Year : 2020

ALK IN THE CONTROL OF THE SYMPATHOADRENAL LINEAGE DIFFERENTIATION AND NEUROBLASTOMA TUMOR PROGRESSION

Vivancos Stalin Lucie

UNIL | Université de Lausanne
Faculté de biologie et de médecine

Laboratoire d'Hématologie-Oncologie Pédiatrique

ALK IN THE CONTROL OF THE SYMPATHOADRENAL LINEAGE DIFFERENTIATION AND NEUROBLASTOMA TUMOR PROGRESSION

Thèse de doctorat ès sciences de la vie (PhD)

Présentée à la

Faculté de biologie et de médecine
de l'université de Lausanne

par

Lucie VIVANCOS STALIN

Master en Pathologie Humaine de la faculté d'Aix-Marseille, France

Jury

Prof. Petr Broz, UNIL, Président

Dr. Raffaele Renella, UNIL, Directeur de Thèse

Dre. Annick Mühlethaler-Mottet, UNIL, co-Directrice de Thèse

Dre. Gudrun Schleiermacher, Institut Curie, Experte

Prof. Jean-Pierre Bourquin, UZH, Expert

Lausanne 2020

UNIL | Université de Lausanne
Faculté de biologie et de médecine

Ecole Doctorale
Doctorat ès sciences de la vie

Imprimatur

Vu le rapport présenté par le jury d'examen, composé de

Président·e	Monsieur	Prof.	Petr	**Broz**
Directeur·trice de thèse	Monsieur	Dr	Raffaele	**Renella**
Co-directeur·trice	Madame	Dre	Annick	**Mühlethaler-Mottet**
Expert·e·s	Madame	Dre	Gudrun	**Schleiermacher**
	Monsieur	Prof.	Jean-Pierre	**Bourquin**

le Conseil de Faculté autorise l'impression de la thèse de

Madame Lucie Marie Lola Vivancos

Master Pathologie Humaine, Université d'Aix-Marseille, France

intitulée

ALK in the control of the sympathoadrenal lineage differentiation and neuroblastoma tumor progression

Lausanne, le 29 mai 2020

pour le Doyen
de la Faculté de biologie et de médecine

Prof. Niko GELDNER
Directeur de l'Ecole Doctorale

TABLE OF CONTENTS

Summary

Neuroblastoma (NB) is an embryonal malignancy derived from the abnormal differentiation of the sympathetic nervous system. NB is a highly heterogeneous disease in terms of clinical, biological and genetic features. NB display an intratumoral heterogeneity and are composed of both neuroblastic and mesenchymal-like cells, displaying a cellular plasticity between both phenotypes. The Anaplastic Lymphoma Kinase (ALK) gene is frequently altered in NB through copy number changes and mutations, with ALK$^{-F1174L}$ and ALK$^{-R1275Q}$ being the most potent activating mutations. ALK amplification and mutations are associated to decrease in the overall free-survival of NB patients. Increased frequencies of ALK mutations have been found at relapse in NB. ALK thus represents a *bona fide* target for NB therapy.

We studied the impact of deregulated ALK signaling during embryonic development on the formation and differentiation of sympathetic neuroblasts. We report that the expression of the human ALK$^{-F1174L}$ mutation in migrating neural crest cells disturbs early sympathetic progenitor differentiation, in addition to increasing their proliferation, both mechanisms being potentially crucial events in the development of embryonal tumors such as NB. Our study suggests that dysregulated signaling of ALK during embryogenesis promotes a precancerous state and may represent an initial and developmental path for NB oncogenesis.

In the second part of this work, we investigated the impact of ALK-wt, ALK$^{-R1275Q}$ and ALK$^{-F1174L}$ -mediated signaling on NB tumorigenesis and progression. ALK isoforms were overexpressed in the human NB cell lines SK-N-Be2c (adrenergic and tumorigenic) and SH-EP (mesenchymal and weakly tumorigenic) through lentiviral vectors. Transduced cells were further injected orthotopically in the adrenal gland of athymic Swiss nude mice or subcutaneously in NOD-SCID-γ mice, respectively. The overexpression of the ALK variants had a low impact on the aggressive NB cell line SK-N-Be2c. In contrast, the expression of ALK-wt, ALK$^{-R1275Q}$ and ALK$^{-F1174L}$ in the SH-EP cell line promotes an aggressive phenotype of the tumors. Indeed, histological and transcriptomic analyses revealed that the overexpression of ALK mediates a change in the cellular phenotype and increases the metastatic potential of the SH-EP tumor cells. Furthermore, we identified the downregulation of genes related to axon guidance, extracellular matrix (ECM) organization in ALK-wt and ALK$^{-F1174L}$ tumors, while these pathways were found upregulated in ALK$^{-R1275Q}$ tumors. Further investigations are

needed to validate these data and to understand the consequences of their deregulation in NB pathogenesis.

To conclude, this work contributed to increase the understanding of ALK mutation as a path to initiate NB-genesis during embryonic development. Moreover, our observations suggest that ALK overexpression and mutations may promote an aggressive phenotype in NB tumors, further opening new research perspectives for the role of ALK deregulated signaling in NB.

Résumé

Le neuroblastome (NB) est une tumeur se développant à partir du système nerveux sympathique (SNS). Le NB est une maladie très hétérogène en termes d'évolution clinique, caractéristiques biologiques et altérations génétiques. Les tumeurs de NB présentent également une hétérogénéité intratumorale. Elles sont composées de cellules adrénergiques et mésenchymateuses qui présentent une plasticité cellulaire. Le gène Anaplastic lymphoma kinase (ALK) est fréquemment amplifié ou muté dans le NB, et ces altérations sont associées à un mauvais pronostic chez les patients. Les mutations ALK$^{-F1174L}$ et ALK$^{-R1275Q}$ sont les mutations les plus fréquentes. De plus, une augmentation du nombre de mutations ponctuelles du gène ALK a été décrite lors des rechutes. ALK constitue ainsi une cible thérapeutique importante dans le NB.

Nous avons étudié l'impact de la mutation ALK$^{-F1174L}$ sur la formation et la différentiation du SNS lors du développement embryonnaire. L'expression de la mutation ALK$^{-F1174L}$ dans les cellules de crête neurale perturbe la formation du SNS, en bloquant la différenciation des progéniteurs sympathiques et en augmentant leur prolifération. Ces deux mécanismes sont des événements cruciaux pour le développement du NB. Notre étude suggère ainsi que l'expression de la mutation ALK$^{-F1174L}$ pendant l'embryogenèse favorise un état précancéreux et serait ainsi impliqué dans l'initiation de la maladie.

Dans un second temps, nous avons étudié l'implication de ALK-wt et des mutations ALK$^{-F1174L}$ et ALK$^{-R1275Q}$ dans la pathogenèse du NB. Les variants ont été surexprimés dans les lignées de NB SK-N-Be2c (adrénergique et tumorigène) et SH-EP (mésenchymateuse et peu tumorigène) par infection lentivirale. Les cellules transduites ont ensuite été injectées respectivement de façon orthotopique dans la glande surrénale de souris athymic Swiss nude mice, ou en sous-cutanée dans des souris NOD-SCID-γ mice. Alors que la surexpression des variants ALK n'a que peu d'impact dans la lignée de NB agressive SK-N-Be2c, la surexpression de ALK-wt, ALK$^{-F1174L}$ et ALK$^{-R1275Q}$ dans la lignée peu tumorigène SH-EP induit un phénotype agressif des tumeurs de NB. En effet, les analyses histologiques et transcriptomiques suggèrent que la surexpression du gène ALK favorise un changement du phénotype cellulaire et montrent une augmentation du potentiel métastatique des tumeurs. De plus, des gènes impliqués dans la formation axonale et l'organisation de la matrice

extracellulaire (ECM) sont négativement régulés dans les tumeurs ALK-wt et ALK$^{-F1174L}$, alors que ceux-ci sont positivement régulés dans les tumeurs ALK$^{-R1275Q}$. Des études approfondies seront nécessaires pour valider ces données et comprendre les conséquences de la modulation de ces gènes dans la pathogenèse du NB.

Pour conclure, ce travail a permis d'apporter une meilleure compréhension de l'impact des mutations du gène ALK au niveau du développement embryonnaire. De plus, nos observations suggèrent que l'amplification et les mutations induisent un phénotype agressif des tumeurs de NB. Ces données ouvrent de nouvelles perspectives de recherche quant au rôle de ALK dans l'initiation et le développement du NB.

ABBREVIATIONS

ADRN	Adrenergic
AKT	Protein kinase B
ALCL	Anaplastic large-cell lymphoma
ALK	Anaplastic lymphoma kinase
ALKAL1	ALK and LTK ligand 1
ALKAL2	ALK and LTK ligand 2
APC	Adenomatous polyposis coli
ARID1A	AT-rich interaction domain 1A
ARID1B	AT-rich interaction domain 1B
ASCL1	Achaete-scute family BHLH transcription factor 1
ATRX	alpha thalassemia/mental retardation syndrome X-linked
BARD1	BRCA1 associated RING domain 1
BMP	Bone morphogenetic protein
BPTF	Bromodomain PHD finger transcription factor
CASC15	Cancer susceptibility 15
CGREF1	Cell growth regulator with EF-hand domain 1
CRKL	CRK like proto-oncogene, adaptor protein
CSMD1	CUB and sushi multiple domains 1
CUX2	Cut like homeobox 2
DNA	Deoxyribonucleic acid
DDX4	Dead-box helicase 4
DHB	Dopamine beta-hydroxylase
DOPA	3,4-dihydroxyphenylalanine
DUSP12	Dual specificity phosphatase 12
EMT	Epithelial-mesenchymal transition
ENTPD2	Ectonucleoside triphosphate diphosphohydrolase 2
FDA	Food and Drug Administration
GATA2	GATA Binding protein 2
GATA3	GATA Binding protein 3
GM-CSF	Granulocyte-macrophage colony-stimulating factor
GN	Ganglioneuroma
GNB	Ganglioneuroblastoma

GWAS	Genome Wide Association Study
HACE1	HECT domain and ankyrin repeat containing E3 protein ubiquitin kinase 1
HAND2	Heart and neural crest derivatives expressed 2
HRAS	HRas proto-oncogene, GTPase
HSD17B12	Hydroxysteroid 17-Beta dehydrogenase 12
IL-2	Interleukine 2
IL-3	Interleukine 3
IL31RA	Interleukine 31 receptor A
INRGSS	International Neuroblastoma Risk Group Staging System
INSM1	Insulinoma-associated 1
INSS	International Neuroblastoma Staging System
JAK	Janus kinase
KI	Knock in
KRAS	Kirsten rat sarcoma viral oncogene homolog
LDLa	Low density lipoprotein class A
LIN28B	Lin-28 homolog B
LMO1	LIN domain only 1
MAM	Mephrin/A5/protein tyrosin phosphatase Mu
MAPK	Mitogen-activated protein kinases
MEKK2/3	Mitogen-activated protein/ERK kinase kinase 2/3
MES	Mesenchymal
MKI	Mitosis-karyorrhexis index
mRNA	Messenger RNA
mTOR	Mammalian target of rapamycin
NB	Neuroblastoma
NCC	Neural crest cell
NF1	Neurofibromin 1
NGS	Next-generation sequencing
NPM	Nucleophosmin
ODZ3	Protein odd oz/ten-M homolog 3
p53	protein 53
PHOX2A	Paired like homeobox 2A
PHOX2B	Paired like homeobox 2B

PI3K	Phosphatidylinositol-4,5-bisphosphate 3-Kinase catalytic subunit alpha
PRRX1	Paired related homeobox 1
PTPN11	Protein tyrosine phosphatase non-receptor type 11
PTPRD	Protein tyrosine phosphatase receptor type D
RET	Ret proto-oncogene
RNA	Ribonucleic acid
ROS1	ROS proto-oncogene 1
RTK	Receptor tyrosine kinase
SA	Sympathoadrenal
SCP	Schwann cell precursor
SDHB	Succinate dehydrogenase complex iron sulfur subunit B
SG	Sympathetic ganglia
SLC45A1	Solute carrier family 45 member 1
SMARCA4	Swi/snf related, matrix associated, actin dependent regulator of chromatin, subfamily A, member 4
SMARCB1	Swi/snf related, matrix associated, actin dependent regulator of chromatin, subfamily B, member 1
SNP	Single nucleotide polymorphism
SNS	Sympathetic nervous system
SOX10	SRY-Box transcription factor 10
STAT	Signal transducer and activator of transcription
TERT	Telomerase reverse transcriptase
TF	Transcription factor
TH	Tyrosine hydroxylase
TKD	Tyrosine kinase domain
TMCO3	Transmembrane and coiled-coil domains 3
TP53	Tumor protein 53
TRA2A	Transformer 2 alpha homolog
TRKB	Tropomyosin receptor kinase B
WT1	Wilms tumor 1
WT	Wild-type

INTRODUCTION

CANCER

Cancer is a major cause of morbidity and mortality. In 2018, 18.1 million of new cases and 9.6 million of cancer-related deaths were estimated to have occurred worldwide[1]. Cancer is the first leading cause of death in developed countries and the second cause in developing countries[1].

The understanding of the biology of cancer has been largely improved over the last 20 years. Pivotal advances have enriched our understanding of the processes involved in the transformation of normal cells into cancer cells. Tumorigenesis is the result of the acquisitions of mutations, genetic or epigenetic alterations in the genome that will consequently drive an uncontrolled cell division and tumor progression[2]. The rate of somatic mutations increases with exposure to exogenous mutagenic sources, including chemicals, radiations, and viruses, and some cancer are directly associated with a specific mutagen exposure (i.e. tobacco for lung cancer, aflatoxin for liver cancer or ultraviolet light for skin cancer)[2,3]. A subset of genes, known as oncogene and tumor suppressor genes, act as drivers of disease and confer growth advantages to the tumor when mutated[2]. Those genes are mainly acting as key regulators to maintain the homeostasis of a tissue, controlling cell cycle progression, or entrance in programmed cell death[2]. In addition to genetic alterations, cancer cells harbor epigenetic changes including DNA methylation and alterations of the chromatin structure which affect gene expression, that contribute to the tumorigenic process and the heterogeneity of the tumor[4]. Cancer is an evolutionary process, based on the continuous acquisition of genetic alterations in individual cells, and the selection of the resulting cells carrying alterations that confer the ability to proliferate and survive more effectively than non-mutated cells. Along the path toward malignancy, the clonal selection leads to the acquisition of multiple functions allowing tumor progression[5]. These biological competent traits, described as hallmarks of cancer, include growth stimulation, evasion of growth suppressors, resistance to cell death, deregulation of cellular energetics, replicative immortality, evasion from the immune destruction, induction of angiogenesis and activation of invasion and metastasis[5]. Until now, researches has

focused on the development of new therapeutic drugs that target one, or several hallmarks in combination[5].

PEDIATRIC CANCER

Pediatric cancers are significantly different from neoplasia in adults, in terms of epidemiology, cellular origin, genetic events and response to therapy[6]. Cancer remains the leading cause of death by disease of children in developed countries[7]. The most common pediatric tumors include brain tumors, lymphoma, neuroblastoma (NB), Wilms tumors, and bone tumors (i.e. osteosarcoma, Ewing sarcoma).

The understanding of the genomic alterations occurring in pediatric cancers has been improved in the past decade mainly through large scale genome sequencing studies[8,9]. Pediatric cancers differ from those in adults particularly in terms of mutational frequency and cancer-driving events. Overall, the mutational burden of pediatric cancers is significantly lower than in the adult tumors, and the cancer-driving genetic events are mostly specific to the diseases in which they arise[8,9]. The chromosomal fusion events that lead to fusion genes are more prevalent in pediatric cancers and often activate genes that are crucial during the development, such as the neurotrophic growth factor receptor family[10,11]. Epigenetic dysregulations are also more frequent in childhood cancers. Point-mutations in histone genes or mutations in epigenetic modifiers (i.e. histone modifying enzyme, chromatin remodeling complexes) contribute to the deregulation of gene expression[8,9,12]. Moreover, a genetic predisposition is involved in at least 10% of pediatric cancers[8,13,14]. Finally, pediatric cancers are mainly embryonal in tissular origin[12]. Evidences suggest that most pediatric cancers originate from stem or progenitor cells in a particular time window, including during embryonic development[12,15]. Mutations in these stem or progenitor cells lead to disturbed cellular divisions and favor self-renewal ability over differentiation[12]. Otherwise, several embryonal cancers arise from precursors that are arrested in undifferentiated stages of development. For example, in rhabdoid tumors, this occurs by inactivation of *SMARCB1* or *SMARCA4*, in Wilms tumors by inactivation of *WT1*, in medulloblastoma by amplification of *MYC* or *MYCN*, in high-grade glioma by mutations in histone genes and in NB by amplification of *MYCN* or aberrant ALK signaling[16].

NEUROBLASTOMA

Epidemiology and clinical presentation

NB is the most common extracranial solid tumor of early childhood, accounting for around 7% of all pediatric cancers[17]. The incidence of NB is 10.2 cases per million children under 15 years old. NB remains relatively lethal, constituting 15% of pediatric oncology deaths. NB occurs in very young children and is the most common malignancy diagnosed during the first year of life, with a median age at diagnosis of 17 months[17]. NB is remarkably heterogeneous, in terms of clinical presentation, evolution, and overall prognosis, with frequent cases of aggressive and metastatic disease at diagnosis (bone marrow, bone, liver, and lymph nodes) or forms with spontaneous regression requiring no therapeutic intervention[17].

Cellular origin

The sympathetic nervous system

NB is an embryonal tumor of the developing sympathetic nervous system (SNS). Together with the parasympathetic system, the SNS belongs to the autonomic nervous system[18]. The SNS is composed of preganglionic neurons that synapse with the postganglionic neurons within sympathetic ganglia (SG) of the sympathetic chain, and the adrenal medulla of the adrenal gland[18]. The chromaffin cells of the adrenal medulla have the same embryonic origin and act as postganglionic neurons[18]. The SNS develops from a subset of neural crest cells (NCCs) giving rise to various cell-types, including neuronal, glial and Schwann cells of the peripheral nervous system, melanocytes, smooth muscle cells, osteoblasts, osteoclasts, adipocytes, and chondrocytes[19]. The neural crest can be divided into four subgroups of migrating population: cranial, cardiac, vagal and trunk neural crest[19]. The SNS develops from the trunk neural crest that give rise to the melanocytes of the skin and to neurons and glia of SG, dorsal root ganglia, Schwann cells and adrenal chromaffin cells[19].

The development of the sympathoadrenal lineage

During embryonic development, the NCCs undergo an epithelial-mesenchymal transition (EMT)[19]. Trunk NCCs forming the sympathoadrenal (SA) lineage migrate toward the ventral side of the neural tube to reach the vicinity of the dorsal aorta, where they receive differentiation signals (Figure1). Sympathetic neuron differentiation is induced by Bone Morphogenetic Proteins (BMPs) 2, 4, and 7 released from the dorsal aorta, upregulating the expression of various transcription factors (TFs) including paired like homeobox 2B (Phox2b), paired like homeobox 2A (Phox2a), achaete-scute family BHLH transcription factor 1 (Ascl1), INSM transcriptional repressor 1 (Insm1), heart and neural crest derivative expressed 2 (Hand2), GATA binding protein 2 (Gata2), GATA binding protein 3 (Gata3), starting from Phox2b and Ascl1 (Figure 1)[20]. The BMP proteins are essential for the initial step of differentiation, and their absence completely prevents the differentiation of sympathetic progenitors at the dorsal aorta[21,22]. The TFs upregulated by the signal released from the dorsal aorta crosstalk and act as a *bone fide* TF network in the initial phase of differentiation. Sox10 is expressed in migrating NCCs, where it mediates their survival, maintenance of multipotency, and inhibition of neuronal differentiation (Figure 1)[23]. It is transiently expressed, with Phox2b, during early sympathetic specification, and lost during neuronal differentiation. However, Sox10 expression is maintained in rare cells of the sympathetic ganglia (SG), where it induces glial cell fate specification and differentiation[23]. During sympathetic specification, $Sox10^+$ NCCs transit to $Sox10^+/Phox2b^+$ immature progenitors and to $Sox10^-/Phox2b^+$ differentiated neuroblasts[24]. The $Sox10^+/Phox2b^+$ progenitors are found in the early phases of neurogenesis until E5 (embryonic days) in the chick embryo and E11.5 in mouse embryo[24,25].

Many studies have confirmed the specific and essential roles of the abovementioned TFs in SA specification, and the absence of even a single member can lead to aberrations in noradrenergic differentiation[20]. Phox2b is a major regulator of the noradrenergic differentiation and its knockout results in the absence of the entire sympathetic nervous system[26]. This is due to the fact that none of the other TFs are expressed in the sympathetic nervous system in the Phox2b knockout mice[26]. Moreover, the noradrenergic differentiation is delayed in Ascl-1 deficient mice and the

same phenotype was observed in mutant mice for Insm1, which acts downstream of Phox2b and Ascl1[27,28]. The absence of Hand2 leads to a progressive loss of neurons and of initial noradrenergic differentiation[29]. Finally, an increased apoptosis of sympathetic neurons is observed in Gata-3 knockout mice with minor effects on neuron differentiation[30]. In parallel, all these TF are also involved in the survival and proliferation of immature sympathetic neurons[20]. While, the knockout of Phox2b results in reduced proliferation of immature sympathetic neurons, in contrast, an antiproliferative effect on immature sympathetic neurons was observed by the overexpression of Phox2b *in vitro* and *in vivo*[31,32]*.* The knockout of Ascl1 in neural crest leads to a strong reduction of the proliferation in SG from E11.5 to E15.5 in mice[28]. The knockout of Insm1 results in a reduced proliferation reflected by smaller SG with normal differentiation[27]. Finally, the knockouts of Hand2 and Gata3 lead to a massive decrease in proliferation of sympathetic progenitors and immature sympathetic neurons[29,30,33].

The noradrenergic differentiation of the SA precursors starts after their migration into the vicinity of the dorsal aorta and is reflected by the expression of the enzymes tyrosine hydroxylase (TH) and dopamine β-hydroxylase (DBH)[20]. TH catalyzes the conversion of tyrosine in dihydroxyphenylalanine (DOPA), which is then converted into dopamine by the DOPA carboxylase[34]. In turn, DBH catalyzes the conversion of dopamine into noradrenaline[34]. At this point, the SA precursors give rise to SG and adrenal chromaffin cells (Figure 1). Of interest, recently a new cellular origin for the chromaffin cells of the adrenal medulla has been reported[35]. A large number of chromaffin cells arise from peripheral glial cells, so-called Schwann cell precursors (SCPs), highlighting that the adrenal medulla is derived from both precursors of the SA lineage and SCPs. The specification of the NCC occurs in early phases of differentiation, around E10.5, where NCCs will separate toward cells forming sympathetic neurons and SCPs. SCPs migrate along the visceral motor nerve to the vicinity of the forming adrenal gland, where they detach from the nerve and form postsynaptic chromaffin cells. The ablation of SCPs, as well as of the visceral motor nerve, leads to a depletion of adrenal chromaffin cells in the forming adrenal medulla. The ablation of the preganglionic nerve also prevents the differentiation of chromaffin cells leading to an accumulation of glial cells in the adrenal medulla[35].

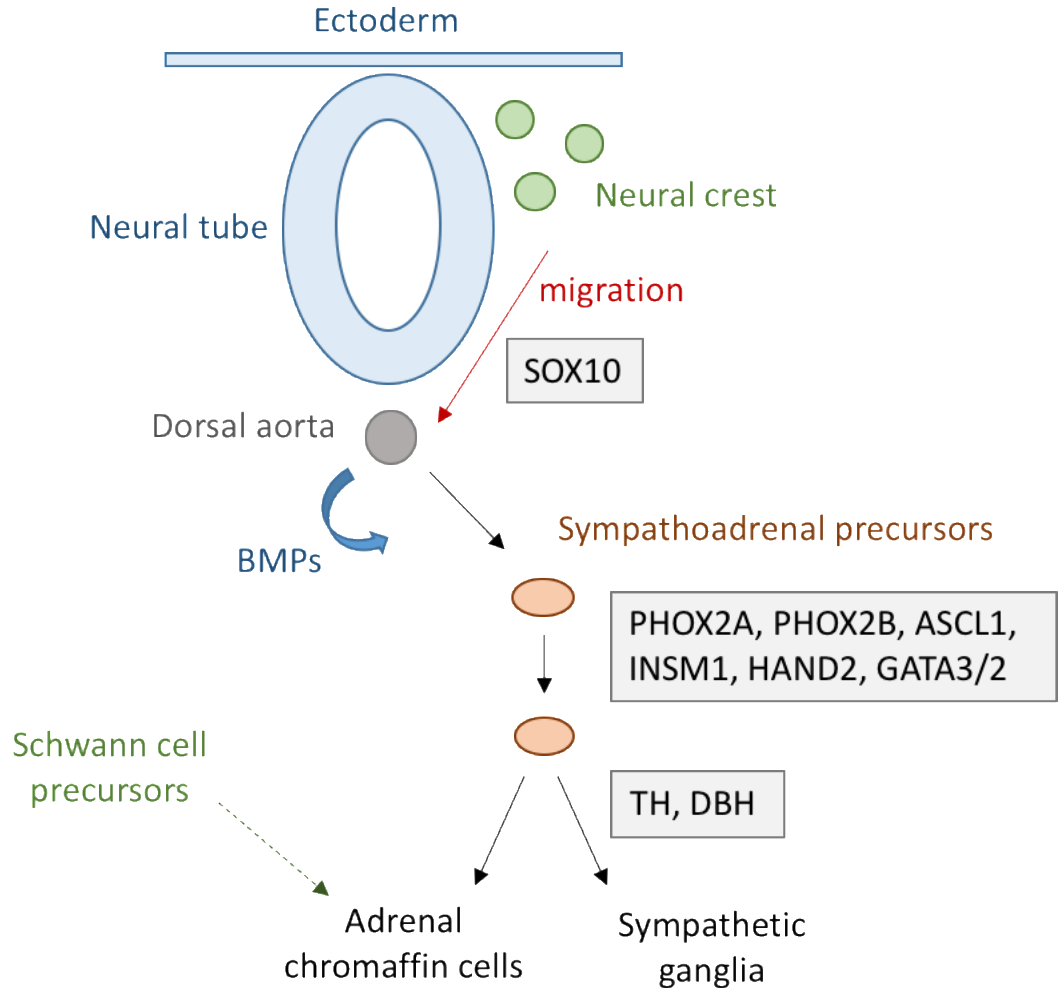

Figure 1. The development of the sympathoadrenal lineage. During embryonic development the neural crest cells undergo epithelial-mesenchymal transition and migrate toward the ventral region of the neural tube to reach the vicinity of the dorsal aorta. Sympathetic neuron differentiation is induced by Bone Morphogenetic Proteins (BMPs) released from the dorsal aorta and involves the expressions of various transcription factors (see grey box). Sympathoadrenal precursors give rise to adrenal chromaffin or SG. The noradrenergic differentiation is characterized by the expression of TH and DBH. Adrenal chromaffin cells also arise from Schwann cell precursors.

The connection between SNS and neuroblastoma development

The connection between the SNS and NB comes from several observations. First, NB can arise along the entire sympathetic system, with the majority of the primary tumors developing in the abdominal region (65%), particularly in the adrenal medulla, or in paraspinal sympathetic ganglia at various sites, including in the neck, chest and pelvis[36]. Second, NB tumors express surface markers of the SNS, such as GD2, which is found on the neuroblastic, but not on the glial lineage[37,38]. Third, NB tumors secrete catecholamine metabolites which are found in increased concentration in the patients' urine[39]. Catecholamines are released from the chromaffin cells of the adrenal medulla and paraspinal ganglia[40]. Finally, the connection between SNS and NB has been highlighted by the observation that the cells within NB tumors display phenotypic and transcriptomic characteristics of the neural crest. Indeed, cell lines derived from NB tumors are defined in three distinct cellular phenotypes and vary in their tumorigenic potential[41]. The N-type (neuronal) cells have the properties of sympathoadrenal neuroblasts and are highly aggressive[42]. The S-type (substrate-adherent) cells lack neuronal characteristics, have the properties of embryonic Schwann/glial/melanocyte cells of the neural crest, and are non or less malignant[42]. The I-type (intermediate) cells have features of both N- and S-type cells and present properties of stem-like cells[43,44]. The I-type cells represent the most aggressive population within a tumor and would be derived from a more primitive stem cell, a common progenitor of the N- and S-type cells.

Recently, two NB cell types were identified in patient-derived cell lines, a mesenchymal (MES) and an adrenergic (ADRN) cell type associated to S- and N-type, respectively, with highly divergent phenotypes and recapitulating the lineage development stage[45,46]. Indeed, MES cells resemble neural crest derived precursors cells (so called NCCs-like), while ADRN cells are committed to the SA lineage, and both cell types can interconvert[46]. These populations have specific super-enhancer landscapes, which are associated to transcription factors (TFs) that compose the core regulatory circuitry (CRC) and govern the cell lineage identity. In NB, MES CRCs of 20 TFs and ADRN CRC of 18 TFs were identified[46]. Among them, PHOX2B, GATA3 and HAND2 are master TFs that define NB cell lines with noradrenergic identity[46,47]. The overexpression of the MES TF PRRX1 or the activation of Notch in ADRN NB cells induces a transition to a MES phenotype[46,48]. Moreover, NCCs-like/MES cells are more

resistant *in vitro* to standard chemotherapy than ADRN cells, and the MES cell population is enriched in post-treated and relapsed NB[46,47].

NB is thought to specifically derive from the proliferation of sympathetic neuroblasts having escaped to apoptotic signals and noradrenergic specification[49]. For now, the specific mechanisms initiating NB from embryonal tissue are still largely unknown. However, mutations in key regulators of the SA lineage may represent potential initial events for NB development[50]. MYCN, PHOX2B, and ALK have previously been identified as potential first hits occurring in the early stages of the embryonic development during the differentiation of the NCCs[50]. For example, MYCN promotes ventral migration and differentiation of NCCs giving rise to dorsal root ganglia and SG[51]. As aforementioned, Phox2b is a major regulator of the noradrenergic differentiation[20]. ALK is expressed in the developing peripheral and central nervous system and the impact of *ALK* alterations on NCCs and sympathetic neuroblasts has been studied by several groups (see below, ALK chapter). Moreover, MYCN, PHOX2B and ALK are frequently altered in NB.

Genetic defects in neuroblastoma

Genetic alterations in sporadic neuroblastoma

Genetic alterations in NB provide prognostic information regarding the risk of the disease. The first somatic genetic alteration identified in NB is the amplification of the oncogene *MYCN*, occurring in approximately 25% of cases[52,53]. It is strongly associated with advanced-stage disease, rapid tumor progression, and treatment failure[52]. Identifying an amplification of *MYCN* is routinely used for the risk classification of NB[54]. Besides, numerical chromosome alterations, including whole chromosome gains or losses, or segmental copy number alterations are frequently observed in sporadic NB[55,56]. Whole-chromosome copy number alterations are associated with low-risk NB and an increased likelihood of survival. Conversely, segmental copy number alterations, including deletions involving chromosomes 1p, 3p, 4p, 11q, and gains within chromosomes 1q, 2p, and 17q are associated with high-risk NB and poor outcomes[57–63]. The unfavorable alteration in chromosome 17q is the most prevalent occurring in 50% of NB[58]. Segmental copy number alterations are the strongest

predictor of relapses, and this independently of *MYCN* amplification[55]. Moreover, patients with both numerical and segmental alterations have a poorer prognosis and the highest risk of relapse[55,56]. Studies additionally identified chromothripsis, corresponding to massive genetic rearrangements, occurring in 18% of high-risk NB, to be associated with poor outcomes[64,65].

Few recurrent mutations with significant frequency were identified in NB tumors in *ALK*, *ATRX*, *PTPN11*, *ARID1A/B* genes and were associated with poor prognosis[66,67]. *ALK* is the most frequently altered gene, occurring in approximately 10% of all cases of neuroblastoma[68–71]. ATRX alterations, including loss-of-function/mutations, were reported to be enriched in older patient cohorts, associated with stage 4 disease and exclusively in tumors without MYCN amplification[72,73]. Genomic rearrangements, near or at the *TERT* locus occur in 20% of high-risk NB, almost exclusively without ATRX and MYCN amplification[74]. Furthermore, sequencing of NB tumors revealed that mutations in RAS and p53 pathways in pretreated NB are associated with poor survival and that patients whose tumors harbor telomere maintenance have a bad prognosis[75]. Overall, low-risk NB lack telomere maintenance mechanisms, high-risk NB display telomere maintenance mechanisms, and ultra-high-risk NB tumors harbor telomere maintenance mechanisms in combination with RAS and/or p53 mutation[75]. Also, structural alterations in genes involved in neuronal cone growth stabilization including *ODZ3*, *PTPRD,* and *CSMD1* were also reported in NB tumors[64].

Several studies reported the loss-of-function/mutation of TP53 in NB cell lines derived from relapse tumors, which might be associated with resistance to therapy [76–78]. More recently, whole-exome sequencing sheds light on the mutational profiles of primary tumors and relapsed NB tumors. Recurrent mutations of *HRAS* and *KRAS*, as well as other mutations in the RAS-MAPK pathways, were identified in 78% of relapsed NB[79,80]. These alterations were found either only in relapses or enriched relative to the primary tumors[79,80]. Moreover, sequencing of the ALK locus identified the occurrence of new ALK mutations in relapsed NB[81]. In addition, whole exome sequencing revealed the acquisition of somatic mutations in *BPTF, TMCO3, CGREF1, CUX2, ENTPD2, SLC45A1, TRA2A* in NB tumors during chemotherapy treatment[82].

Genetic predisposition to neuroblastoma

Most NB tumors are sporadic; however, about 1-2% of cases are familial and defined by the presence of several affected individuals within the same family. In these situations, NB generally appears at a younger age and is often associated with the presence of multifocal primary tumors[83]. The disease can show different degrees of severity, with the presence of low-risk and high-risk NB within the same family.

The first gene of predisposition identified for familial NB was *PHOX2B*, a TF playing an essential role during sympathetic differentiation, as described above. Loss-of-function mutations in PHOX2B are found in approximately 10% of familial NB and are mostly associated with other neural-crest disorders, called neurocristopathies, such as Hirschsprung's disease or congenital hypoventilation syndrome[84–87]. Families harboring a mutation in the gene *PHOX2B* have variable penetrance for these neurocristopathies[88].

More recently, the anaplastic lymphoma kinase (*ALK*) gene was identified as a second NB predisposition gene[69,71]. Constitutional activating ALK mutations are found in approximately 50% of familial NB[71]. However, their penetrance is incomplete, and it is considered that only 50% of carriers of ALK mutations develop NB[89]. This incomplete penetrance may be explained by a lack of acquisition of additional genetic events. Mutations in PHOX2B and ALK represent early events during malignant transformation. However, there are familial NB cases that do not present mutations in these genes, and additional predisposing genes remain to be discovered. Recently, germline mutations in *TP53*, *SDHB*, *PTPN11*, *APC*, and *NF1* have been reported to occur in rare patients with NB[14,90,91].

Moreover, various susceptibility loci were identified by Genome-Wide Association Studies (GWAS) and associated with either high-risk or low-risk NB[88,92]. GWAS identified *BARD1*, *CASC15*, *HACE1*, *LIN28B*, *LMO1* as associated with high-risk NB[88]. SNPs in *BARD1*, at chromosome 2q35 are associated to stage 4 disease[93]. Three SNPs were identified in chromosome 6p22 within the long coding RNA tumor suppressor gene *CASC15* and the predicted genes *FLJ22536* and *FLJ44180*[94,95]. Patients who are homozygotes for this risk allele have a high risk to undergo metastatic stage 4 disease with *MYCN* amplification[94,95]. Aberrations within LMO1 at chromosome

11p15.4 have been reported in 12% of NB and are associated with aggressive forms[96]. Subsequently, SNPs within *HACE1* and *LIN28B* were both found in chromosome 6q16[97]. *HACE1* is a tumor suppressor gene that has been described to inhibits the growth of several cancer cell types, including NB[98]. *LINB28* is an oncogene involved in stem cell differentiation known to regulate let-7 expression. High expression of LIN28B and low levels of let-7 have been reported in various cancers[99]. In NB, the low expression of *HACE1* and, in contrast, high expression of *LINB28* are associated with high-risk NB and poor overall survival[97]. Regarding the low-risk group, GWAS identified SNPs within *DUSP12* at 1q23.3, *DDX4,* and *IL31RA* both in 5q11.2 and *HSD17B12* at 11q11.2[100].

Tumor histology

Together with ganglioneuroma (GN) and ganglioneuroblastoma (GNB), NB belongs to the group of peripheral neuroblastic tumors[101]. Neuroblastic tumors have been classified according to their degree of differentiation/maturation by the Neuroblastoma Pathology Committee[101,102] (Figure 2). The neuroblastic tumors are defined in 4 categories: ganglioneuroma (Schwannian stroma-dominant), GNB intermixed (Schwannian stroma-rich), GNB nodular (Schwannian stroma-rich/stroma-dominant and stroma poor) and NB (Schwannian stroma-poor)[101]. Mature tumors, with high Schwann cell content, are the least aggressive and occur in young patients, whereas immature/stroma-poor neuroblastic tumors occur in older children and tend to be extremely aggressive[101]. GN and intermixed GNB are linked to a favorable prognosis, and nodular GNB with unfavorable outcome[101]. NB is the most undifferentiated tumor, with less than 50% of Schwann cell content. According to the International Neuroblastoma Pathology Classification, the grade of histology, the mitosis-karyorrhexis (MKI) index, and the age of the patient at diagnosis are taken into consideration for the distinction of NB into favorable or unfavorable histology[101]. Globally, undifferentiated NB at any age and any MKI have the most unfavorable prognostic; but poorly differentiated or differentiated NB with high MKI index in older children are also of unfavorable outcomes[101] (Figure 2).

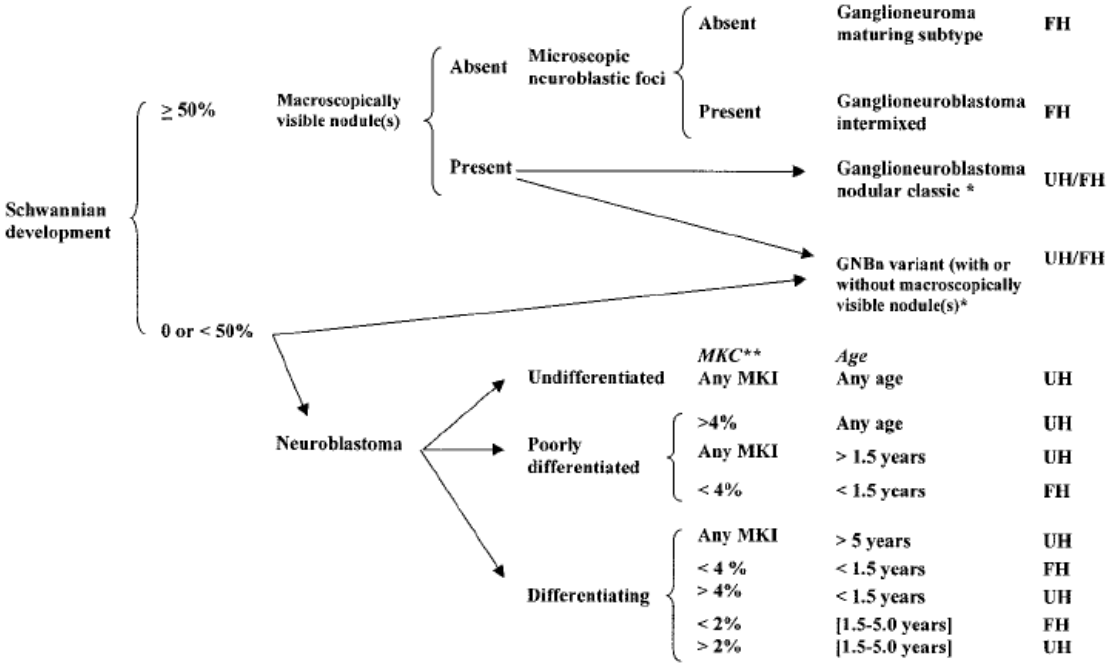

Figure 2. International Neuroblastoma Pathology Classification. Neuroblastoma belongs to the family of neuroblastic tumors with Ganglioneuroma and Ganglioneuroblastoma (GNBn). UH as Unfavorable Histology and FH as Favorable Histology. Peuchmaur et al., *Cancer*, 2003.

Clinical risk factors and classification

The International Neuroblastoma Staging System (INSS) was accepted in 1988 for newly diagnosed NB[103]. The INSS included the degree of tumor resection, the presence of lymph node involvement and the infiltration of the tumor[103,104]. In 2009, the International Neuroblastoma Risk Group Staging System (INRGSS) has been proposed as pre-treatment consensus (Figure 3)[105]. The INRGSS is based on the age at diagnosis, the INRG tumor stage which depend on the invasion of the tumor: L1/L2 for localized tumors, M for metastatic disease and MS, the grade of differentiation of the tumor, the *MYCN* status, the 11q aberrations, and the DNA ploidy of the tumors[54]. The INRGSS proposes 16 distinct risk groups and classifies NB in term of 5-year event-free survival rates into 4 categories as very low risk (>85%), low risk (>75 to <85%), intermediate-risk (>50 to <75%) and high risk (<50%) (Figure 3). Globally, older children with metastatic stages have the most unfavorable prognosis, with a high risk of refractory disease. In contrast, younger children with localized tumors have a good

response to treatment and can frequently be cured. Stage MS occurs in 5% of NB, in children under 1 year of age, and corresponds in small localized tumors with distant metastasis in the liver, skin, or bone marrow. This special form of metastatic NB has the particularity to almost always spontaneously regress without any treatment[17].

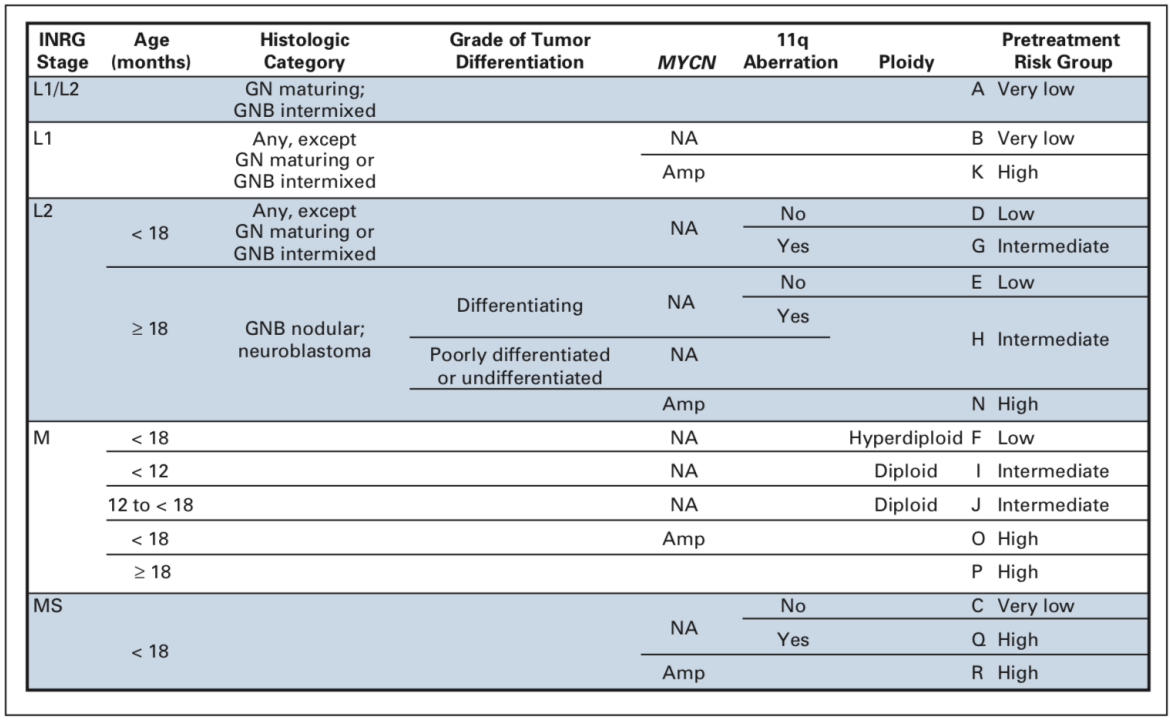

INRG Stage	Age (months)	Histologic Category	Grade of Tumor Differentiation	*MYCN*	11q Aberration	Ploidy	Pretreatment Risk Group
L1/L2		GN maturing; GNB intermixed					A Very low
L1		Any, except GN maturing or GNB intermixed		NA			B Very low
				Amp			K High
L2	< 18	Any, except GN maturing or GNB intermixed		NA	No		D Low
					Yes		G Intermediate
	≥ 18	GNB nodular; neuroblastoma	Differentiating	NA	No		E Low
					Yes		H Intermediate
			Poorly differentiated or undifferentiated	NA			
				Amp			N High
M	< 18			NA		Hyperdiploid	F Low
	< 12			NA		Diploid	I Intermediate
	12 to < 18			NA		Diploid	J Intermediate
	< 18			Amp			O High
	≥ 18						P High
MS	< 18			NA	No		C Very low
					Yes		Q High
				Amp			R High

Figure 3. International Neuroblastoma Risk Group staging system. Cohn et al., *J. Clin. Oncol.,* 2009.

Risk-stratification and treatment

The risk-stratification system has been designed to determine the optimal therapeutic strategy depending on the favorable or unfavorable prognosis of NB[54]. Patients having low- and intermediate-risk NB have an excellent event-free and overall survival[106]. For these patients, the objective is to achieve cures and reduce therapeutic intensity. Although in the last decades the treatment for lower stages disease has been improved, the survival rates for children with high-risk NB remains dramatically low, with long-term survival rates being inferior to 40% despite intensive treatments. Children with high-risk NB are clinically treated with a combination of chemotherapies, surgical resection, high-dose chemotherapy with an hematopoietic stem-cell rescue,

radiation therapy, immunotherapy (dinutuximab, GM-CSF, IL-2) and 13-cis retinoic acid[107]. The treatment of high-risk NB is based on three phases: a first phase of induction, a phase of consolidation, and a final phase to maintain the remission and eliminate any residual disease[107].

Molecular targeted therapy

Refractory NB prompted extensive research in the last few years aiming to generate new targeted drugs in the last few years. Targeted therapies have been developed to prevent or eradicate the residual disease, and they are in clinical studies or already currently used in the clinic[108,109]. The use of topoisomerase inhibitors including topotecan and irinotecan, radioactive molecules such as radioactive I-MIBG, anti-GD_2 monoclonal antibodies, and 13-cis-retinoic acid constitute clinical standard of care for the treatment for high-risk refractory disease[36,108]. Aurora kinase inhibitors reducing the stability of the oncogenic transcription factor *MYCN*, and PI3K/AKT/mTOR pathways inhibitors are currently being evaluated for their effects in combination with chemotherapy[108,109]. Finally, the use of tyrosine kinase inhibitors have shown results in the treatment of refractory NB. Indeed, clinical trials with tyrosine kinase inhibitors targeting TrkB, which acts as an oncogenic kinase in a subset of NB, gave promising results for patients with high-risk refractory NB[110]. Moreover, extensive efforts have been made for the development of tyrosine kinase inhibitors targeting *ALK*, which represents an important therapeutic target in NB[68–71,111].

In vivo model of neuroblastoma

The most frequently employed mouse model for NB remains up to these days the TH-MYCN mouse developed by Weiss et al. in 1997[112]. In this model, the expression of *MYCN* is under the control of a tyrosine hydroxylase promoter leading to the development of NB. Of interest, this model was the first demonstration that MYCN amplification can cause NB from sympathetic precurcors[112]. Tumors grow with a long latency period and the mice do not develop metastasis in the bone marrow, and thus this model did not reflect the aggressive form of the disease[112]. However, the period of latency was reduced, and the penetrance increased when TH-MYCN mice were crossed with mice deficient for the tumor suppressors Nf1 and Rb1[112]. Moreover, a

metastatic model has been generated by using TH-MYCN mice lacking Caspase-8 expression in the neural crest[113]. A second MYCN-driven NB mouse model has been generated by Althoff et al. in 2015[114]. The Cre-conditional induction of *MYCN* in dopamine β-expressing-cells (DBH) leads to the development of neuroblastic tumors in mice. This model, called *LSL-MYCN*;Dbh-iCre mice model, closely recapitulates the biology of the human NB tumor in terms of localization, histology, and chromosomal alterations[114]. Moreover, *LINB28* has also been reported to generate NB tumors when overexpressed in the SA lineage of mice and to increase the oncogenic potential of *MYCN*[115]. Finally, several *in vivo* models have been developed to study the implication of *ALK* in the developing sympathetic nervous system (see below). Recently, the analysis of the genetic profile of mouse NB tumors driven by *ALK$^{-F1174L}$*, *MYCN*, *MYCN/ALK$^{-F1174L}$* and *Lin28B* revealed a low number of genetic alterations that were enriched for genes that are mutated in the human form of the disease[116].

ANAPLASTIC LYMPHOMA KINASE

ALK structure and expression

The ALK gene, located on chromosome 2p23.2, encodes for a transmembrane receptor tyrosine kinase (RTK) of 1620 amino acids. Together with the leucocyte tyrosine kinase and the ROS receptor, ALK belongs to the insulin receptor (IR) superfamily. Like all other RTKs, ALK is composed of an amino-terminal extracellular domain, a transmembrane domain, and an intracellular tyrosine kinase domain (TKD). The extracellular domain of ALK contains glycine-rich regions and additional LDLa (low density lipoprotein class A) and MAM (mephrin/A5/protein tyrosin phosphatase Mu) domains[117]. ALK possesses an intracellular TKD domain and remains inactive without ligand-dependent activation. Like other IRs, ALK has a Y'XXX'Y autophosphorylation motif (Y'RAS'YYY) in the activation loop and the tyrosine Y1278, Y1282, and Y1283 are sequentially phosphorylated during activation[118].

ALK is mainly expressed during embryogenesis and is mostly downregulated after birth. In mouse, rat, and chick, ALK is strictly expressed in the developing peripheral and central nervous system including thalamic nuclei, spinal cord motoneurons, and sympathetic and enteric ganglia[119–122]. ALK has also been described to be expressed

in the motor nuclei of the brainstem[123]. Moreover, the analysis of the developing SA lineage reported the mRNA expression of ALK in sympathetic neuroblasts at E12.5 and E13.5 in mice embryo[35]. In adult tissue, ALK is expressed in the dentate gyrus and in the CA1 and CA3 regions of the hippocampus[124]. In zebrafish, ALK expression has only been reported in the developing central nervous system[125].

ALK ligands

Pleiotrophin and midkine have been reported as potential activating ligands of mammalian ALK[126,127]. Midkine has been described to activate ALK in cultured chick sympathetic neuroblasts and human glioblastoma cells[128,129]. In contrast, the role of pleiotrophin remains controversial, as the specific activation of ALK by pleiotrophin has not been well proved[130–132]. Moreover, the dimerization of the ALK receptor occurs with heparin but not with midkine and pleiotrophin, suggesting that heparin might be a co-ligand for the dimerization and activation of the receptor[133]. More recently, the secreted proteins FAM150A and FAM150B (also named augmentor-β and augmentor-α or ALKAL1 and ALKAL2) were identified as potent activating ALK ligands that bind the glycine-rich region[134–138]. FAM150A has been reported to bind and activate ALK[134,139]. FAM150B induces the neuronal differentiation of human NB NB1 and PC12 cells[138]. Moreover, FAM150B stimulates the transformation of ALK-expressing NIH/3T3 cells and induces IL-3 independent growth of Ba/F3 cells expressing ALK[135].

Physiological function of ALK in the SA lineage

The physiological role of ALK during embryonal development remains elusive. However, analysis of its expression pattern, as well as its importance in familial and sporadic NB, suggests a key role in the central and peripheral nervous system development. In zebrafish, ALK is required for neurogenesis[125]. Indeed, the overexpression of ALK during early development leads to an increased proliferation and aberrant neurogenesis, while the knock-down severely affects the differentiation and survival of neurons in the central nervous system[125]. In mice, the knockout of ALK is viable, however, it leads to alterations of neurological functions, including reduced hippocampal neurogenesis, behavior defects, and impacts the hypothalamic-pituitary-

gonadal axis[124,140–142]. Many studies have been made to understand the physiological role of ALK in the developing SA lineage. The chick model revealed the first direct evidence for the role of ALK in the control of sympathetic neuron proliferation *in vitro* and *in vivo*[129]. While the overexpression of ALK strongly increased the proliferation of sympathetic neurons, the pharmacological inhibition of ALK, as well as the knock-down of ALK and midkine decreased their proliferation[129].

Contributions of ALK in cancer

A chromosomal translocation involving the ALK locus was first described in Anaplastic Large Cell Lymphoma (ALCL), a rare non-Hodgkin lymphoma, by Morris *et al*. in 1994[143]. ALK was fused with the nucleophosmin (NPM) gene, forming a constitutively expressed protein NPM-ALK[143]. Since the discovery of its implication in ALCL, the ALK gene has been found in fusion products with a variety of partners (e.g. inflammatory myofibroblastic tumor, non-small-cell lung cancer, diffuse large B cells carcinoma), overexpressed in its wild-type form (e.g. retinoblastoma, rhabdomyosarcoma, melanoma, glioblastoma, Ewing's sarcoma), or selectively mutated in many other cancers (e.g. anaplastic thyroid cancer and NB)[144]. Most information regarding the downstream pathways of ALK come from the analysis of oncogenic fusion proteins, such as NPM-ALK[144]. Overall, ALK activates multiple pathways including PI3K-AKT, JAK-STAT, CRKL-C3G, and RAS/MAPK, which in turn induce differentiation, survival, proliferation, migration, and angiogenesis[144]. Recently phosphoproteomic analysis confirmed PI3K-AKT-FOXO3, CRKL-C3G, MEKK2/3-MEK5-ERK5, JAK-STAT, MAPK and RAS/JNK pathways as downstream signaling of ALK, following inhibition with ALK inhibitors crizotinib or lorlatinib in NB cell lines[145,146]. Moreover, various studies have reported *MYCN* as a transcriptional target of ALK activated full-length, via Pi3k/AKT, MEK1/2, or STAT3[147–149].

ALK acts as a hotspot for the translocation in a wide variety of loci, as reflected by the multiple fusion proteins that have been discovered in cancers[144]. The translocations lead to the generation of ALK fusion protein that dimerize to constitutively activate ALK signaling pathways. The aberrant ALK signaling is dictated by the fusion partner, and the tissue of expression, and the fusion protein involved will define the pathological

consequences[144]. While the amplification of the *ALK* locus and overexpression of the ALK protein has been reported in various types of cancers, the importance of its role in the initiation and progression of cancer remains unclear[144]. In NB, the amplification of ALK is associated with *MYCN* amplification, suggesting that they act concomitantly in NB progression[150]. ALK mutations directly affect ALK expressing tissues, leading to the perturbation of the physiological functions of the receptor and the constitutive activation of ALK downstream pathways[144,151]. This is the case for NB, where aberrant ALK mutations may perturb the SA system development and could initiate the tumor.

ALK and neuroblastoma

The expression of ALK in NB was first reported by Lamant *et al.* in 2000[152]. Various studies demonstrated that ALK is amplified in NB cell lines and tumor patient samples. A meta-analysis of 709 NB tumors reported ALK amplification in approximately 2% of NB[150]. They were almost exclusively associated with MYCN amplification and occurred in around 7% of *MYCN*-amplified primary tumors[150]. *ALK* gene gain was also detected in 91.8% of NB tumors with gain of chromosome 2p and was associated with MYCN gain[150]. Overall, gain of chromosome 2, including the ALK locus is correlated with increased ALK expression and is associated with poor survival[69,150].

ALK point-mutations and their implication in neuroblastoma

In 2008, several groups reported the presence of ALK mutations in both cases of familial and sporadic NB[68–71]. ALK-TKD point-mutations have been described in 6 to 12% of sporadic NB cases, with conserved loci[68–70,153]. Three major ‘hot-spots’, accounting for 85% of mutations, have been reported: R1275 (mutated to Q or L, 43%), F1174 (mutated to L, S, I, C or V, 30%) and F1245 (mutated to V or C, 12%) that are all ligand-independent oncogenic mutations[154]. The mutations ALK$^{-R1275Q}$, occurring in both familial and sporadic cases, and ALK$^{-F1174L}$, restricted to sporadic cases, are the most prevalent. The mutation F1174L is not found in familial NB, suggesting that it might be lethal during embryonic development. However, the mutations F1174L and F1245V have been reported as *de novo* germline mutations in a syndromic form of NB associating congenital tumors with a severe encephalopathy and brainstem

malformations in two patients[155]. In familial NB, three distinct germline mutations were identified: R1192P, G1128A and R1275Q, the latter being the most frequent[69,71].

ALK point mutations were identified in NB mainly in the TDK and can be classified into three classes[156]. The first class corresponds to gain-of-function ligand-independent mutations. Globally, these mutations occurring in the TDK are the most frequent in NB and lead to the constitutive activation of ALK downstream signaling pathways[144,151]. The second class is ligand-dependent mutations, such as D109IN, T1151M, and A1234T that are not constitutively active and require activation with ligand or agonist antibody[156]. Finally, the last class is kinase-dead mutations, which are inactive in their TKD and only involves the mutation I1250T which has been found in one patients[71,156]. In this case, the stimulation with agonist ALK antibodies fail to lead to the tyrosine phosphorylation, and the I1250T mutation is unable to activate downstream signaling or to mediate neurite outgrowth[157].

A meta-analysis of NB tumors reported $ALK^{-R1275Q}$ and $ALK^{-F1174L}$ mutations to be as present as prevalent in prognostically unfavorable as in favorable NB[150]. However, $ALK^{-F1174L}$ was observed in a higher frequency in *MYCN*-amplified tumors and displays a higher degree of autophosphorylation and carries transforming capacity[150,158]. Furthermore, patients with concomitantly amplified MYCN and mutated $ALK^{-F1174L}$ have significantly poorer outcomes[150,158,159]. NGS-sequencing analysis of clinical NB samples revealed the occurrence of subclonal events (defined as a mutated allele fraction below 20%) of the ALK mutations, highlighting that they are more frequent than what was shown previously[159]. Moreover, Sanger sequencing analysis reported the occurrence of ALK mutations at relapse[81]. Overall, subclonal ALK mutations may contribute to tumor evolution and relapse, suggesting that targeted therapy could be indispensable for a definitive cure[81,159].

Genomic rearrangement of ALK in neuroblastoma

The amplification of an abnormal ALK gene lacking exon 2 and 3 leading to the overexpression of a short-form of ALK protein (ALK^{del2-3}) has been reported in the NB1 cell line[160]. ALK^{del2-3}-transduced NIH/3T3 cells display increase colony-forming

capacity in soft agar and tumorigenicity in nude mice[160]. In the NB CLB-Bar cell line, a genomic rearrangement lead to the expression of a 170 kDa protein lacking part of the extracellular domain encoded by exon 4 to 11 (ALK^{D4-11}) and this is associated with an amplification of the ALK locus[161]. NIH/3T3 cells expressing ALK^{D4-11} show increased proliferation and colony-forming capacity compared to cells expressing ALK-wt. Moreover, the analysis of NB tumors revealed that the rearranged allele ALK^{D4-11} was observed only at relapse. In both cases, these truncated forms lead to an increased kinase activity of the ALK variants[160,161]. These studies show that genomic rearrangements are alternative mechanisms of the deregulation of the *ALK* gene in NB.

Studying the implication of ALK in NCCs and sympathoblasts

Since its discovery in NB, many studies have been conducted to study the impact of deregulated ALK signaling in the cells at the origin of the disease. NB arises from a subset of NCCs of the SA lineage, however, for now, it is not clearly defined if alterations of *ALK* occur in NCCs or more likely in differentiated progenitors that would already have acquired noradrenergic properties[117].

The forced *in vitro* expression of oncogenic drivers in NCCs or sympathetic progenitors has been studied by several groups. Olsen and colleagues reported that MYCN can induce NB when expressed in primary NCCs[162]. Indeed, the subcutaneous injection of NCCs transfected with MYCN leads to the generation of NB tumors that resemble their human counterparts[162]. In 2013, MYCN and $ALK^{-F1174L}$ were reported to be sufficient to drive NB from NCCs[163]. The subcutaneous injection of immortalized Joma1 NCCs overexpressing MYCN or $ALK^{-F1174L}$ led to the formation of NB-like tumors[163]. In another study, the expression of $ALK^{-R1275Q}$ and $ALK^{-F1174L}$ mutations, as well as ALK-wt, were reported to display oncogenic properties in NCCs[164]. The orthotopic injection of ALK-expressing MONC-1 and Joma1 NCCs, immortalized with v-Myc or tamoxifen-inducible $Myc\text{-}ER^{T}$, gave rise to various tumor types. The $ALK^{-F1174L}$ mutation had the strongest effects on tumor growth and generated undifferentiated tumors. This study provided the first demonstration that ALK-wt protein was sufficient to initiate the formation of aggressive tumors when overexpressed in NCCs, even in the absence of the oncogene MYCN[164].

Different results were obtained by the overexpression of ALK in sympathetic progenitors relative to the observations in NCCs. ALK mutations have been shown to affect sympathetic neuroblasts by increasing their proliferation in various studies. In a chick embryo model, the overexpression of the ALK$^{-F1174L}$ and ALK$^{-R1275Q}$ mutations, as well as of the ALK-wt protein leads to an increase of proliferation of primary sympathetic neurons[129]. Moreover, in cultured sympathetic neuroblasts, ALK$^{-F1174L}$ first induced an increased proliferation, but then led to an arrest of proliferation and an increased differentiation after long-term in culture[165]. This is in accordance with observation in the rat PC12 pheochromocytoma and the human SK-N-SH NB cell lines, where ALK-wt overexpression was reported to induce neurite differentiation[166,167].

Evaluation of the oncogenic potential of *ALK* in transgenic animal models

The implication of ALK in NB tumor initiation has been explored over the last years through various animal models by the direct overexpression of ALK in sympathetic precursors. The first report of the oncogenic potential of ALK in NB was made by the mice model developed by Heukamp et al. in 2012[168]. Transgenic mice expressing ALK$^{-F1174L}$ under the control of the β-actin promoter were crossed with DBHiCre and TH-IRES-Cre mice to restrict the expression of the ALK mutation in sympathetic neuroblasts. In this model, the expression of ALK$^{-F1174L}$ was sufficient to drive NB. However, the generation of tumors was of incomplete penetrance and long latency[168]. In the model developed by Berry et al. in 2012, the overexpression of the ALK$^{-F1174L}$ mutation in sympathetic precursors under the control of the TH-promoter was not sufficient to generate tumors in mice[169]. However, tumors appeared when ALK$^{-F1174L}$ were crossed with *TH-MYCN* mice. The coexpression of the two oncogenes leads to the development of tumors with an earlier onset, full penetrance, and enhanced lethality[169].

The Knock-In (KI) model developed by Janoueix-Lerosey and colleagues allowed an improved understanding of the role of ALK mutations in sympathetic development. In this system, the mutations ALK$^{-F1178L}$ and ALK^{-1279Q} (ALK$^{-F1174L}$ and ALK$^{-R1275Q}$ in human) are expressed under the control of the endogenous promoter[170]. The homozygous expression of ALK$^{-F1178L}$ in KI mice induces high neonatal lethality, suggesting that this mutation may not be compatible with survival in mice when

expressed above a critical threshold[123]. This is in agreement with the severe phenotype of patients carrying the *de novo* germline mutations[155]. Moreover, an increased size and an enhanced proliferation of neuroblasts were observed in SG of the *Alk* KI embryos, suggesting that ALK mutations act at early stages in disturbing neuroblastic proliferation[170]. While the *Alk* KI mice do not develop tumors, the generation of tumors occurs when the ALK$^{-F1178L}$ and ALK$^{-R1279Q}$ KI mice are crossed with the *TH-MYCN* mice. The tumor onset was of shorter latency in *TH-MYCN/ALK$^{-F1178L}$* mice relative to *TH-MYCN/ALK$^{-R1279Q}$* mice. Moreover, the tumors that were generated by crossing *Alk-mutant* KI with TH-MYCN mice displayed a more differentiated phenotype when compared to MYCN-only driven tumors[170]. Another KI model for the ALK$^{-R1275Q}$ mutation has been developed and shows that ALK$^{-R1275Q}$ leads to the generation of NB tumors in cooperation with MYCN and favors the metastatic dissemination by the perturbation of the extracellular matrix[171].

In zebrafish, the same results were obtained with the *dβh:ALKF1174L* model. Fish expressing ALK$^{-F1174L}$ under the control of the dβ*h* promoter did not develop tumors[172]. In contrast, the crossing of *dβh:ALKF1174L* with *dβh:EGFP-MYCN* led to the generation of NB tumors. The coexpression of *ALK* and *MYCN* tripled the disease penetrance and accelerated tumor onset relative to the fish expressing MYCN alone[172].

Targeting ALK in neuroblastoma

Several ALK inhibitors have been investigated *in vitro*, in mouse models of NB or in clinical trials. One of the mechanisms of action of these small molecules is the interference with the ATP binding to the TKD[111]. Only one year after the discovery of ALK mutations in 2008, early-phase clinical trials with crizotinib (XALKORI®, Pfizer) were initiated for patients with NB but unfortunately failed to show significant effects[173]. Crizotinib has also been reported to have limited effects on the F1174 mutations in NB cell lines[154]. Several others ALK inhibitors have been approved by the FDA and vary in their efficiency in NB pre-clinical models[158,174,175]. Moreover, these inhibitors have been evaluated in pre-clinical studies in combination with chemotherapy or downstream target agents such as PI3K and mTOR inhibitors[169,176–179]. Lorlatinib (PF-06463922, Pfizer) is part of the last generation of ALK/ROS1 inhibitors approved by the FDA in 2018[111]. Lorlatinib has the particularity to target the amplification of the wild-

type form and several ALK mutations including R1275Q and F1174L. Promising *in vitro* and *in vivo* results were obtained with lorlatinib, as it was reported to be more efficient than all other previously studied ALK inhibitors. *In vitro*, lorlatinib was reported to be 10-30 times more efficient than crizotinib, and, *in vivo*, lorlatinib induced a complete regression of crizotinib-resistance xenografts and PDXs NB tumors[180,181]. These encouraging results prompted the first pediatric phase I for lorlatinib in ALK-driven relapsed or refractory NB in 2017, as a single agent or in combination with topotecan and cyclophosphamide (Phase I/II-NANT, New Approaches to Neuroblastoma Therapy, NTC03107988).

AIM OF THE PROJECT

This thesis is articulated around two distinct projects. The first project was dedicated to study the involvement of ALK deregulated signaling in the differentiation of the SA lineage during embryonic development. Although ALK mutations have been identified as predisposing to NB and may constitute a “first hit” in NB genesis, their role in the differentiation of the SA lineage and in the initial steps of NB development remain unclear. Therefore, we investigated the implication of the ALK-F1174L mutation on the differentiation of NCCs committed to the SA lineage by analyzing the acquisition of sympathetic and noradrenergic markers in developing SGs during embryonic development. We aimed to improve the understanding of the implication of ALK deregulated signaling in the initial steps of the NB genesis.

The objective of the second project was to investigate the involvement of ALK-wt, ALK$^{-F1174L}$ and ALK$^{-R1275Q}$ activating mutations in the tumorigenesis and progression of NB. For this purpose, these ALK variants were stably expressed in NB cell lines and transduced cells were injected in immunocompromised mice. We then analyzed ALK impact on the tumor growth, the tumoral cell dissemination and on the transcriptomes of the primary tumors. The objective of this study was to identify new genes/signaling pathways activated *in vivo* by ALK-wt, ALK$^{-F1174L}$ and ALK$^{-R1275Q}$ activating mutations.

RESULTS

PART I

Publication

Expression of the Neuroblastoma-Associated ALK-F1174L Activating Mutation During Embryogenesis Impairs the Differentiation of Neural Crest Progenitors in Sympathetic Ganglia

ALK mutations have been identified as predisposing to NB and may constitute a "first hit" in NB genesis. The impact of ALK signaling in sympathetic neurogenesis has been investigated in several *in vitro* and *in vivo* models and shed light on a potential role of ALK deregulated signaling in disturbing the balance between proliferation and differentiation of sympathetic precursors[129,164,165,170]. Previous analyses of the ALK^{-F1178} and ALK$^{-R1279Q}$ KI mice reported an enlargement of sympathetic ganglia (SG) at birth and in adults, due to an enhanced proliferation of neuroblasts[170]. Moreover, a published study from our laboratory suggested that ALK activating mutations may impair the differentiation capacity of NCCs[164]. However, the role of ALK activating mutations in the differentiation of the SA lineage and in the initial step of NB development remain unclear.

Therefore, the objective of this study was to investigate the involvement of the ALK-F1174L activating mutation in the differentiation of NCCs committed to the SA lineage during embryonic development. Transgenic mice carrying a conditional ALK-F1174L allele were crossed with Sox10-Cre mice, restricting its expression to migrating NCCs. We studied the impact of the ALK-F1174L mutation on SG formation and neuroblast differentiation during early embryonic stages by analyzing the expression of TFs that control the development of the SA lineage. Embryos from embryonic stages (E) 9.5 to 14.5 were obtained. *Sox10-Cre;LSL-ALK-F1174L* displayed an embryonic lethality from E12.5 with impaired hematopoietic development. Moreover, the ALK-F1174L mutation affected SG formation. First, we observed an enlargement of SG with perturbed architecture and cellular disorganization at E10.5 and E11.5. Secondly,

Sox10-Cre;LSL-ALK-F1174L mutant SG were mainly undifferentiated, with a large increased of Sox10^{+} cells at both E10.5 and E11.5. Third, ALK-F1174L impaired noradrenergic differentiation as almost no TH was detected in mutant SG. Fourth, the neuronal differentiation was also affected by ALK-F1174L expression as highlighted by the reduced upregulation of the pan-neuronal marker βIII-tubulin in *Sox10-Cre;LSL-ALK-F1174L* SG. Furthermore, at E10.5, ALK-F1174L mediated an increased proliferation of Phox2b^{+} progenitors in *Sox10-Cre;LSL-ALK-F1174L* SG relative to WT, reflecting an inhibition of the transient cell-cycle withdrawal displayed by sympathetic neuroblasts at this stage. In addition, we analyzed ALK endogenous expression pattern by *in situ* hybridization via the RNAscope® assay (ACD) in Phox2b^{+} progenitors to precisely determine the onset of ALK expression in neuroblasts of the developing sympathetic nervous system. ALK mRNA was previously detected starting from E12.5 in the sympathetic chain[121]. Interestingly, while ALK was undetectable in Phox2b^{+} cells at E9.5, we observed ALK mRNA expression starting from E10.5 in the sympathetic trunk of WT embryos. Altogether, we report for the first time that the expression of the ALK-F1174L mutation in NCCs during embryonic development profoundly disturbs early sympathetic progenitor differentiation, in addition to increasing their proliferation, both mechanisms being potential crucial events in NB oncogenesis.

frontiers in Oncology

ORIGINAL RESEARCH
published: 16 April 2019
doi: 10.3389/fonc.2019.00275

Expression of the Neuroblastoma-Associated ALK-F1174L Activating Mutation During Embryogenesis Impairs the Differentiation of Neural Crest Progenitors in Sympathetic Ganglia

Lucie Vivancos Stalin[1], *Marco Gualandi*[2], *Johannes Hubertus Schulte*[3,4,5], *Raffaele Renella*[1], *Olga Shakhova*[2] *and Annick Mühlethaler-Mottet*[1]*

[1] Pediatric Hematology-Oncology Research Laboratory, DFME, University Hospital of Lausanne, CHUV-UNIL, Lausanne, Switzerland, [2] Translational Oncology, Department of Hematology and Oncology, University Hospital Zürich, Zurich, Switzerland, [3] Department of Pediatric Hematology, Oncology and SCT, Charité—Universitätsmedizin Berlin, Corporate Member of Freie Universität Berlin, Humboldt-Universität zu Berlin, and Berlin Institute of Health, Berlin, Germany, [4] Berlin Institute of Health, Berlin, Germany, [5] German Cancer Consortium, Partner Site Berlin and German Cancer Research Center, Heidelberg, Germany

OPEN ACCESS

Edited by:
Sabine Wislet,
University of Liège, Belgium

Reviewed by:
Aldo Pagano,
University of Genoa, Italy
Stavros Taraviras,
University of Patras, Greece

***Correspondence:**
Annick Mühlethaler-Mottet
annick.muhlethaler@chuv.ch

Specialty section:
This article was submitted to Molecular and Cellular Oncology, a section of the journal Frontiers in Oncology

Received: 31 October 2018
Accepted: 25 March 2019
Published: 16 April 2019

Citation:
Vivancos Stalin L, Gualandi M, Schulte JH, Renella R, Shakhova O and Mühlethaler-Mottet A (2019) Expression of the Neuroblastoma-Associated ALK-F1174L Activating Mutation During Embryogenesis Impairs the Differentiation of Neural Crest Progenitors in Sympathetic Ganglia. Front. Oncol. 9:275. doi: 10.3389/fonc.2019.00275

Neuroblastoma (NB) is an embryonal malignancy derived from the abnormal differentiation of the sympathetic nervous system. The Anaplastic Lymphoma Kinase (*ALK*) gene is frequently altered in NB, through copy number alterations and activating mutations, and represents a predisposition in NB-genesis when mutated. Our previously published data suggested that ALK activating mutations may impair the differentiation potential of neural crest (NC) progenitor cells. Here, we demonstrated that the expression of the endogenous *ALK* gene starts at E10.5 in the developing sympathetic ganglia (SG). To decipher the impact of deregulated ALK signaling during embryogenesis on the formation and differentiation of sympathetic neuroblasts, *Sox10-Cre;LSL-ALK-F1174L* embryos were produced to restrict the expression of the human ALK-F1174L transgene to migrating NC cells (NCCs). First, ALK-F1174L mediated an embryonic lethality at mid-gestation and an enlargement of SG with a disorganized architecture in *Sox10-Cre;LSL-ALK-F1174L* embryos at E10.5 and E11.5. Second, early sympathetic differentiation was severely impaired in *Sox10-Cre;LSL-ALK-F1174L* embryos. Indeed, their SG displayed a marked increase in the proportion of NCCs and a decrease of sympathetic neuroblasts at both embryonic stages. Third, neuronal and noradrenergic differentiations were blocked in *Sox10-Cre;LSL-ALK-F1174L* SG, as a reduced proportion of Phox2b$^+$ sympathoblasts expressed βIII-tubulin and almost none were Tyrosine Hydroxylase (TH) positive. Finally, at E10.5, ALK-F1174L mediated an important increase in the proliferation of Phox2b$^+$ progenitors, affecting the transient cell cycle exit observed in

normal SG at this embryonic stage. Altogether, we report for the first time that the expression of the human ALK-F1174L mutation in NCCs during embryonic development profoundly disturbs early sympathetic progenitor differentiation, in addition to increasing their proliferation, both mechanisms being potential crucial events in NB oncogenesis.

Keywords: ALK, neuroblastoma, differentiation, sympathetic ganglia, neural crest cells, SOX10, PHOX2B, mouse embryos

INTRODUCTION

Neuroblastoma (NB) is a pediatric malignancy of the sympathetic nervous system (SNS) which may arise in the adrenal medulla (47%) or along the entire sympathetic chain (53%) (1, 2). NB is considered to originate from a subset of neural crest cells (NCCs) committed to the sympathoadrenal (SA) lineage (3). However, recent studies described Schwann cell precursors (SCP) as a new cellular origin for the adrenal medulla, highlighting an additional cellular origin for adrenal NB (4).

NCCs are a transient and multipotent cell population of the developing embryos. During embryogenesis NCCs undergo epithelial-mesenchymal transition, and migrates toward their final destination where they differentiate into various cell types (5). The transcription factor (TF) Sox10 is expressed from ∼E9 in trunk migrating NCCs where it mediates their survival, aids in the maintenance of multipotency and inhibits neuronal differentiation (6). NCCs of the sympathetic lineage follow a ventrolateral path to reach the vicinity of the dorsal aorta where bone morphogenetic proteins (BMPs) induce sympathetic neuron differentiation (5). This involves the expression of various TFs, including Paired-like homeobox 2a/b (Phox2a/b), Achaete-scute family BHLH transcription factor 1 (Ascl1), Insulinoma-associated 1 (Insm1), heart and neural crest derivatives expressed protein 2 (Hand2), and gata binding protein 3 (Gata3), acting as a network controlling the differentiation and specification of the NCCs into noradrenergic neurons (7). Early steps of noradrenergic differentiation are characterized by the upregulation of the enzymes tyrosine hydroxylase (TH) and dopamine β-hydroxylase (DBH), both involved in catecholamine biosynthesis, as well as other neuronal markers, including βIII-tubulin. The absence of even a single member of the TF network can lead to deregulation in sympathetic neuroblast proliferation, survival and/or noradrenergic differentiation (7).

NB is considered to constitute an embryonal tumor according to its tissue of origin, its early onset in childhood, and its ability to spontaneously regress. NB tumorigenesis is thought to be initiated *in utero* as an embryonal precancerous condition, and to arise through proliferation of sympathetic neuroblasts having escaped to apoptotic signals and to noradrenergic specification (8). For now, the specific mechanisms initiating NB are still largely unknown. Mutations or deregulations of key regulators of the sympathoadrenergic (SA) lineage may represent potential initial events for NB development, and MYCN, PHOX2B and ALK have previously been identified as potential first hits (8, 9).

The Anaplastic Lymphoma Kinase *(ALK)* gene is frequently altered in sporadic NB through amplification, copy number gain, overexpression, and mutations, and it has been defined as a predominant driver of familial NB (10, 11). The *ALK* gene encodes a receptor tyrosine kinase with an expression restricted to the central and peripheral nervous system (12–14). Point-mutations in its tyrosine kinase domain (TKD) have been reported in 8% of sporadic NB cases, with three major "hot-spots" mutations at position R1275, F1174, and F1245 (15–19). ALK-R1275Q, occurring in both familial and sporadic cases, and ALK-F1174L, restricted to sporadic cases, are reportedly the most potent activating mutations (19).

The expression of ALK-wt, ALK-F1174L, or ALK-R1275Q in NC progenitors or in sympathetic neuroblasts is not sufficient to drive NB tumor formation in absence of MYCN or other NB prototypical genetic alterations (20–23). However, ALK-F1174L and ALK-R1275Q have been described to strongly potentiate MYCN-mediated NB tumorigenesis in transgenic and knock-in (KI) animal models, highlighting their cooperation in sympathetic neuroblast progenitors and confirming their roles as possible initial events in NB initiation (20, 21, 23–25).

The precise role of ALK activating mutations during the initial stages of NB development remains unclear. However, the impact of ALK signaling in sympathetic neurogenesis has been investigated in several *in vitro* and *in vivo* models. ALK knockdown (shRNA) and its pharmacological inhibition (i.e., by TAE-684) were both associated with a decrease in the proliferation of chick sympathetic neuroblasts, while overexpression of ALK-wt or the ALK-F1174L or ALK-R1275Q variants increased their proliferation (26). In addition, ALK-F1174L induced a transient increase in the proliferation of chick primary sympathetic neuroblasts, followed by their differentiation after prolonged culture (27). Furthermore, an increased SG size was observed from embryonic to adult stages in $ALK^{-F1178L}$ KI mice, associated with an enhanced proliferation of sympathetic neuroblasts and a prolonged duration of neurogenesis (23). However, in a recent study, we demonstrated that ALK-F1174L expression in the murine NC progenitor MONC-1 cell line generated undifferentiated tumors upon orthotopic implantation in nude mice. In contrast, MONC-1 parental cells gave rise to NB or osteochondrosarcoma, suggesting that ALK activating mutations may impair the differentiation capacity of NCCs (22).

In this study, we investigated the impact of the human ALK-F1174L mutation *in vivo* on sympathetic neuroblast differentiation using *Sox10-Cre;LSL-ALK-F1174L* mice. The aim was to improve our understanding of the implication of ALK deregulated signaling in the initial steps of NB genesis.

RESULTS

ALK-F1174L Causes Embryonic Lethality When Expressed in NCCs Prior to SA Lineage Commitment

To assess the impact of the human ALK-F1174L activating mutation on the development and differentiation of the SNS, *Sox10-Cre;LSL-ALK-F1174L* embryos were generated. This model allowed to restrict the expression of the ALK-F1174L variant to migrating $Sox10^+$ cells before sympathetic lineage commitment. We observed that such lineage-specific expression of ALK-F1174L mediated an embryonic lethality in 100% of E12.5 *Sox10-Cre;LSL-ALK-F1174L* embryos ($n = 4$) (**Figure 1**). A similar phenotype was also observed in 1/8 and 1/3 *Sox10-Cre;LSL-ALK-F1174L* embryos at E10.5 and E11.5, respectively (data not shown).

Endogenous ALK mRNA Is Detectable in Sympathetic Ganglia Starting at Stage E10.5

ALK is widely expressed in the developing nervous system. A previous report described the detection of ALK mRNA and protein in murine SG starting at E12.5 and E13.5 respectively (12). Here, we took advantage of a recently developed and highly sensitive *in situ* Hybridization (ISH) method, the RNAscope® assay (Advanced Cell Diagnostics, Inc), to precisely define the onset of ALK mRNA expression in the developing sympathetic chain of *WT* embryos. We observed ALK specific signals starting as early as E10.5 in the sympathetic trunk, while ALK mRNA was undetectable in migratory NCCs at E9.5 (**Figure 2**). Thus, in our *Sox10-Cre;LSL-ALK-F1174L* model the expression of the ALK-F1174L variant precedes the expression of the endogenous form by nearly 1.5 day.

ALK-F1174L Affects Sympathetic Ganglia Formation and Early Sympathetic Progenitors Differentiation

Due to the early embryonic lethality, we focused our analysis of the impact of ALK-F1174L expression in NCCs on the development and differentiation of the sympathetic chain, as the initial structure of the adrenal medulla appears at E12.5. During sympathetic lineage specification around E9.5, migrating $Sox10^+/Phox2b^-$ NCCs transform into progenitors co-expressing Sox10 and Phox2b, and then the majority of SG cells switch to $Sox10^-/Phox2b^+$ immature sympathetic neuroblasts (7). While Sox10 expression is rapidly lost during neuronal differentiation, it is maintained in a minority of cells where it induces glial cell fate specification and differentiation (28, 29).

By IF co-staining for Sox10 and Phox2b, we first observed an elevated number of $Sox10^+$ cells in *Sox10-Cre;LSL-ALK-F1174L* embryos at E9.5 and E10.5 (**Figure 3A**). $Sox10^+$ NCCs still migrate ventro-laterally in *Sox10-Cre;LSL-ALK-F1174L* embryos. However, an abnormal number of cells were found in the dorsal root ganglia and in the region lateral to the dorsal aorta, where the ventral root and the sympathetic trunk formed indistinct structures. The expression pattern of the human ALK-F1174L transgene was similar to that of Sox10 in *Sox10-Cre;LSL-ALK-F1174L* embryos at E10.5 (**Supplementary Figure 1**). For further experiments, we focused our analyses at E10.5 and E11.5, as NCCs are still migrating toward the dorsal aorta at E9.5. We observed an alteration in the formation of the sympathetic chain in *Sox10-Cre;LSL-ALK-F1174L* embryos with an important increase in SG section areas at E10.5 and E11.5, by 3.3 and 2.2-fold, respectively, relatively to *WT* embryos (**Figures 3B,C**, upper panel). This observation was confirmed by an increased number of cells per SG section measured in *Sox10-Cre;LSL-ALK-F1174L* embryos relative to *WT* at both embryonic stages (**Figure 3C**, lower panel). Moreover, *Sox10-Cre;LSL-ALK-F1174L* SG displayed a pattern of disorganized architecture. Indeed, $Sox10^+$ cells were found localized in the entire section of the ganglion at E11.5, while they were confined to the periphery in *WT* embryos (represented by arrows, **Figure 3B**), as previously described (28, 30).

Subsequently, we investigated the impact of the ALKF-1174L mutation on the transition from NCCs to sympathetic neuroblasts. We assessed the proportions of $Sox10^+/Phox2b^-$, $Sox10^+/Phox2b^+$, and $Sox10^-/Phox2b^+$ cells in SG sections co-stained for Sox10 and Phox2b. At E10.5, the percentage of $Sox10^+/Phox2b^-$ cells was markedly increased in *Sox10-Cre;LSL-ALK-F1174L* relative to *WT* SG (32.4 vs. 4.4%), while the proportions of $Sox10^+/Phox2b^+$ (38.2 vs. 52.5%) and $Sox10^-/Phox2b^+$ cells (29.4 vs. 43.1%) were significantly decreased (**Figure 4A**, upper panel). At E11.5, the fractions of $Sox10^+/$ $Phox2b^-$ and $Sox10^+/$ $Phox2b^+$ cells were increased in *Sox10-Cre;LSL-ALK-F1174L* embryos relative to *WT* (32.5 vs. 10.4% and 29.9 vs. 5.2%, respectively), while the sympathetic neuroblast population was decreased (37.6 vs. 84.4%) (**Figure 4A**, lower panel). At E11.5, in *WT* embryos, as expected the majority of sympathetic progenitors (84.4%) had lost the expression of Sox10, while $Sox10^+/Phox2b^-$ and $Sox10^+/Phox2b^+$ cells represented 10.4 and 5.2%, respectively (**Figures 4B,C**, upper panels). In contrast, in *Sox10-Cre;LSL-ALK-F1174L* SG, no significant variations in the proportions of those three cell populations were observed between the two embryonic stages (**Figures 4B,C**, lower panels). Our results thus demonstrate that the ALK-F1174L mutation plays a decisive role in impairing the initial sympathetic differentiation by affecting the transition from NCCs to sympathetic neuroblasts.

ALK-F1174L Impairs Noradrenergic Differentiation of Sympathetic Progenitors

To further assess the impact of the ALK-F1174L mutation on the noradrenergic differentiation of sympathetic progenitors, the expression of the early noradrenergic marker tyrosine hydroxylase (TH) was analyzed by co-staining with Phox2b. We quantified the fraction of TH^+ cells over the total $Phox2b^+$ cells, and we observed that TH was expressed in only rare cells in *Sox10-Cre;LSL-ALK-F1174L* SG at both E10.5 and E11.5 (**Figure 5A**). At E10.5, we detected only 10.1% of $TH^+/Phox2b^+$ neuroblasts in *Sox10-Cre;LSL-ALK-F1174L*

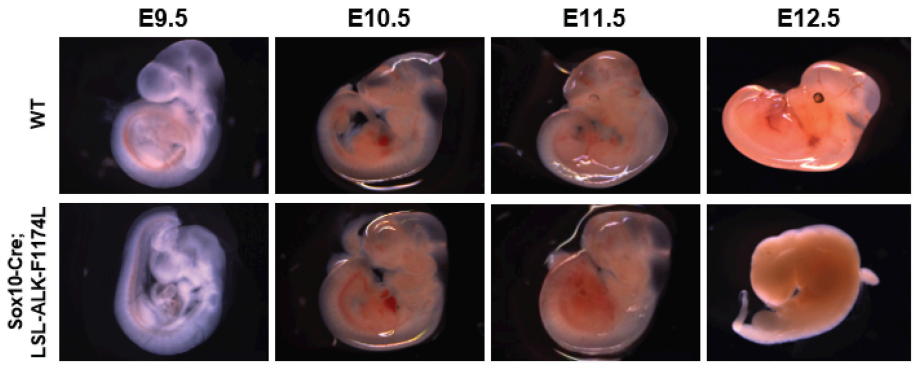

FIGURE 1 | ALK-F1174L expression in Sox10$^+$ cells NCCs mediates an embryonic lethality. Representative images of both *WT* and *Sox10-Cre;LSL-ALK-F1174L* embryo phenotypes for stages from E9.5 to E12.5. Embryos were genotyped by PCR as described in the Material and Method section.

SG, when compared to *WT* SG (43.8%) (**Figure 5B**). At stage E11.5, the fraction of TH$^+$ cells increased in *WT* SG relative to E10.5, reaching 85.3% of Phox2b$^+$ cells (**Figures 5B,C**, left panel). In contrast, in *Sox10-Cre;LSL-ALK-F1174L* SG, the proportion of TH$^+$/Phox2b$^+$ cells remained weak (11.8%) and equivalent to E10.5 (**Figures 5B,C**, right panel).

We investigated whether the rare TH-positive cells observed in *Sox10-Cre;LSL-ALK-F1174L* SG may result from NCCs that failed to effectively express the ALK-F1174L transgene. Therefore, *ALK-F1174L* embryos (E10.5) were labeled by IF staining to detect the human ALK (h-ALK) protein (**Figure 5D**). Surprisingly, 76.5% of TH$^+$ cells were negative for h-ALK in the analyzed sections. This demonstrates that TH expression resulted from the lack of Cre-loxP-mediated recombination in NCCs and that TH was also drastically repressed in ALK-F1174L expressing sympathetic neuroblasts. These results indicate that the ALK-F1174L mutation plays a crucial role in blocking sympathetic neuroblasts differentiation and inhibiting noradrenergic differentiation of sympathetic progenitors at early developmental stages.

Noradrenergic differentiation is controlled by a TF network, comprising at the top of the cascade Phox2b and Ascl1, and immediately downstream Insm1 (7). To further understand the mechanisms mediating the blockage of noradrenergic differentiation observed in *Sox10-Cre;LSL-ALK-F1174L* embryos, we evaluated Ascl1 and Insm1 expression in SG at E10.5 by ISH. Specific Ascl1 and Insm1 signals were mainly localized within Phox2b$^+$ cells in *WT* and *Sox10-Cre;LSL-ALK-F1174L* SG (**Supplementary Figure 2**). However, we observed a reduction in the number of ISH signals for both Ascl1 and Insm1 when reported to the SG section area in *Sox10-Cre;LSL-ALK-F1174L* SG relative to *WT* (**Supplementary Figure 2**). The decreased expression of both TF in SG may result from the incomplete sympathetic differentiation observed in *Sox10-Cre;LSL-ALK-F1174L* SG characterized by the reduced proportion of Phox2b$^+$ cells. However, it may not explain the lack of noradrenergic differentiation mediated by the ALK-F1174L mutation.

ALK-F1174L Affects Neuronal Differentiation

We then assessed whether the ALK-F1174L mutation might also perturb the physiological acquisition of neuronal marker by double IF staining for Phox2b associated to the early pan-neural marker βIII-tubulin. The expression of the neuronal marker βIII-tubulin appears rapidly after Phox2b upregulation at E10.5 and was described both in Sox10$^+$/Phox2b$^+$ and Sox10$^-$/Phox2b$^+$ sympathetic progenitors (29). We quantified the fraction of βIII-tubulin$^+$ cells over the total Phox2b$^+$ cell population. The proportions of βIII-tubulin$^+$ cells were reduced in *Sox10-Cre;LSL-ALK-F1174L* SG relative to *WT* SG at E10.5 (36.1 vs. 64.3%) and E11.5 (35.1 vs. 81.8%) (**Figures 6A,B**). Moreover, similarly to the acquisition of sympathetic and noradrenergic markers, no statistically significant changes were observed between E10.5 and E11.5 in *Sox10-Cre;LSL-ALK-F1174L* SG (36.1 and 35.1%, respectively) (**Figures 6B,C**, right panel), while the proportion of βIII-tubulin$^+$ cells increased in *WT* SG (64.3–81.8%, respectively) (**Figures 6B,C**, left panel).

At E11.5, the proportion of the Phox2b$^+$ cell population represented 89.6% in *WT* SG versus 67.5% in *Sox10-Cre;LSL-ALK-F1174L* SG (**Figure 4C**), corresponding to a 1.33-fold reduction. However, the proportion of βIII-tubulin$^+$ cells at E11.5 dropped from 81.8 to 35.1% between *WT* and *Sox10-Cre;LSL-ALK-F1174L* SG, corresponding to a 2.3-fold reduction (**Figure 6C**). This suggests that the reduced expression of neuronal marker did not only result from the incomplete sympathetic differentiation, but also from a direct impact of ALK-F1174L on the regulation of neuronal differentiation. These data indicate that the ALK-F1174L mutation impairs the expression of the early neuronal marker βIII-tubulin, although its impact is minor than on TH expression.

ALK-F1174L Increases the Proliferation of Undifferentiated Sympathetic Progenitors in Sympathetic Ganglia

The abnormally increased SG size observed in *Sox10-Cre;LSL-ALK-F1174L* embryos could be explained by an increased proliferation of NCCs and/or sympathetic progenitors. To verify

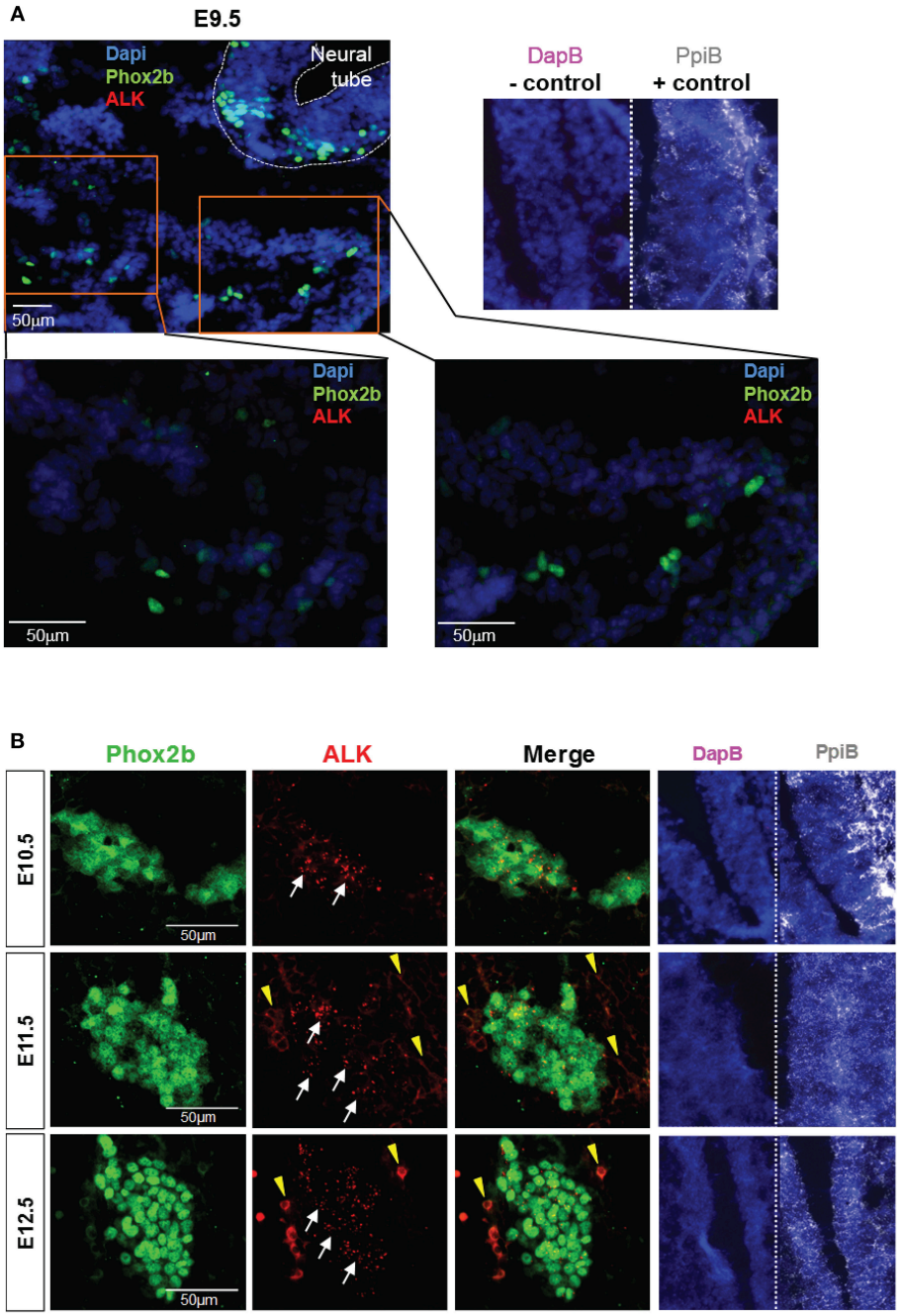

FIGURE 2 | ALK mRNA is expressed from E10.5 in SG. Analysis of endogenous ALK mRNA expression in *WT* embryos. **(A)** Representative pictures of ALK ISH (red) staining of *WT* embryos at E9.5 (magnifications: x20 for top panel and x40 for lower panels). **(B)** Representative pictures of ALK ISH (red) staining in *WT* SG from E10.5 to E12.5 (×40 magnification). **(A,B)** Phox2b IF (green) staining was applied after ISH to highlight migrating sympathoblasts and SG. Specific ALK ISH signals (red, small dots) are identified by white arrows, and non-specific signals (diffuse cytoplasmic or membranous staining) by yellow arrowheads. Numbers of embryos analyzed: E9.5 $n = 3$, E10.5 $n = 4$, E11.5 $n = 3$, and E12.5 $n = 2$. Representative images of ISH with the positive control probe Mm-Ppib (white), showing mRNA integrity of the embryo sections, and the negative control DapB (pink), showing absence of the background due to molecule trapping in the tissue, are also displayed for each embryonic stages with Dapi staining (blue).

this hypothesis, we analyzed the proportion of proliferating Phox2b$^+$ cells in *WT* and *Sox10-Cre;LSL-ALK-F1174L* SG by Phox2b and Ki67 co-staining. Results showed that the proportion of Ki67$^+$ cells over total Phox2b$^+$ progenitors was significantly increased in *Sox10-Cre;LSL-ALK-F1174L* SG compared to *WT* SG (mean of 80 vs. 29.2%) at E10.5 (**Figures 7A,B**). At E11.5, the proportion of proliferating Phox2b$^+$ cells, mainly composed of sympathetic neuroblasts, increased in *WT* SG (82.2%) reaching

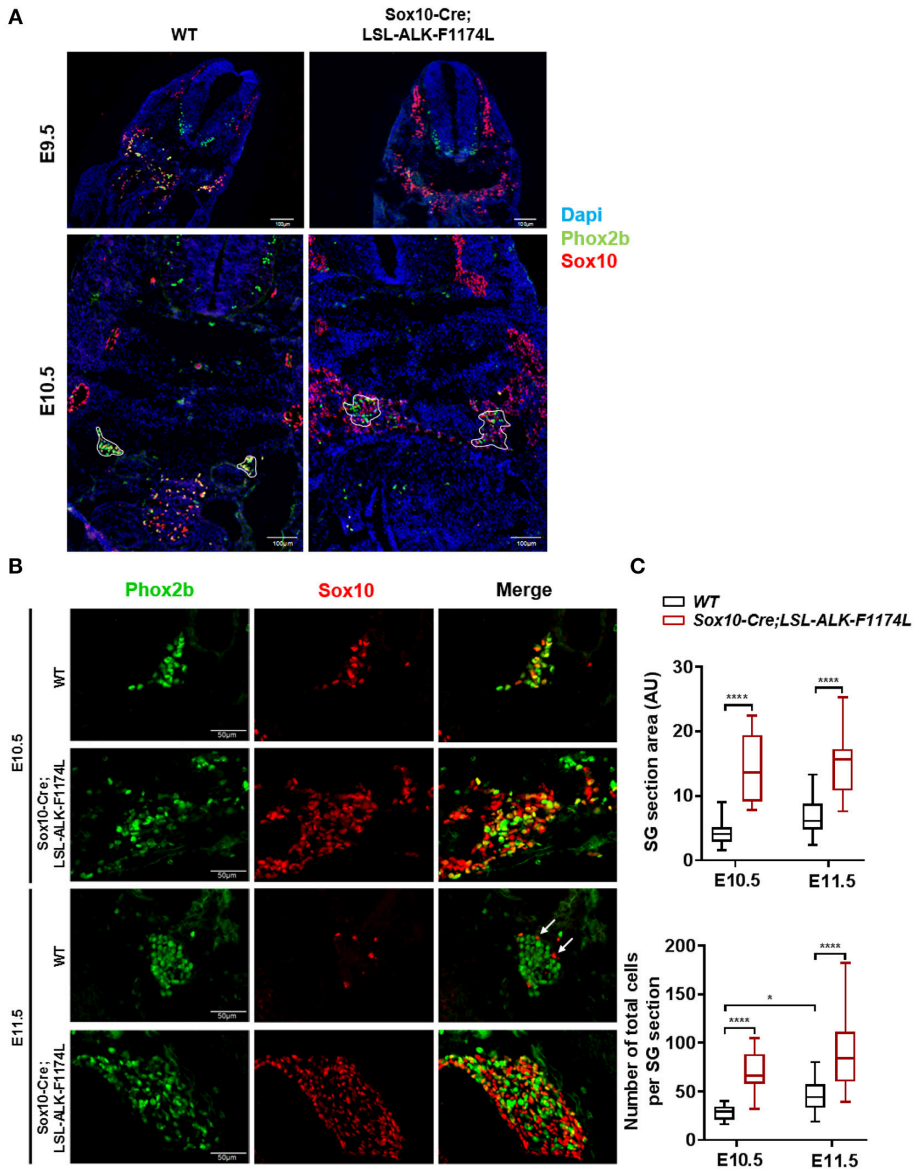

FIGURE 3 | Increased SG size in *Sox10-Cre;LSL-ALK-F1174L* embryos. **(A)** Representative images of *WT* and *Sox10-Cre;LSL-ALK-F1174L* embryo sections stained for Sox10 (red) and Phox2b (green), with DAPI (blue) at E9.5 and E10.5 (x10 magnification). SG are surrounded by white circle. **(B)** Representative images of SG IF staining for Sox10 (red) and Phox2b (green) (x40 magnification). **(C)** Box-plot of SG section areas in arbitrary units (AU) (upper panel) and of the total numbers of cells per SG section (lower panel) at E10.5 and E11.5 in *WT* and *Sox10-Cre;LSL-ALK-F1174L* embryos (One-way Anova multiple comparison, $^{****}p < 0.0001$, $^{*}p = 0.0306$, not significant (ns) comparisons are not shown). Numbers of SG sections analyzed at E10.5 and E11.5, respectively: *WT* $n = 22$ and $n = 23$, *Sox10-Cre;LSL-ALK-F1174L* $n = 14$ and $n = 16$.

the proportions observed in *Sox10-Cre;LSL-ALK-F1174L* SG at both E10.5 and E11.5 (**Figures 7A,B**). These results indicate that ALK-F1174L expressing neuroblasts at E10.5 display an markedly high proliferation rate.

DISCUSSION

NB is thought to derive from aberrant NC development during embryogenesis. ALK mutations have been identified as predisposing to NB and may constitute a "first hit" in NB genesis. Here we studied the involvement of deregulated ALK signaling on sympathetic ganglia formation and neuroblast differentiation during early embryonic development.

In our *Sox10-Cre;LSL-ALK-F1174L* mouse model, as ALK-F1174L transgene expression was not restricted to the SA lineage-committed NCCs, the embryonic lethality may result from ALK-F1174L-mediated effects on $Sox10^{+}$ migrating NCCs and their progeny. Alternatively, it could be caused by the absence of TH expression, as norepinephrine deficiency has been described to mediate embryonic death at mid-gestation (31–33).

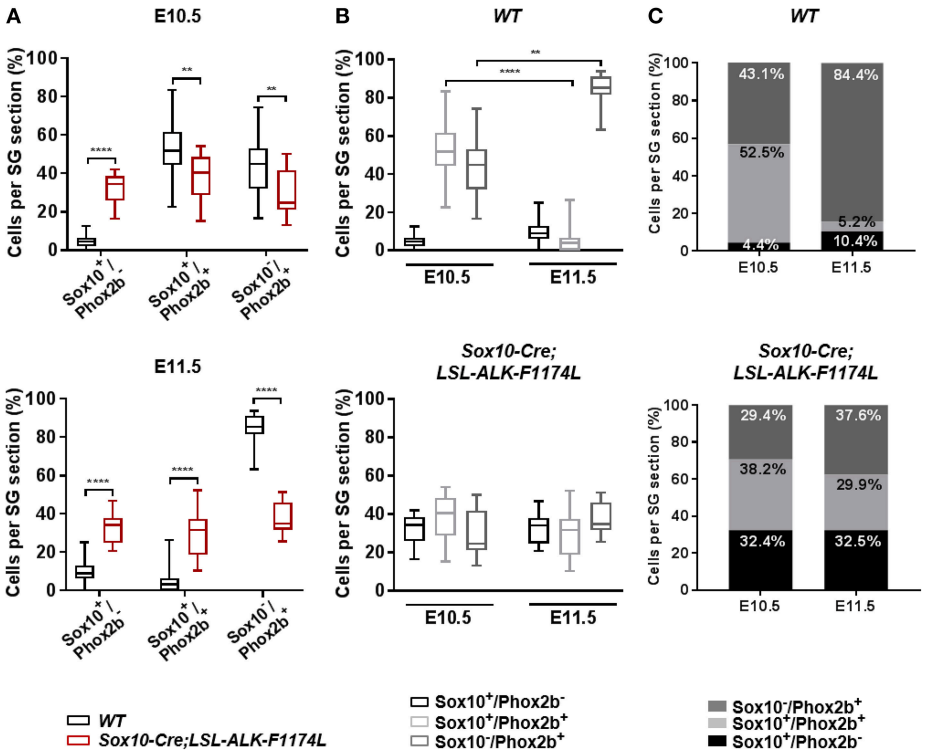

FIGURE 4 | ALK-F1174L affects the differentiation of sympathetic progenitors. **(A)** The fractions of Sox10$^+$/Phox2b$^-$, Sox10$^+$/Phox2b$^+$, and Sox10$^-$/Phox2b$^+$ cell populations in *WT* and *Sox10-Cre;LSL-ALK-F1174L* embryos at E10.5 (top) and E11.5 (bottom) are shown in Box-plots (Mann Whitney test or unpaired *t*-test depending on data distributions, $^{****}p < 0.0001$, $^{**}p < 0.01$). **(B)** The evolution from E10.5 to E11.5 of the three cell populations in *WT* (top) and *Sox10-Cre;LSL-ALK-F1174L* (bottom) embryos are illustrated in Box-plots (Krukal-Wallis and One-way Anova respectively, paired comparisons, $^{****}p < 0.0001$, $^{**}p = 0.0043$, ns comparisons are not shown). Numbers of SG sections analyzed at E10.5 and E11.5, respectively: *WT* $n = 22$ and $n = 23$, *Sox10-Cre;LSL-ALK-F1174L* $n = 14$ and $n = 16$. **(C)** The mean percentages of each cell population are plotted in grouped representations at E10.5 and E11.5 for *WT* (top) and *Sox10-Cre;LSL-ALK-F1174L* (bottom) embryos.

ALK deregulated signaling in *Sox10-Cre;LSL-ALK-F1174L* embryos did not impair the migration of NCCs as Sox10$^+$ cells were still able to migrate ventrolaterally. Nonetheless, the abnormal number of cells observed in the ventral roots and regions lateral to the dorsal aorta, at E9.5 and in particular at E10.5 strongly suggest that ALK-F1174L elicits an abnormal proliferation of the Sox10$^+$ NCCs at early embryonic stages.

In *WT* embryos, the proportionality of the three cell populations were in line with previously published data, reflecting a physiological sympathetic differentiation (7, 29, 34). In contrast, ALK-F1174L caused a transitional block in NCCs as the sympathetic specification was only incompletely initiated, and a large proportion of Sox10$^+$/Phox2b$^-$ NCCs remained present both at E10.5 and E11.5. This observation may result from an ALK-F1174L-mediated inhibition of NCCs responsiveness to BMPs signaling. Alternatively, as an abnormal number of Sox10$^+$ NCCs reached the vicinity of the dorsal aorta in *Sox10-Cre;LSL-ALK-F1174L* embryos, the amount of BMPs may not be sufficient to stimulate the integrality of these NCCs. Moreover, a complex reciprocal and dose-dependent inhibition loop between Sox10 and Phox2b is involved in sympathetic ganglia differentiation: at higher levels, Sox10 inhibits Phox2b expression, while at lower levels it is required for the initial upregulation of Phox2b (35). In addition, Phox2b negatively controls Sox10 expression (30, 36) but has also been shown to upregulate its own expression (37). In our model, the maintenance of Sox10 expression in *Sox10-Cre;LSL-ALK-F1174L* SG suggests that ALK-F1174L may affect the regulatory loop between Sox10 and Phox2b.

Furthermore, we observed a decrease in cells expressing βIII-tubulin, reflecting the incomplete acquisition of neuronal properties in *Sox10-Cre;LSL-ALK-F1174L* SG. This effect was not only due to the reduced proportion of sympathetic neuroblasts but also involved a direct ALK-F1174L-mediated inhibition of neuronal differentiation. Importantly, we highlight an important block in the acquisition of the noradrenergic marker TH in *Sox10-Cre;LSL-ALK-F1174L* SG. This indicates that even cells responding to BMPs signaling were unable to acquire noradrenergic features. Further experiments are necessary to elucidate the specific molecular mechanisms driving these observations, but one hypothesis would be that ALK-F1174L dysregulates the TF network essential for the initiation of noradrenergic differentiation. However, our data suggest that Ascl1 and Insm1 may not be involved as these TF were globally

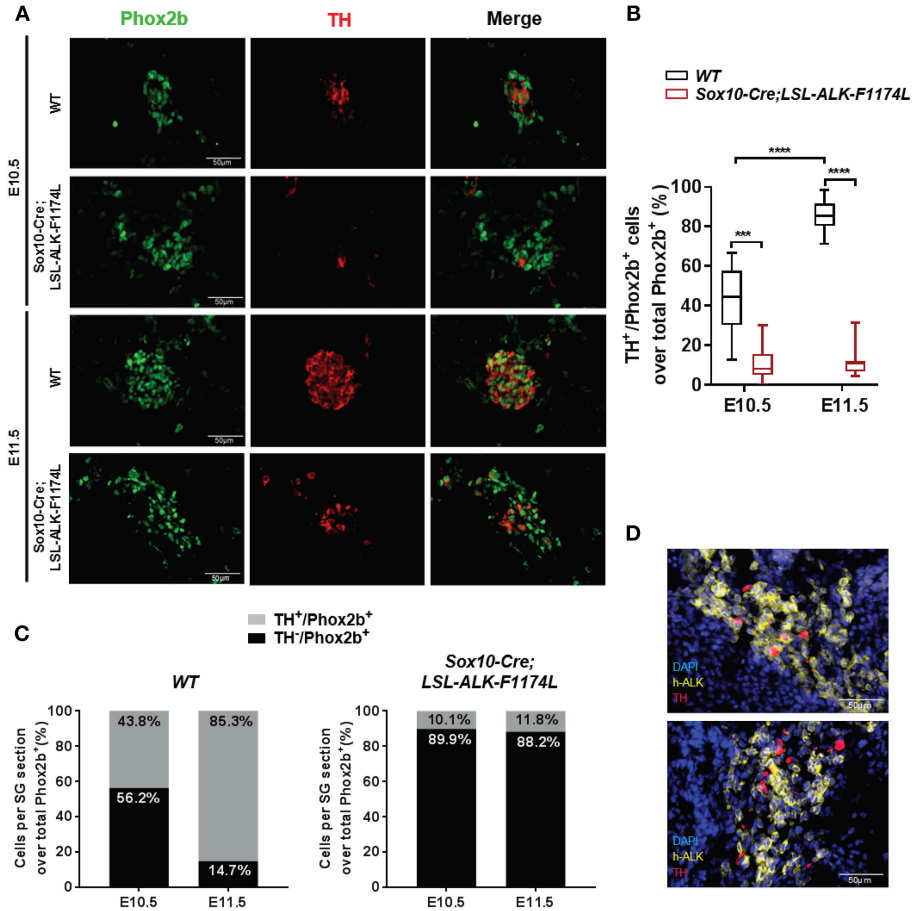

FIGURE 5 | ALK-F1174L expression in sympathoblasts impairs noradrenergic differentiation. **(A)** Representative IF images of TH (red) and Phox2b (green) staining in *WT* and *Sox10-Cre;LSL-ALK-F1174L* embryos at E10.5 and E11.5 (x40 magnification). **(B)** The quantifications of the proportions of $Phox2b^+/TH^+$ cells over total $Phox2b^+$ cells in *WT* and *Sox10-Cre;LSL-ALK-F1174L* embryos are illustrated in Box-plot for E10.5 and E11.5 (Kruskal-Wallis test, multiple comparisons, $^{****}p < 0.0001$, $^{***}p = 0.0003$, ns comparisons are not shown). Numbers of SG sections analyzed at E10.5 and E11.5, respectively: *WT* $n = 30$ and $n = 30$; *Sox10-Cre;LSL-ALK-F1174L* $n = 18$ and $n = 16$. **(C)** Mean percentages of $TH^-/Phox2b^+$ and $TH^+/Phox2b^+$ cell populations are plotted in grouped representations at E10.5 and E11.5 for *WT* (left panel) and *Sox10-Cre/LSL-ALK-F1174L* SG (right panel) embryos. **(D)** Representative IF images of double staining for human ALK (h-ALK) (yellow) and TH (red) in two *Sox10-Cre/LSL-ALK-F1174L* embryos at E10.5. Numbers of SG sections analyzed: $n = 10$.

detected in $Phox2b^+$ cells in *Sox10-Cre;LSL-ALK-F1174L* SG. Our finding that ALK blocks differentiation of NCCs during embryogenesis is in accordance with previous reports in tumors derived from the NC progenitor cell lines, MONC1 and JoMa1, expressing ALK mutations (22, 38). However, an opposite role for ALK in mediating neurite outgrowth was reported in rat pheochromocytoma (PC12) cells, the human SK-N-SH NB cell line and sympathetic neuroblasts (27, 39, 40). In addition, a more differentiated phenotype was observed in NB tumors expressing a constitutively activated ALK variant in combination with MYCN when compared to MYCN-only driven tumors (23). These contrasting findings suggest that sympathetic neuroblasts may respond differentially to ALK-mediated signaling depending on their maturational stage, as previously suggested (27, 41).

Embryonal tumors, such as NB, are thought to originate from an excessive proliferation of the tissue of origin prior to birth, coupled with an incomplete differentiation. In *Sox10-Cre;LSL-ALK-F1174L* embryos, the reduced sympathetic differentiation was associated with an increased expansion of $Sox10^+$ NCCs, an enhanced proliferation of $Phox2b^+$ progenitors at E10.5, and an enlarged size of *Sox10-Cre;LSL-ALK-F1174L* SG. These data are in accordance with the $ALK^{-F1178L}$ KI model, which displayed enlarged stellate and superior cervical ganglia at birth and in adult mice, together with an elevated proliferation of neuroblasts at E14.5, and at birth (23). Similar involvement of ALK signaling in promoting proliferation of NCC progenitors and sympathetic neuroblasts has also previously been described in various models (22, 26, 27, 38).

Interestingly, the control of neurogenesis in the SNS is unique among neuronal cells as it is not linked to exit from cell cycle. Indeed, neuroblasts of the SNS continue to divide after initial neuronal differentiation and display two phases of proliferation (26, 42, 43). The first phase consists of an initial expansion of NC progenitors, which comprise both $Sox10^+/Phox2b^-$ and

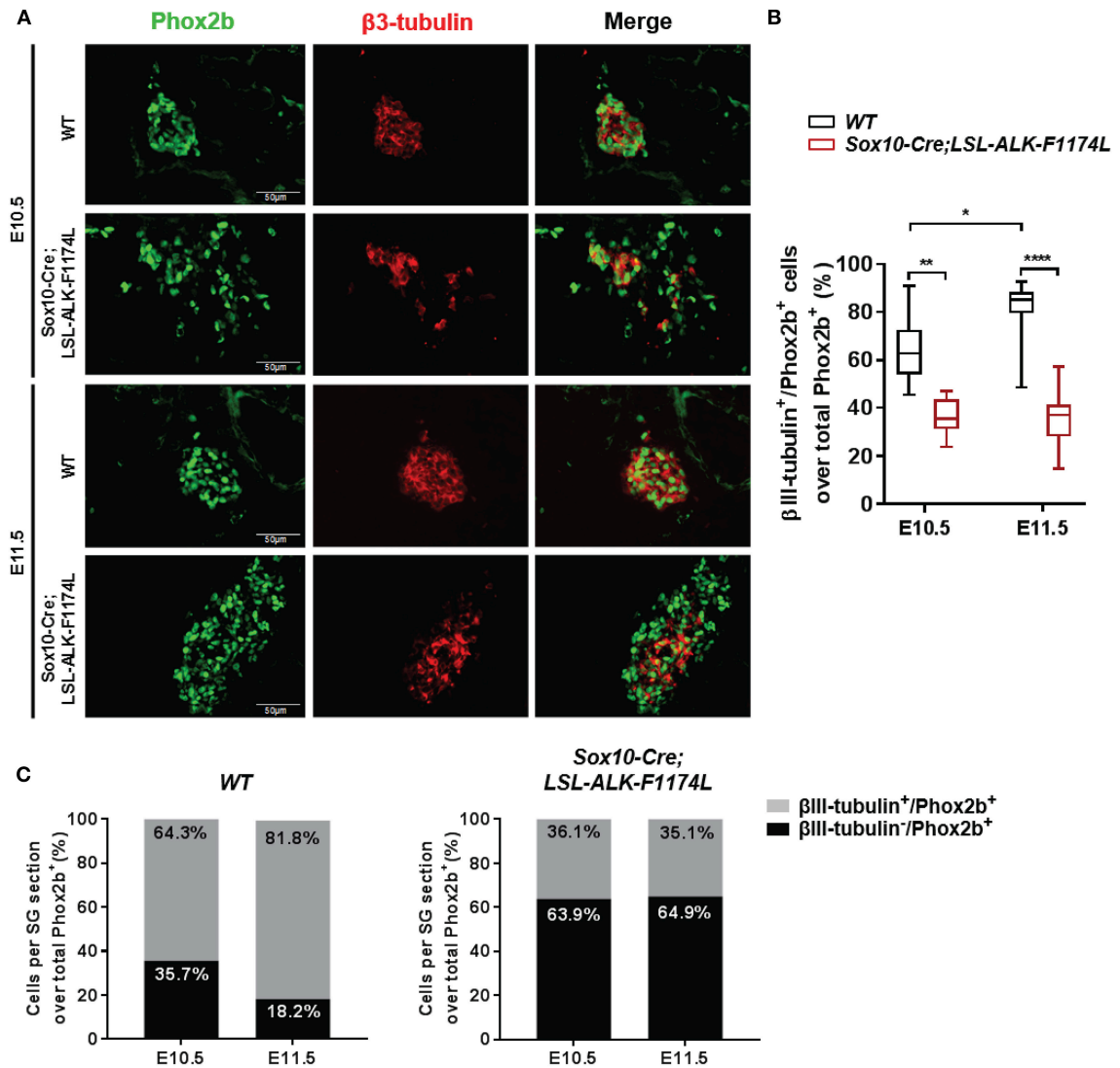

FIGURE 6 | *Sox10-Cre;LSL-ALK-F1174L* SG displayed reduced neuronal differentiation. **(A)** Representative IF images of Phox2b (green) and βIII-tubulin (red) staining (x40 magnification). **(B)** Box-plot illustration of the fractions of βIII-tubulin$^+$ cells over total Phox2b$^+$ cells per section at E10.5 and E11.5 in *WT* and *Sox10-Cre;LSL-ALK-F1174L* embryos (Kruskal-Wallis test, paired comparisons, $^{****}p < 0.0001$, $^{**}p = 0.0034$, $^{*}p = 0.023$, ns comparisons are not shown). Numbers of SG sections analyzed at E10.5 and E11.5, respectively: *WT* $n = 20$ and $n = 28$, *Sox10-Cre;LSL-ALK-F1174L* $n = 12$ and $n = 13$. **(C)** The mean percentages of βIII-tubulin$^-$/Phox2b$^+$ and βIII-tubulin$^+$/Phox2b$^+$ cell populations are plotted in grouped representations at E10.5 and E11.5 for *WT* (left panel) and *Sox10-Cre;LSL-ALK-F1174L* (right panel) embryos.

Sox10$^+$/Phox2b$^+$ cells. Then, a transient cell cycle exit occurs at E10.5 in cells displaying Sox10 downregulation together with upregulation of neuronal (βIII-tubulin, Hu) and noradrenergic (TH) markers (29, 43). Subsequently, the majority of immature noradrenergic neuroblasts (TH$^+$) undergo a second wave of proliferation starting at E11.5 in mouse (7, 29). Our results in *WT* embryos are consistent with these reports, as 29% of Phox2b$^+$ cells were proliferating at E10.5 and 82% at E11.5. In contrast, the abnormal and high proliferation index of Phox2b$^+$ cells (80%) in *Sox10-Cre;LSL-ALK-F1174L* SG at E10.5, suggests that the ALK-F1174L mutation may prevent neuroblast progenitors from exiting the cell cycle. The mechanisms mediating the transient cell cycle exit are not clearly understood. However, it has been suggested that Sox10 might drive the proliferation of NCCs, and that the loss or the reduction of Sox10 expression could be involved (29, 35). In addition, only the cells with reduced or complete Sox10 downregulation expressed βIII-tubulin and TH at E10.5, and they displayed a proliferation arrest (29). We can thus hypothesize that in *Sox10-Cre;LSL-ALK-F1174L* SG, the persistently elevated expression of Sox10 may impede neuroblast progenitors from exiting the cell cycle and therefore prevent their differentiation.

It is worth noting that neuroblastoma-like premalignant lesions were identified in human fetuses or neonates via mass-screening and autopsies in prior independent studies (8, 44, 45). As they occur at much higher rates than the

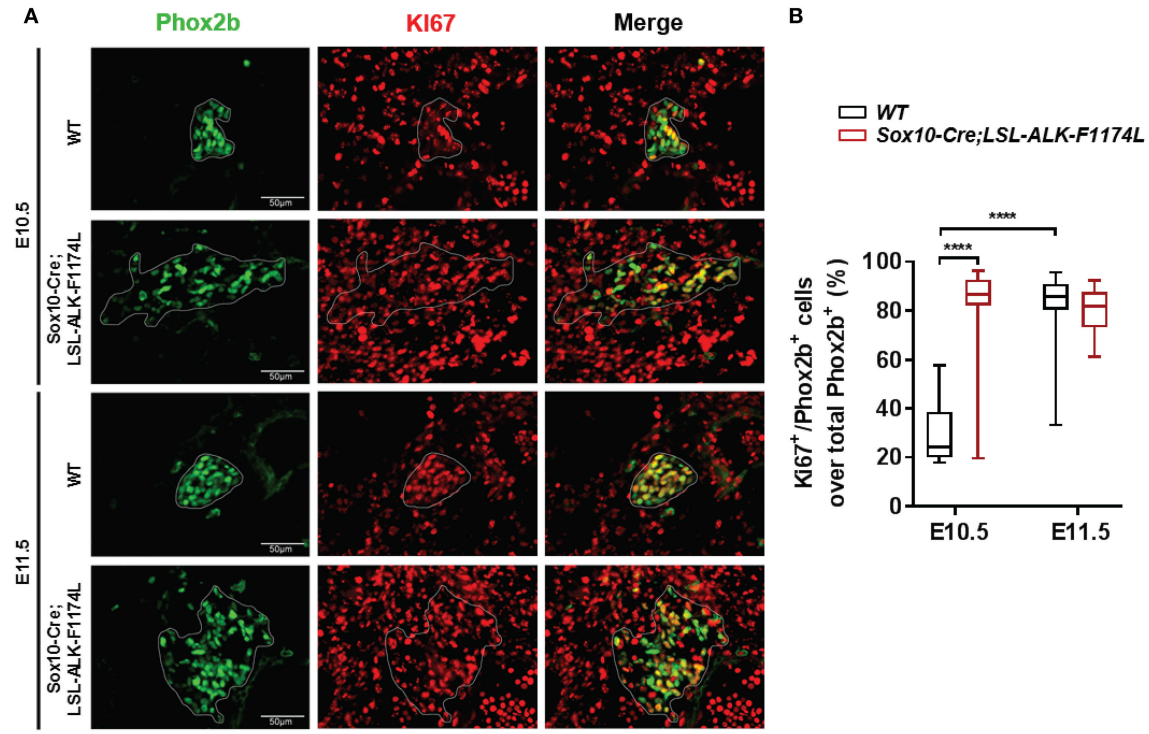

FIGURE 7 | Increased proliferation of Phox2b$^+$ cells in *Sox10-Cre;LSL-ALK-F1174L* SG. **(A)** Representative IF images of Phox2b (green) and Ki67 (red) staining at E10.5 and E11.5 in *WT* and *Sox10-Cre;LSL-ALK-F1174L* SG (x40 magnification). SG are surrounded by white circles. **(B)** Blox-plot representation of the fractions of Phox2b$^+$/Ki67$^+$ over total Phox2b$^+$ cells in *WT* and *Sox10-Cre;LSL-ALK-F1174L* SG at E10.5 and E11.5 (Kruskal-Wallis test, multiple comparisons, $^{****}p < 0.0001$, ns comparisons are not shown). Numbers of SG sections analyzed at E10.5 and E11.5, respectively: *WT* $n = 24$ and $n = 22$, *Sox10-Cre;LSL-ALK-F1174L* $n = 16$ and $n = 16$.

incidence of NB, it was speculated that the majority might indeed regress or mature spontaneously (8, 46, 47). Similarly, clusters of hyperplastic proliferating βIII-tubulin and TH negative cells were described in SG as well as in adrenal glands of newborn WT mice (34, 48). These hyperplastic clusters in SG were found to disappear postnatally at 14 days in WT mice, while they increased in size during the first postnatal weeks in the TH-MYCN NB mouse model, and even gave rise to NB-like tumors (48). Such precancerous clusters were shown to express Phox2b in the TH-MYCN mice, but lacked TH expression (49). These cells could represent the cellular origin of NB. Indeed, NB tumors, derived from TH-MYCN mice or from xenografts of human NB cell lines, were found mainly composed of proliferating undifferentiated Phox2b$^+$/TH$^-$ sympathetic progenitors (49). Importantly, these cells constitute large fractions of SG in our *Sox10-Cre;LSL-ALK-F1174L* model. We can thus hypothesize that deregulated ALK signaling, due to mutation or overexpression, in rare NCCs during embryonic development could promote the expansion of precursors of preneoplastic lesions. Further studies should focus on whether such precancerous states are also more prevalent and biologically persistent in the ALK$^{-F1178L}$ or the AKL$^{-R1279Q}$ KI model after birth.

The limitations of the experiments presented herein are mostly due to the fact that the expression of the ALK-F1174L variant in our model is anterior by nearly 1.5 days and possibly different i.e., more elevated than the one resulting from the endogenous gene. Thus, the observed ALK-F1174L-mediated impacts are more striking in our model as compared to the ALK$^{-F1178L}$ KI model. Indeed, this KI model displayed lethality between 24 and 48 h after birth in homozygous mice (23). However, increased SG sizes and neuroblast proliferation were also observed in the ALK$^{-F1178L}$ KI model (23). In addition, the early lethality of our model also limited the time-frame for the analyses relating to the differentiation of SG. We cannot exclude that the expression of the ALK-F1174L variant could mediate a delay in SA differentiation, as observed in murine Ascl1 and Insm1 knock-out models (50–52). However, as the transition from NCCs to sympathetic neuroblasts occurs between E9.5 and E11.5, we could precisely study the impact of ALK-F1174L during the initial phase of sympathetic lineage specification. Moreover, the ALK-F1174L mutation is not found in familial NB, but restricted to sporadic cases (19), suggesting that activation of ALK above a critical threshold might not be compatible with survival. Nevertheless, although no mutations at positions F1174 and F1245 were identified in familial NB cases, *de novo* germline mutations, ALK-F1174V and ALK-F1245V, were reported in two independent cases of congenital NB associated with CNS developmental defects (53). This potentially indicates that activating mutations

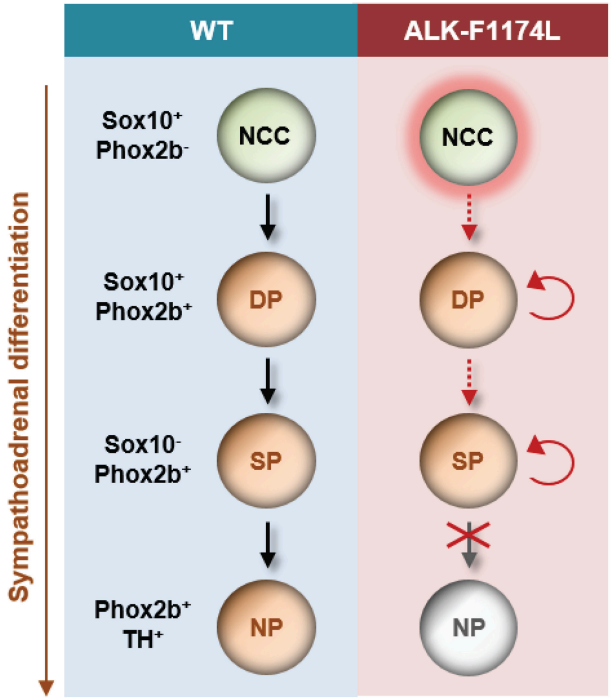

FIGURE 8 | Schematic model proposed for the impact of the ALK-F1174L mutation on sympathetic differentiation. The expression of the ALK-F1174L mutation in NCCs affects various steps of the sympathetic differentiation during SA lineage development. ALK-F1174L increases the number of NCCs at early embryonic stages (marked by red halo). The transition from NCCs to Sox10$^+$/Phox2b$^+$ progenitors, and further to sympathetic progenitors is incomplete in *Sox10-Cre;LSL-ALK-F1174L* embryos (red dashed arrows). The expression of Sox10 is maintained in a large proportion of cells, while the cell population upregulating Phox2b is reduced, and no variation occur between embryonic stages. The Sox10$^-$/Phox2b$^+$ sympathetic progenitors do not acquire noradrenergic properties highlighting that ALK-F1174L hinders their maturation into noradrenergic neurons. The proportion of proliferating Phox2b$^+$ cells is increased in *Sox10-Cre;LSL-ALK-F1174L* SG at E10.5 (red circular arrows). Thus, ALK deregulation leading to reduced SA differentiation and proliferative excess may be an essential path for NB initiation. NCC, neural crest cell; DP, differentiating progenitor; SP, sympathetic progenitor; NP, noradrenergic progenitor.

at position F1174 can occur *de novo* in the germline and result in NB and severe CNS abnormalities. Finally, whilst our findings are mostly descriptive, this study opens new avenues for further mechanistic investigations to decipher the precise molecular underpinnings of ALK-mediated perturbations of the proliferative and differentiative checks and balances in place in SG, as well as in adrenal chromaffin cells. This is of particular interest, as the majority of adrenal chromaffin cells were recently described to originate from SCP rather than from a common SA progenitor (4).

In conclusion, our study is the first demonstration of a role for the ALK-F1174L mutation in disturbing the balance between proliferation and differentiation in the sympathetic lineage *in vivo* at early embryonic stages. This occurs by (a) an increase in neuroblast proliferation, and (b) a block in neuronal and noradrenergic differentiation (**Figure 8**). Our data strongly suggest that dysregulated signaling of ALK during embryogenesis promotes a precancerous state, and thus may represent an initial and developmental path for NB oncogenesis.

MATERIALS AND METHODS

Generation of LSL-ALK-F1174L Mice

The human ALK cDNA, harboring the ALK F1174L mutation (synthetized by GenScript), was cloned downstream of a chicken actin gene (CAG) promoter followed by loxP-flanked strong transcriptional termination site (LSL). The transgene was placed upstream of an internal ribosome entry site (IRES) and a second open reading frame coding for the luciferase gene (Fluc) in a proprietary plasmid (Taconic-Artemis, Cologne, Germany). The CAG-LSL-ALK(F1174L)-IRES-Fluc vector [LSL-ALK(F1174L)] was introduced into the ROSA26 locus of C57BL/6 embryonic stem cells by recombinase-mediated cassette exchange. Recombinant clones were isolated, validated by Southern blotting and chimera were generated by injection into blastocysts. Chimera were crossbred to C57BL/6NTac and offspring positive for the ALK(F1174L) was obtained and maintained by backcrossing on C57BL/6NTac mice. Further details about generation and characterization of the C57BL/6NTac-Gt(ROSA)26Sortm3196(CAG-ALK*F1174L)Arte mouse strain will be published elsewhere (Schulte et al., unpublished).

Animal Breeding and Genotyping

The *LSL-ALK-F1174L* transgenic mice were crossed with *Sox10-Cre* mice (54). The mouse pairs were let to stand one night and the midday of the following day was considered as E0.5. Pregnant mice were killed by cervical dislocation for embryos collection. Embryos were fixed in Histofix (Roti® Histofix 4% formaldehyde, Roth) from 15 min at room temperature (RT) to overnight at +4°C, depending on embryos size, and incubated overnight in 30% sucrose (in 1x PBS) for tissue preservation. Then, embryos were embedded in optimal cutting temperature (OCT, Sakura Finetek) compound and frozen at −80°C. This study was carried out in accordance with the guidelines of the Swiss Animal Protection Ordinance and the Animal Experimentation Ordinance of the Swiss Federal Veterinary Office (FVO). The protocol was approved by the veterinary authorities of Canton of Zurich.

Genomic DNA was extracted from the tip of embryos tails and genotyping was performed by PCR using the following primers to detect Sox10-Cre and LSL-ALK-F1174L transgenes: Cre-for: 5′-CTATCCAGCAACATTTGGGCCAGC-3′ and Cre-rev: 5′-CCAGGTTACGGATATAGTTCATGAC-3′; LSL-ALK-for: 5′-CCATCAGTGACCTGAAGGAGG-3′ and LSL-ALK-rev: 5′-CACGTGCAGAAGGTCCAGC-3′.

Cycling condition were: 5′ at 94°C, 35 cycles of 40″ at 94°C, 40″ at 55°C (Cre) or 60°C (ALK) and 1′ at 72°C, followed by 7′ at 72°C. Embryos carrying either the Sox10-Cre or LSL-ALK-F1174L transgene, or none are referred to as *WT* embryos, while embryos carrying both transgenes are referred to as *Sox10-Cre;LSL-ALK-F1174L* embryos.

Immunofluorescence Analyses

Transverse cryosections of 10 μm were made using a cryostat and every fifteenth or twentieth embryonic section were deposited on the same glass slide (∼10 sections/slide), separating each section by 150 or 200 μm, respectively.

For immunofluorescence (IF) analyses embryos sections were fixed in 4% paraformaldehyde for 5 min, then washed in PBS (3 × 5 min, same for all following washes) and treated for permeabilization with 0.5% Triton X-100 in PBS for 5 min. After washes, slides were incubated with a blocking solution (5% Goat serum, 0.1%Triton X-100 in PBS) for 45 min at RT, and then overnight at 4°C with primary antibodies diluted in PBS. The next day, after washes, corresponding secondary antibodies (diluted at 1/500 in PBS) were added for 1 h at RT, and then incubated with fluorescent mounting medium for 30 min (Dako, 1/5000). The following primary antibodies were used to detect Phox2b (Santa Cruz Biotechnology, #sc-376997, 1/100), Sox10 (Cell Signaling Technology, #89356S, 1/200); Ki67 (Abcam, #ab 15580, 1/200), TH (Abcam, #ab 76442, 1/500), βIII-tubulin (Cell Signaling Technology, #5568, 1/200), ALK (Cell Signaling, D5F3® #3633, 1/100); and revealed using the secondary Ab: Goat-a-Mouse-Alexa Fluor® 488 (ThermoFisher scientific, #A-11001), Goat-a-Rabbit- Alexa Fluor ® 647 (ThermoFisher scientific, #A-21246), Goat-a-Chicken-Alexa Fluor® 647 (Abcam, #ab 150175).

In situ Hybridization

ISH experiments were performed using the RNAscope® technology (Advanced Cell Diagnostics, Inc) at the Histology Core Facility of the EPFL. RNAscope Multiplex Fluorescent V1 assay (Advanced Cell Diagnostics, Cat. No. 320850) was performed according to manufacturer's protocol on 10 μm fixed frozen cryosections, hybridized with the probes Mm-Alk1-C1 (ACD, Cat. No. 501131), Mm-Ascl1-CDS-C3 (ADC, Cat. No. 476321-C3), Mm-Insm1-C1 (ADC, Cat. No. 430621), 3Plex positive control Mm-Ppib (ACD, Cat. No. 313911), and negative control DapB (ACD, Cat. No. 310043) at 40°C for 2 h and revealed with Atto550 for C1 and Atto647 for C3.

Imaging and Quantitative Analyses of Sympathetic Ganglia

Images for IF and ISH analyses were acquired using a fluorescence microscope (Leica DFC 345 FX, Leica). For each embryo, one slide was analyzed for each staining conditions. SG were defined as Phox2b^{+} regions near the dorsal aorta as analyzed by IF staining. To estimate the proportion of the different cell populations, all embryo sections of the slide presenting SG were analyzed. Cells were counted in SG bilaterally. For IF analyses, three *WT* embryos were analyzed for both E10.5 and E11.5, while three and two *Sox10-Cre;LSL-ALK-F1174L* embryos were analyzed for E10.5 and E11.5, respectively for Sox10/Phox2b, Phox2b/TH, Phox2b/βIII-tubulin, and Phox2b/Ki67 double stainings. The precise numbers of SG sections analyzed for each staining are indicated in the respective Figure Legends.

Areas of SG sections were quantified using Image J software (National Institute of Health, USA). The SG surfaces delimited by Phox2b positive regions was measured using the Sox10/Phox2b co-staining analyses and are given in arbitrary unit (AU). IF labeled cell populations were manually counted using the Leica Microsystem LAS AF software (Version 2.6.0, build 7266). Cell proportions were calculated by counting the number of cells comprised in of each cell population normalized to the total number of cells investigated per each SG sections. These later correspond to the total number of cells/SG section for Sox10/Phox2b staining or total number of Phox2b+ cells/SG section for βIII-tubulin/Phox2b, TH/Phox2b, and Ki67/Phox2b staining. All SG sections analyzed were independently represented on the graphs using Box-plot representation, illustrating the minimum to maximum and the median value of measurements. Quantifications of TH/h-ALK co-staining were performed using a confocal microscope (Zeiss LSM 710) and the Zeiss Blue software.

Statistical Analysis

Statistical analyses were performed using GraphPadPrism 6.0 (GraphPad Software Inc., San Diego, CA, USA). D'Agostino-Pearson normality test was performed for each data set, and depending on data distribution, they were analyzed with unpaired two-tailed parametric *t*-test or non-parametric Mann Whitney test to compare two different conditions, or by one-way Anova or Kruskal-Wallis test for multiple comparisons. Only statistically significant comparisons are indicated in the graphs.

ETHICS STATEMENT

This study was carried out in accordance with the guidelines of the Swiss Animal Protection Ordinance and the Animal Experimentation Ordinance of the Swiss Federal Veterinary Office (FVO). The protocol was approved by the veterinary authorities of Canton of Zurich.

AUTHOR CONTRIBUTIONS

LV performed all major experimental work. LV and MG performed *in vivo* experiments. LV and AM-M analyzed the data. JS produced the *LSL-ALK-F1174L* mouse model. AM-M and OS designed and coordinated experiments. LV and AM-M prepared figures and drafted the manuscript. LV, RR, and AM-M interpreted the data and edited the manuscript. All authors read, commented and approved the final manuscript.

FUNDING

This work was supported by grants from the Swiss National Science Foundation (Project grant #310030-163407 to AM-M), FORCE (to AM-M and RR) and the Kinderkrebsforschung Schweiz (to AM-M). The work in Shakhova's laboratory was supported by grants to OS from Promedica UBS, Julius Müller and FORCE Foundations.

ACKNOWLEDGMENTS

We thank Dr. Maria Vittoria Sepporta for her rereading of the manuscript.

SUPPLEMENTARY MATERIAL

The Supplementary Material for this article can be found online at: https://www.frontiersin.org/articles/10.3389/fonc.2019.00275/full#supplementary-material

REFERENCES

1. Maris JM. Recent advances in neuroblastoma. *N Engl J Med*. (2010) 362:2202–11. doi: 10.1056/NEJMra0804577
2. Vo KT, Matthay KK, Neuhaus J, London WB, Hero B, Ambros PF, et al. Clinical, biologic, and prognostic differences on the basis of primary tumor site in neuroblastoma: a report from the international neuroblastoma risk group project. *J Clin Oncol*. (2014) 32:3169–76. doi: 10.1200/jco.2014.56.1621
3. Cheung NK, Dyer MA. Neuroblastoma: developmental biology, cancer genomics and immunotherapy. *Nat Rev Cancer*. (2013) 13:397–411. doi: 10.1038/nrc3526
4. Furlan A, Dyachuk V, Kastriti ME, Calvo-Enrique L, Abdo H, Hadjab S, et al. Multipotent peripheral glial cells generate neuroendocrine cells of the adrenal medulla. *Science*. (2017) 357:eaal3753. doi: 10.1126/science.aal3753
5. Lumb R, Schwarz Q. Sympathoadrenal neural crest cells: the known, unknown and forgotten? *Dev Growth Differ*. (2015) 57:146–57. doi: 10.1111/dgd.12189
6. Kelsh RN. Sorting out Sox10 functions in neural crest development. *Bioessays*. (2006) 28:788–98. doi: 10.1002/bies.20445
7. Rohrer H. Transcriptional control of differentiation and neurogenesis in autonomic ganglia. *Eur J Neurosci*. (2011) 34:1563–73. doi: 10.1111/j.1460-9568.2011.07860.x
8. Marshall GM, Carter DR, Cheung BB, Liu T, Mateos MK, Meyerowitz JG, et al. The prenatal origins of cancer. *Nat Rev Cancer*. (2014) 14:277–89. doi: 10.1038/nrc3679
9. Ratner N, Brodeur GM, Dale RC, Schor NF. The "neuro" of neuroblastoma: neuroblastoma as a neurodevelopmental disorder. *Ann Neurol*. (2016) 80:13–23. doi: 10.1002/ana.24659
10. Huber K, Janoueix-Lerosey I, Kummer W, Rohrer H, Tischler AS. The sympathetic nervous system: malignancy, disease, and novel functions. *Cell Tissue Res*. (2018) 372:163–70. doi: 10.1007/s00441-018-2831-0
11. Ritenour LE, Randall MP, Bosse KR, Diskin SJ. Genetic susceptibility to neuroblastoma: current knowledge and future directions. *Cell Tissue Res*. (2018) 372:287–307. doi: 10.1007/s00441-018-2820-3
12. Vernersson E, Khoo NK, Henriksson ML, Roos G, Palmer RH, Hallberg B. Characterization of the expression of the ALK receptor tyrosine kinase in mice. *Gene Exp Patterns*. (2006) 6:448–61. doi: 10.1016/j.modgep.2005.11.006
13. Hurley SP, Clary DO, Copie V, Lefcort F. Anaplastic lymphoma kinase is dynamically expressed on subsets of motor neurons and in the peripheral nervous system. *J Comp Neurol*. (2006) 495:202–12. doi: 10.1002/cne.20887
14. Degoutin J, Brunet-de Carvalho N, Cifuentes-Diaz C, Vigny M. ALK (Anaplastic Lymphoma Kinase) expression in DRG neurons and its involvement in neuron-Schwann cells interaction. *Eur J Neurosci*. (2009) 29:275–86. doi: 10.1111/j.1460-9568.2008.06593.x
15. Janoueix-Lerosey I, Lequin D, Brugieres L, Ribeiro A, de Pontual L, Combaret V, et al. Somatic and germline activating mutations of the ALK kinase receptor in neuroblastoma. *Nature*. (2008) 455:967–70. doi: 10.1038/nature07398
16. Chen Y, Takita J, Choi YL, Kato M, Ohira M, Sanada M, et al. Oncogenic mutations of ALK kinase in neuroblastoma. *Nature*. (2008) 455:971–4. doi: 10.1038/nature07399
17. George RE, Sanda T, Hanna M, Frohling S, Luther W II, Zhang J, et al. Activating mutations in ALK provide a therapeutic target in neuroblastoma. *Nature*. (2008) 455:975–8. doi: 10.1038/nature07397
18. Caren H, Abel F, Kogner P, Martinsson T. High incidence of DNA mutations and gene amplifications of the ALK gene in advanced sporadic neuroblastoma tumours. *Biochem J*. (2008) 416:153–9. doi: 10.1042/BJ20081834
19. Bresler SC, Weiser DA, Huwe PJ, Park JH, Krytska K, Ryles H, et al. ALK mutations confer differential oncogenic activation and sensitivity to ALK inhibition therapy in neuroblastoma. *Cancer Cell*. (2014) 26:682–94. doi: 10.1016/j.ccell.2014.09.019
20. Zhu S, Lee JS, Guo F, Shin J, Perez-Atayde AR, Kutok JL, et al. Activated ALK collaborates with MYCN in neuroblastoma pathogenesis. *Cancer Cell*. (2012) 21:362–73. doi: 10.1016/j.ccr.2012.02.010
21. Berry T, Luther W, Bhatnagar N, Jamin Y, Poon E, Sanda T, et al. The ALK(F1174L) mutation potentiates the oncogenic activity of MYCN in neuroblastoma. *Cancer Cell*. (2012) 22:117–30. doi: 10.1016/j.ccr.2012.06.001
22. Montavon G, Jauquier N, Coulon A, Peuchmaur M, Flahaut M, Bourloud KB, et al. Wild-type ALK and activating ALK-R1275Q and ALK-F1174L mutations upregulate Myc and initiate tumor formation in murine neural crest progenitor cells. *Oncotarget*. (2014) 5:4452–66. doi: 10.18632/oncotarget.2036
23. Cazes A, Lopez-Delisle L, Tsarovina K, Pierre-Eugene C, De Preter K, Peuchmaur M, et al. Activated Alk triggers prolonged neurogenesis and Ret upregulation providing a therapeutic target in ALK-mutated neuroblastoma. *Oncotarget*. (2014) 5:2688–702. doi: 10.18632/oncotarget.1883
24. Heukamp LC, Thor T, Schramm A, De Preter K, Kumps C, De Wilde B, et al. Targeted expression of mutated ALK induces neuroblastoma in transgenic mice. *Sci Transl Med*. (2012) 4:141ra91. doi: 10.1126/scitranslmed.3003967
25. Schönherr C, Ruuth K, Kamaraj S, Wang CL, Yang HL, Combaret V, et al. Anaplastic Lymphoma Kinase (ALK) regulates initiation of transcription of MYCN in neuroblastoma cells. *Oncogene*. (2012) 31:5193–200. doi: 10.1038/onc.2012.12
26. Reiff T, Huber L, Kramer M, Delattre O, Janoueix-Lerosey I, Rohrer H. Midkine and Alk signaling in sympathetic neuron proliferation and neuroblastoma predisposition. *Development*. (2011) 138:4699–708. doi: 10.1242/dev.072157
27. Kramer M, Ribeiro D, Arsenian-Henriksson M, Deller T, Rohrer H. Proliferation and survival of embryonic sympathetic neuroblasts by MYCN and activated ALK signaling. *J Neurosci*. (2016) 36:10425–39. doi: 10.1523/JNEUROSCI.0183-16.2016
28. Callahan T, Young HM, Anderson RB, Enomoto H, Anderson CR. Development of satellite glia in mouse sympathetic ganglia: GDNF and GFR alpha 1 are not essential. *Glia*. (2008) 56:1428–37. doi: 10.1002/glia.20709
29. Gonsalvez DG, Cane KN, Landman KA, Enomoto H, Young HM, Anderson CR. Proliferation and cell cycle dynamics in the developing stellate ganglion. *J Neurosci*. (2013) 33:5969–79. doi: 10.1523/JNEUROSCI.4350-12.2013
30. Nagashimada M, Ohta H, Li C, Nakao K, Uesaka T, Brunet JF, et al. Autonomic neurocristopathy-associated mutations in PHOX2B dysregulate Sox10 expression. *J Clin Invest*. (2012) 122:3145–58. doi: 10.1172/JCI63401
31. Thomas SA, Matsumoto AM, Palmiter RD. Noradrenaline is essential for mouse fetal development. *Nature*. (1995) 374:643–6. doi: 10.1038/374643a0
32. Morikawa Y, Zehir A, Maska E, Deng C, Schneider MD, Mishina Y, et al. BMP signaling regulates sympathetic nervous system development through Smad4-dependent and -independent pathways. *Development*. (2009) 136:3575–84. doi: 10.1242/dev.038133
33. Lim KC, Lakshmanan G, Crawford SE, Gu Y, Grosveld F, Engel JD. Gata3 loss leads to embryonic lethality due to noradrenaline deficiency of the sympathetic nervous system. *Nat Genet*. (2000) 25:209–12. doi: 10.1038/76080
34. Chan WH, Anderson CR, Gonsalvez DG. From proliferation to target innervation: signaling molecules that direct sympathetic nervous system development. *Cell Tissue Res*. (2018) 372:171–93. doi: 10.1007/s00441-017-2693-x
35. Kim J, Lo L, Dormand E, Anderson DJ. SOX10 maintains multipotency and inhibits neuronal differentiation of neural crest stem cells. *Neuron*. (2003) 38:17–31. doi: 10.1016/S0896-6273(03)00163-6
36. Seo H, Hong SJ, Guo S, Kim HS, Kim CH, Hwang DY, et al. A direct role of the homeodomain proteins Phox2a/2b in noradrenaline neurotransmitter identity determination. *J Neurochem*. (2002) 80:905–16. doi: 10.1046/j.0022-3042.2002.00782.x

37. Cargnin F, Flora A, Di Lascio S, Battaglioli E, Longhi R, Clementi F, et al. PHOX2B regulates its own expression by a transcriptional auto-regulatory mechanism. *J Biol Chem*. (2005) 280:37439–48. doi: 10.1074/jbc.M508368200
38. Schulte JH, Lindner S, Bohrer A, Maurer J, De Preter K, Lefever S, et al. MYCN and ALKF1174L are sufficient to drive neuroblastoma development from neural crest progenitor cells. *Oncogene*. (2013) 32:1059–65. doi: 10.1038/onc.2012.106
39. Gouzi JY, Moog-Lutz C, Vigny M, Brunet-de Carvalho N. Role of the subcellular localization of ALK tyrosine kinase domain in neuronal differentiation of PC12 cells. *J Cell Sci*. (2005) 118(Pt 24):5811–23. doi: 10.1242/jcs.02695
40. Motegi A, Fujimoto J, Kotani M, Sakuraba H, Yamamoto T. ALK receptor tyrosine kinase promotes cell growth and neurite outgrowth. *J Cell Sci*. (2004) 117(Pt 15):3319–29. doi: 10.1242/jcs.01183
41. Janoueix-Lerosey I, Lopez-Delisle L, Delattre O, Rohrer H. The ALK receptor in sympathetic neuron development and neuroblastoma. *Cell Tissue Res*. (2018) 372:325–37. doi: 10.1007/s00441-017-2784-8
42. Rohrer H, Thoenen H. Relationship between differentiation and terminal mitosis: chick sensory and ciliary neurons differentiate after terminal mitosis of precursor cells, whereas sympathetic neurons continue to divide after differentiation. *J Neurosci*. (1987) 7:3739–48. doi: 10.1523/JNEUROSCI.07-11-03739.1987
43. Hendershot TJ, Liu H, Clouthier DE, Shepherd IT, Coppola E, Studer M, et al. Conditional deletion of Hand2 reveals critical functions in neurogenesis and cell type-specific gene expression for development of neural crest-derived noradrenergic sympathetic ganglion neurons. *Dev Biol*. (2008) 319:179–91. doi: 10.1016/j.ydbio.2008.03.036
44. Beckwith JB, Perrin EV. *in situ* neuroblastomas: a contribution to the natural history of neural crest tumors. *Am J Pathol*. (1963) 43:1089–104.
45. Shimada H. *in situ* neuroblastoma: an important concept related to the natural history of neural crest tumors. *Pediatr Dev Pathol*. (2005) 8:305–6. doi: 10.1007/s10024-005-2162-5
46. Woods WG, Tuchman M, Robison LL, Bernstein M, Leclerc JM, Brisson LC, et al. A population-based study of the usefulness of screening for neuroblastoma. *Lancet*. (1996) 348:1682–7. doi: 10.1016/S0140-6736(96)06020-5
47. Nuchtern JG. Perinatal neuroblastoma. *Semin Pediatr Surg*. (2006) 15:10–6. doi: 10.1053/j.sempedsurg.2005.11.003
48. Hansford LM, Thomas WD, Keating JM, Burkhart CA, Peaston AE, Norris MD, et al. Mechanisms of embryonal tumor initiation: distinct roles for MycN expression and MYCN amplification. *Proc Natl Acad Sci USA*. (2004) 101:12664–9. doi: 10.1073/pnas.0401083101
49. Alam G, Cui H, Shi H, Yang L, Ding J, Mao L, et al. MYCN promotes the expansion of Phox2B-positive neuronal progenitors to drive neuroblastoma development. *Am J Pathol*. (2009) 175:856–66. doi: 10.2353/ajpath.2009.090019
50. Hirsch MR, Tiveron MC, Guillemot F, Brunet JF, Goridis C. Control of noradrenergic differentiation and Phox2a expression by MASH1 in the central and peripheral nervous system. *Development*. (1998) 125:599–608.
51. Pattyn A, Guillemot F, Brunet JF. Delays in neuronal differentiation in Mash1/Ascl1 mutants. *Dev Biol*. (2006) 295:67–75. doi: 10.1016/j.ydbio.2006.03.008
52. Wildner H, Gierl MS, Strehle M, Pla P, Birchmeier C. Insm1 (IA-1) is a crucial component of the transcriptional network that controls differentiation of the sympatho-adrenal lineage. *Development*. (2008) 135:473–81. doi: 10.1242/dev.011783
53. de Pontual L, Kettaneh D, Gordon CT, Oufadem M, Boddaert N, Lees M, et al. Germline gain-of-function mutations of ALK disrupt central nervous system development. *Hum Mutat*. (2011) 32:272–6. doi: 10.1002/humu.21442
54. Matsuoka T, Ahlberg PE, Kessaris N, Iannarelli P, Dennehy U, Richardson WD, et al. Neural crest origins of the neck and shoulder. *Nature*. (2005) 436:347–55. doi: 10.1038/nature03837

Conflict of Interest Statement: The authors declare that the research was conducted in the absence of any commercial or financial relationships that could be construed as a potential conflict of interest.

Supplementary Material

Expression of the neuroblastoma-associated ALK-F1174L activating mutation during embryogenesis impairs the differentiation of neural crest progenitors in sympathetic ganglia

Vivancos Stalin Lucie, Gualandi Marco, Schulte Johannes Hubertus, Renella Raffaele, Shakhova Olga, Mühlethaler-Mottet Annick*

*** Correspondence:** Mühlethaler-Mottet Annick: Annick.Muhlethaler@chuv.ch

1.1 Supplementary Figures

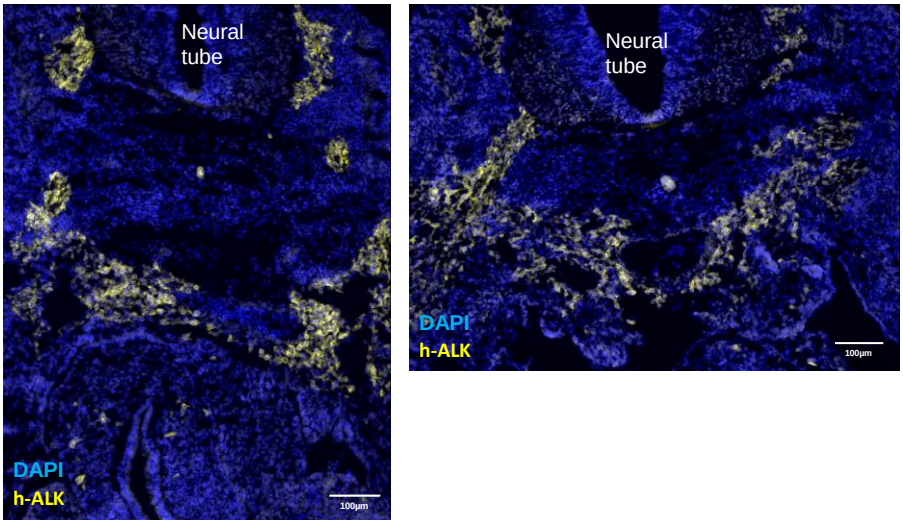

Supplementary Figure 1. Expression pattern of the ALK-F1174L transgene (h-ALK) in *Sox10-Cre;LSL-ALK-F1174L* embryos. Representative images of IF staining for h-ALK (yellow) at E10.5 (x10 magnification) in two *Sox10-Cre;LSL-ALK-F1174L* embryos.

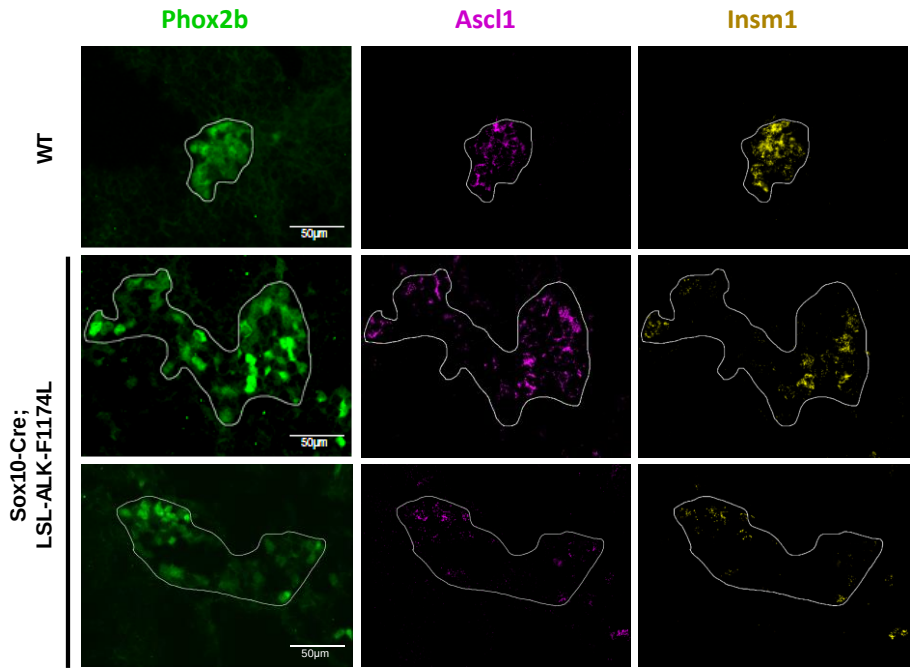

Supplementary Figure 2. Analysis of Ascl1 and Insm1 expression in SG at E10.5. Representative images of ISH staining for Ascl1 (purple) and Insm1 (yellow) in *WT* and *Sox10-Cre;LSL-ALK-F1174L* embryos at E10.5 (x40 magnification). Phox2b IF (green) staining was applied after ISH to highlight SG. SG are surrounded by white circle. Numbers of embryos analyzed: *WT* n=2 and *Sox10-Cre;LSL-ALK-F1174L* n=3.

PART II

INVESTIGATION OF THE INVOLVMENT OF ALK-wt and ALK ACTIVATING MUTATIONS IN TUMORIGENESIS AND PROGRESSION OF NEUROBLASTOMA

INTRODUCTION

ALK mutations are present in 10% of primary NB, and ALK$^{-F1174L}$ and ALK$^{-R1275Q}$ mutations are the most potent ALK activating mutations observed in NB tumors[158]. The expression of ALK$^{-F1174L}$ and ALK$^{-R1275Q}$ mediated the transformation of Ba/3F and NIH3T3 cells[70,148,182]. While MYCN alone was unable to transform NIH3T3 cells, the co-transfection of ALK mutants and MYCN strongly increased the transformation when compared to ALK mutation alone[148]. Overall, AKL$^{-F1174L}$ has been described to display a higher oncogenic potential than ALK$^{-R1275Q}$ in several models[148,164,170]. ALK$^{-F1174L}$ and ALK$^{-R1275Q}$ both strongly potentiate MYCN-mediated NB tumorigenesis in transgenic and knock-in (KI) animal models, highlighting their cooperation in sympathetic neuroblast progenitors and confirming their roles as possible initial events in NB formation[169,170,172]. Moreover, patients harboring both ALK$^{-F1174L}$ and MYCN amplification have the poorer outcomes[150,158]. ALK-wt has been reported to display oncogenic potential in NCCs, however, it does not potentiate the effects of MYCN in the zebrafish model and was unable to transform Ba/3F and NIH3T3 cells[70,148,164,172]. Furthermore, high levels of ALK-wt contributes to unfavorable phenotype in primary NB[183].

The identification of activated ALK as a druggable target in NB raised the hope for more successful therapy and prompted the initiation of several clinical trials with small-molecule inhibitors, such as phase I with crizotinib for patients with refractory NB[173,184]. However, resistances frequently occurred in patients, which showed the need to have a more comprehensive understanding of the ALK signaling pathways and target genes[185]. The activation of MAPK/ERK, PI3K/AKT/mTOR and MYC/MYCN signaling by ALK mutants has been well described in several studies in NB[68–71,148,168,169,186,187]. Transcriptomic profiling of ALK-inhibitors treated NB cell lines allowed to establish an 77-gene ALK-driven signature in NB cell lines and identified a negative MAPK feedback loop and RET as an ALK activated target genes[186]. This 77-genes signature

gradually decreases from 2h after TAE-treatment[187]. Moreover, 41% of the ALK 77-gene signature were also identified in gene expression profile after treatment with crizotinib and lorlatinib[145]. The *RET* gene is a target of activated ALK, and has been identified at the mRNA level in both human NB cell lines and primary tumors, as well as in the tumors generated by the KI *MYCN/ALK$^{-F1174L}$* mice[170,186]. Moreover, *ETV5*, previously identified in the ALK signature, has been reported to be upregulated upon ALK activation through the MAPK axis via MEK/ERK, and to be able to drive *RET* gene transcription[188,189]. However, pathways and genes activated through ALK deregulated signaling *in vivo* remain largely to be discovered.

Cell lines derived from NB tumors occur in three different subtypes, each with specific morphology and behavior: the non-invasive S-type cells with glial or schwannian-like characteristics, the invasive N-type composed of sympathoadrenal neuroblast and the I-type displaying feature of both phenotype and representing the most aggressive population[42,45,190]. Using patient-derived NB cell lines, Versteeg and colleagues have characterized a mesenchymal (MES) cell type associated to S-type cells and that resemble neural crest derived precursors cells, and an adrenergic (ADRN) cell type associated to N-type cells and displaying properties of the SA progenitors[45,46]. These cell types can interconvert, and the lineage identity is defined by the expression of TFs that compose the CRC[46,47]. Overall, MES cells are more resistant *in vitro* to standard chemotherapy and the MES cell population is enriched in post-treated and relapsed NB[46,47] (see introduction page 15).

In this study, we analyzed the impact of the ALK-wt, ALK$^{-R1275Q}$ and ALK$^{-F1174L}$ signaling *in vivo*. For this purpose, we used the SK-N-Be2c cell line displaying I-type/ADRN identity, and the SH-EP cell line corresponding to the S/MES-type. The ALK-wt, ALK$^{-F1174L}$ and ALK$^{-R1275Q}$ variants were stably expressed through lentiviral transduction in the SK-N-Be2c and SH-EP cell line, and the transduced cells were injected orthotopically in the adrenal gland of athymic Swiss mice or subcutaneously in NOD-SCID-γ mice, respectively. We conducted RNA sequencing on the generated tumors to unveil common or ALK-status specific downstream target genes specifically activated by ALK-wt overexpression, ALK$^{-F1174L}$ and ALK$^{-R1275Q}$ activating mutations *in vivo.* We hypothesized that the validation of new genes/signaling pathways could bring

new information about the pathways activated through ALK deregulated signaling and open new potential targets for NB therapy.

MATERIAL & METHODS

Cell culture

Two NB cell lines were used in this study: the SK-N-Be2c and the SH-EP cell lines. The SK-N-BE(2) NB cell line was established from a bone marrow biopsy taken from child with disseminated NB after repeated courses of chemotherapy and radiotherapy. SH-EP cell line originates from SK-N-SH cell line, which derives from highly involved bone marrow of a 4-year-old girl with stage 4 NB. Authentication of both cell lines was performed by microsatellite short tandem repeat analysis (Microsynth, Switzerland). Cell lines were cultured in Dubelco's modified Eagle's medium (D-MEM) (Gibco, Paisley, UK), supplemented with 1% penicillin/streptomycin (Gibco) and 10% heat inactivated Foetal Calf Serum (FCS) (BioWest, South American) and under standard culture conditions in humidified incubator at 37°C with 5% CO_2.

Plasmid construction and lentiviral infection

The human ALK cDNA *EcoR1-Pme1* fragments, isolated from ALK-wt, ALK-F1174L and ALK-R1275Q-pcDNA3 constructs (gift from Dr I. Janoueix-Lerosey[191]) were introduced into *EcoR1-Pme1* sites of the lentiviral vector pLiVpuro_C located downstream of the EF1-α promoter and containing the puromycin resistance gene (kind gift from Pr. Ivan Stamenkovic)[192]. All ALK-expressing vectors were verified by DNA sequencing of the complete ALK sequence.

The pLiVpuro_C vector with or without *ALK-wt*, *ALK-F1174L* and *ALK-R1275Q* genes was inserted by lentiviral infection into SK-N-Be2c and SH-EP cells. The day before transduction, $2x10^6$ 293T cells were plates on 6-well plates in DMEM, 10% FCS. 250 µL of a DNA solution containing 10 µg of pLiVpuro_C, 7.5 µg of pCMV**Δ**8 and 2.5 µg of pMD2.G, was mixed with 250 µl $CaCl_2$ 0.5 M and incubated at room temperature (RT) for 10 min. The $CaCl_2$/DNA mix was added to a HBS buffer pH 7.1 (280 mM Nacl, 10 mM KCl, 1.5 mM Na2HPO4-2H2O, 12 mM Glucose, 50 mM HEPES), incubated 15 min at RT, and then added onto 239T cells. Cells were incubated at 37°C for 8h. Viral medium was replaced by fresh culture medium DMEM/10% FCS and cells were incubated 48h at 37°C. Viral supernatant was harvested, supplemented with 8 µg/ml polybrene (Sigma Aldrich, MO, USA), filtrated through a 0.45 µm filter (Milian SA,

Geneva, Switzerland) and added to NB cells, preliminary seeded in a 6-well plate the day before, at a density of $2x10^5$ cells per well. After 24h of incubation of NB cells at 37°C, viral supernatant was replaced by fresh DMEM/10% FCS. The SK-N-Be2c and SH-EP cells were treated for two weeks with 5 µg/ml and 1 µg/ml of puromycin (Gibcom Lifes ® Technologies™), respectively.

Immunoblotting

Cells were lysed in RIPA buffer (10 mM Tris-Hcl (pH 7.4), 150 mM NaCl, 5 mM EDTA, 25 mM β-glycerophosphate, 10% glycerol, 1% NP40, 0.25 % Na-deoxycholate, 20 mM NaF, 1 mM Na-pyrophosphate, 1 mM Na_3VO_4 and 1x protease inhibitor cocktail (Complete mini, EDTA-free, Roche, Mannheim, Germany). Cell lysates were centrifugated at 15'000 rpm at 4°C during 15 min. Supernatant was recovered and protein concentration was measured using Bio-rad protein assay (Bio-Rad, CA, USA). 30 µg protein lysate were loaded on Mini-PROTEAN TGX Gels 4-15% 10 wells (Bio-Rad), transferred to PVDF membrane (Bio-Rad). Proteins were detected using monoclonal rabbit antibody for ALK (D5F3®, Cell signaling technologies, MA, USA) and monoclonal mouse antibody for β-Actin (Sigma-Aldrich, MO, USA); using secondary antibody goat anti-Rabbit IgG/HRP (Dako, CA, USA) and peroxidase AffiniPure goat anti-mouse IgG (Jackson ImmunoResearch, UK); using WesternBright Sirius Kit or WesternBright Quantum kit (Advansta, CA, USA).

***In vivo* studies**

Animal experiments were carried out with athymic Swiss nude mice (Crl:NU(Ico)-Foxn1^{nu}) and NOD-SCID-γ (NSG™) mice in accordance with established guidelines for animal care of the Swiss Animal Protection Ordinance and the Animal Experimentation Ordinance of the Swiss Federal Veterinary Office (FVO). Animal experimentation protocols were approved by the Swiss FVO (authorization numbers: VD2995 and VD3372). All reasonable efforts were made to reduce suffering, including anesthesia for painful procedures. For surgical procedures, mice were anaesthetized using isoflurane (Baxter) and received paracetamol as analgesia the day before the surgery. For orthotopic implantations, $5x10^4$ NB cells were resuspended in 10 µl of PBS and injected in left adrenal gland of 6 mice per groups as previously

described[193,194]. Briefly, the implantation was performed through an incision above the kidney practiced under microscope and incisions were closed with continuous suture. Tumor growth were followed by ultrasound every 7 to 14 days at the Cardiovascular Assessment Facility (University of Lausanne, UNIL). For subcutaneous implantation, groups of 6 mices were injected in the right flank with $5x10^5$ cells suspended in 200 ul 1:1 mix of DMEM and BD Matrigel™ Basement Membrane Matrix (BD Biosciences, Bedford, MA, USA). The grafted animals were then twice weekly monitored with calipers for tumor growth assessment. The tumor volume was calculated using the formula: volume = 4/3×π×(depth×sagittal×transversal)/6 for ortho tumors and volume = (length x $width^2$)/2 for sc tumors. For both orthotopic and subcutaneous implantation mice with tumor volumes around ~1000 mm^3 were sacrificed using CO_2. The tumors were split into pieces for paraffin-embedded tissue, RNA or protein extraction (snap frozen in liquid nitrogen), and tumor cell dissociation.

Tumor cell dissociation and establishment of tumor-derived cell

Tumors were cut into fragments and further mechanically minced using sterile scissors. The tumor tissues were enzymatically digested using the Tumor Dissociation Kit (Miltenyi Biotec, USA) and gentleMACS™ Dissociator (Miltenyi Biotec, USA) according to the manufacturer's instructions, followed by filtration through CellTricks® (50µm, Partek, Germany). Viable cells were propagated like parental cells and called tumor-derived cells (TDC).

Immunohistochemistry

All immuno-labeling were performed at the Lausanne Mouse Pathology Facility (UNIL). Hematoxylin and eosin (H&E) staining was performed on all subcutaneous and orthotopic tumors. Immunohistochemistry (IHC) was performed using monoclonal rabbit antibody for ALK (D5F3®, Cell signaling technologies). Human cells in mouse lungs were detected by ISH experiments, performed at the Histology Core Facility of the EPFL using the Alu positive probe II (Roche Diagnostics, Cat. No. 05272041001) and the Ventana Discovery ULTRA automate (Roche Diagnostics, Rotkreuz, Switzerland). For each mice, 3 lungs sections distant from 300 µm/mice were analyzed

for subcutaneous models and imaged using a BX43 Olympus microscope and the CellSens Entry 1.18 imaging software (LEAD Technologies, Inc.).

RNA isolation

Total RNA from cell line and tumors were extracted using RNeasy or miRNeasy mini kit (Qiagen, Germany), respectively. RNA concentration was measured using a Nanodrop (Agilent Technologies, CA, USA). For the RNA sequencing, each RNA tumor was quantified by Qubit Fluorometer (Life Technologies) and RNA integrity was verified using the Agilent 2100 Bioanalyzer system (Agilent Technologies).

RNA sequencing

RNAseq was performed at the iGE3 Genomics platform (University of Geneva). The total RNA ribo-zero gold kit from Illumina was used for the library preparation with 200 ng of total RNA as input. Library molarity and quality were assessed with the Qubit and Tapestation using a DNA High sensitivity chip (Agilent Technologies). Libraries were pooled at 2 nM and loaded for clustering on 2 lanes of a Single-read Illumina Flow cell. Reads of 100 bases were generated using the TruSeq SBS chemistry on an Illumina HiSeq 4000 sequencer.

Real-Time qPCR

CDNA were prepared from 0.5 µg of RNA using PrimeScript™ reagent kit according to the manufacturer's instruction (TAKARA Bio Inc., Shiga,Japan). The expression level of selected genes identified by RNA sequencing was validated by semi-quantitative real-time PCR (RT Q-PCR) using the Rotor Gene 6000 real-time cycler (Corbett). Cycling conditions were 5 min at 95°C, 40 cycles of 10 sec at 95°C, 20 sec at 60°C, and 1 sec at 72°C with the QuantiFast SYBR® green kit (Qiagen). The expression level ratio of each selected genes was evaluated relatively to the level of the housekeeping gene *HPRT1* using the ΔC_t method.

Human specific pairs of primers:

VAV1 (5'-AAAGAGAACCATCAGCAGGC-3' and 5'-TCTTGATGATGTCACCCTCC-3')

RAC2 (5'-ACTGAAGGAGAAGAAGCTGG-3' and 5'-CGAACACGGTTTTCAGGCC-3')

FYN (5’- CAGAGCTGGTCACCAAAGG-3’ and 5’-TCATGCAGAGAGATGGGC-3’)

ETV5 (5’-AGCTCTTCAGAATCGTGAG-3’ and 5’-TCTCGATCTGAGGAATGCAG-3’)

ITGAV (5’-CATGCCACCAAGCTTTGGC-3’ and 5’-ACAGTGATAACTGGTCTGGC-3’)

HPRT1 (5’-TGACACTGGCAAAACAATGCA-3’ and 5’ GGTCCTTTTCACCAGCAAGCT-3’)

Cell viability

Tumor-derived cells ($5x10^3$) in 100 µl DMEM/10% FCS were plated in quadruplicates in a 96-well plate (Thermo Scientific ™, USA). After 24h the culture media was aspirated and 100 µl fresh DMEM/10% FCS was added containing the following compounds: doxorubicin (Sigma-Aldrich) and cisplatin (Sigma-Aldrich) (0.01, 0.1, 0.5, 1 and 10 µM), and lorlatinib (Sigma-Aldrich) (0.001, 0.01, 0.1, 0.5, 1, 2, 5, 10, 20 µM). Dimethyl sulfoxide (DMSO, Sigma-Aldrich) was used to dissolve the compounds. DMSO concentrations fixed at the maximal concentration used for the compounds (10 or 20 µM) was used as the vehicle controls. Water was added in the border of the plate to reduce evaporation and cells were incubated at 37°C. Cell viability was assessed after 48h using the proliferation kit CellTiter 96® Aqueous Non-radioactive Cell proliferation Assay (Promega, WI, USA) according to the manufacturer’s protocol. OD was measured using Hidex Sens Microplate Reader (Hidex, Finland). Cell culture medium was used to calculate background signal that was subtracted from all measurements. Normalized dose-response curves were generated by non-linear regression and IC_{50} values were calculated with GraphPad Prism 5.04 software (GraphPad Software, Inc.).

ETV5 expression after lorlatinib treatment

Tumor-derived cells ($2x10^5$) were plated in 6-well plates in DMEM/10% FCS. After 24h the media was aspirated, and fresh media with or without lorlatinib (2 µM) was added. After 8h cells were detached with trypsin and total RNAs were extracted with RNeasy kit (Qiagen) as described above.

Statistical analysis

Statistical significance of results was analyzed using one-way ANOVA analysis using GraphPad Prism 5.04 software (GraphPad Software, Inc.).

Bioinformatics analysis

All bioinformatic analysis were performed by Dr. Viviane Praz. SK-N-Be2c (T_Be) and SHEP (T_SHEP) RNAseq samples were analyzed separately, as two independent experiments.

Mapping:

For all samples, fastq files with 100 nucleotides long single-end reads were mapped with STAR version 2.5.2b on both the Human genome version Hg19 and the Mouse genome version Mm10 simultaneously. The following options were changed from the default parameters: --outSAMmultNmax 50 --outFilterMatchNminOverLread 0.4 --quantMode TranscriptomeSAM. Transcriptome annotations in gtf format for both organisms were downloaded from the gencode website (https://www.gencodegenes.org).

Per gene quantification:

Reads mapped on the transcriptomes of the two organisms were then parsed and split in one file per organism with an in-house per script. Reads with matches on both Human and Mouse were discarded from the Mouse file. Per-gene quantification was then calculated independently for each organism using rsem version 1.3.0. Counts and rpkm values were extracted in two tables.

Expression analysis:

All RNAseq per gene data quality checks and analysis were done in RGenes with a log2(rpkm) value above 1 in at least one sample were kept, thus corresponding to 17912 genes in SHEP and 18065 in SK-N-Be2c tumors for Human data. Principal Component Analysis were done using the log2(rpkm) values. Clustering analysis were performed on the scaled log2(rpkm) values using euclidean distance measures and the ward.D2 agglomeration method. Differential analyses were performed using the

raw data counts in the DESeq2 package (Bioconductor, bioconductor.org). For each comparison, the cutoffs for fold-change (FC) and adjusted p-values to call differentially transcribed genes were set to 1 and 0.05, respectively.
Heatmaps for sample correlations and for specific gene lists were generated using the heatmap.2 function on DESeq2 normalized counts, in log2.

Functional analysis:
Functional analysis was performed in two different ways : 1) by using the GseaPreranked mode in the GSEA java applet from the BROAD Institute (*https://software.broadinstitute.org › gsea).* For each comparison, the data was ranked according the log2(FC) between the two compared conditions. 2) by applying a hypergeometric test on selected genes lists against gene sets from GO (Molecular Function, Biological Process and Cellular Component), KEGG pathways, REACTOME pathways, or BIOCARTA pathways. The gene lists used in the test were generated by either applying the above-mentioned cutoffs for FC and adjusted p-value for each comparison, or by intersecting those lists to obtain genes having a similar response in different comparisons.

ALK Activity Score Calculations:
Differentiation pathways gene expression of the ALK signatures was quantified by defining a rank-based pathway activity score. Genes were ranked according to decreasing expression levels for each RNAseq separately. The ranks of the genes in the ALK signature were summed up for each tumor. For each gene signature, the rank sums were divided by the average rank sum for the cohort, followed by log2 transformation, thus giving a cohort-comparative score for each tumor. A pathway activity score of zero corresponds to cohort average activity for the pathway, a positive value corresponds to above cohort average activity, and a negative value corresponds to below average activity.

RESULTS

ALK-overexpression has no impact on the growth of SK-N-Be2c tumors and has limited consequences on their transcriptomes

We aimed to compare the genes and signaling pathways mediated by the distinct ALK variants *in vivo*. For this purpose, the ALK-wt, ALK$^{-F1174L}$ and ALK$^{-R1275Q}$ variants were stably expressed through lentiviral transduction in the MYCN-amplified and tumorigenic SK-N-Be2c cell line. Although SK-N-Be2c-pLIV cells express a weak level of the endogenous ALK-wt protein, a strong overexpression of the three ALK variants was obtained (Figure 1A). The transduced cells were injected orthotopically in the adrenal gland of athymic Swiss mice. Mice engrafted with the SK-N-Be2c cells (6 mice/groups) developed tumors within 40 days, and ALK-overexpression had no impact on tumor growth (Figure 1B). The expression of ALK in the SK-N-Be2c tumors was assessed by IHC staining. It confirmed the overexpression of ALK in ALK-wt, ALK$^{-F1174L}$ and ALK$^{-R1275Q}$ tumors relative to the control pLIV. Moreover, we also observed a low expression of ALK in the SK-N-Be2c control group (Figure 1C).

The histologic analysis showed that all SK-N-Be2c tumors were stroma-poor tumors with undifferentiated or poorly differentiated neuroblasts. Thus, ALK-overexpression did not affect the histologic phenotype (Figure 1D).

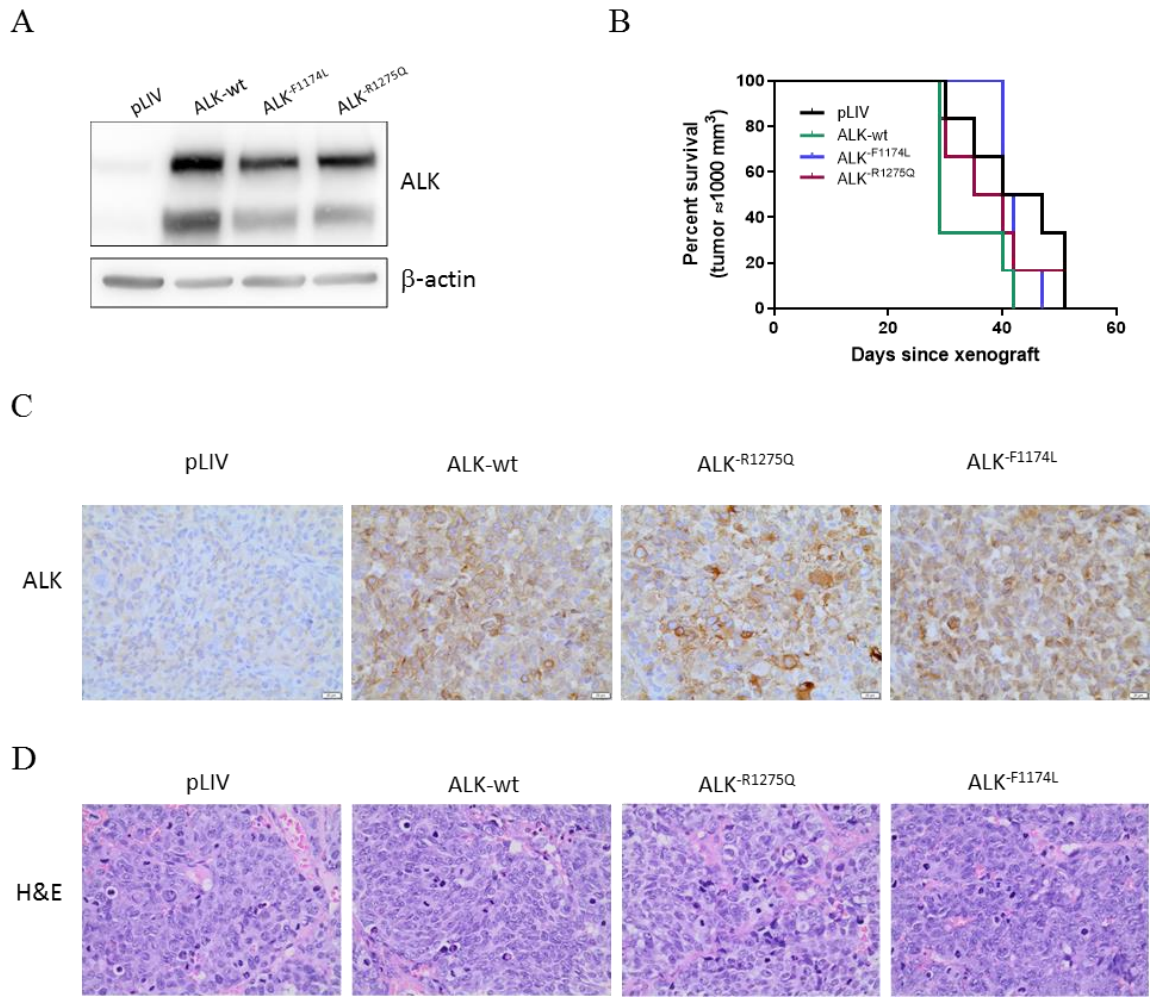

Figure 1. ALK overexpression has no impact on the SK-N-Be2c tumor growth. (A) Establishment of SK-N-Be2c ALK-overexpressing cell lines. The expression of ALK was analyzed by western blot in SK-N-Be2c transduced cell lines. **(B)** Tumor growth of the SK-N-Be2c tumors. Survival curve comparison show not statistical difference between the groups (log rank test). N= 6 mice/group. **(C)** Representative images of ALK expression in SK-N-Be2c tumors (x40, scale bar = 20 µm). **(D)** Representative images of H&E staining in SK-N-Be2c tumors (x40).

The transcriptional consequences of ALK overexpression were investigated by RNA sequencing on four SK-N-Be2c-derived tumors per group. Unsupervised hierarchical clustering showed that SK-N-Be2c tumors were not clustered in distinct groups, reflecting a homogeneity of the transcriptional profiles among the groups of tumors (Supplementary Figure S1). Moreover, as the tumor SK-N-Be2c_F1 was very distant from its group, it was removed for the bioinformatic analysis (Supplementary Figure S1). Genes with a log2(fold-change)≥ 1 or ≤ -1 and an adjusted p value ≤ 0.05 were considered as differentially expressed (DE). The number of DE genes relative to control tumors was higher in the ALK$^{-F1174L}$ tumors (963 genes) than in ALK-wt (282

genes) and ALK$^{-R1275Q}$ expressing tumors (102 genes), with a majority of downregulated genes (Figure 2A). *PCDHB7* and *PCDHB8* were the genes deregulated with the lowest FC and p-value in the ALK$^{-F1174L}$ tumors (Figure 2B).

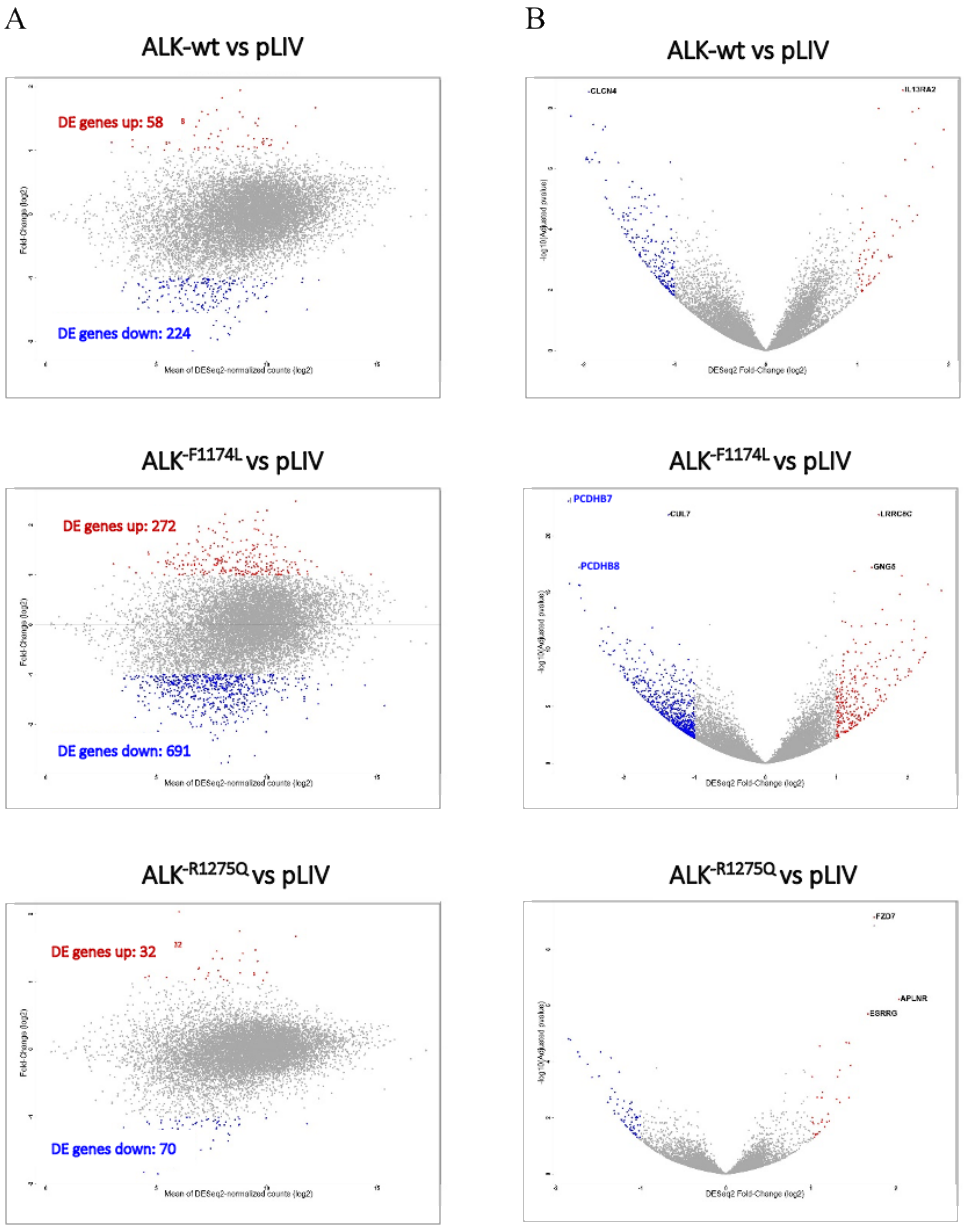

Figure 2. RNA sequencing analysis of SK-N-Be2c ALK-overexpressing tumors relative to control pLIV. (A) MVA plots representing the genes detected in ALK-expressing tumors relative to pLIV, plotted according to their log2(mean normalized counts) and log2(FC) with the DE genes upregulated (noted in red) and downregulated (noted in blue) genes. **(B)** Volcano plots representing the genes detected in ALK-expressing tumors relative to pLIV, plotted according to their log2(mean normalized counts) and log2(FC) with the DE genes upregulated (noted in red) and downregulated (noted in blue) genes. *PCDHB7* and *PCDHB8* are highlighted in blue in ALK$^{-F1174L}$ vs pLIV tumors.

The analysis of common and specific DE genes revealed 80 genes shared by the three groups of ALK-expressing tumors relative to the control group (Figure 3A). ALK$^{-F1174L}$ tumors displayed 75% of specific genes (727 genes), while 20% of specific genes were found in ALK-wt tumors (57 genes) and only 5% were specific to the ALK$^{-R1275Q}$ group (5 genes) (Figure 3A). Interestingly, for each paired comparison between ALK-overexpressing tumors, all the DE genes in common were positively correlated and the majority were downregulated (Figure 3B).

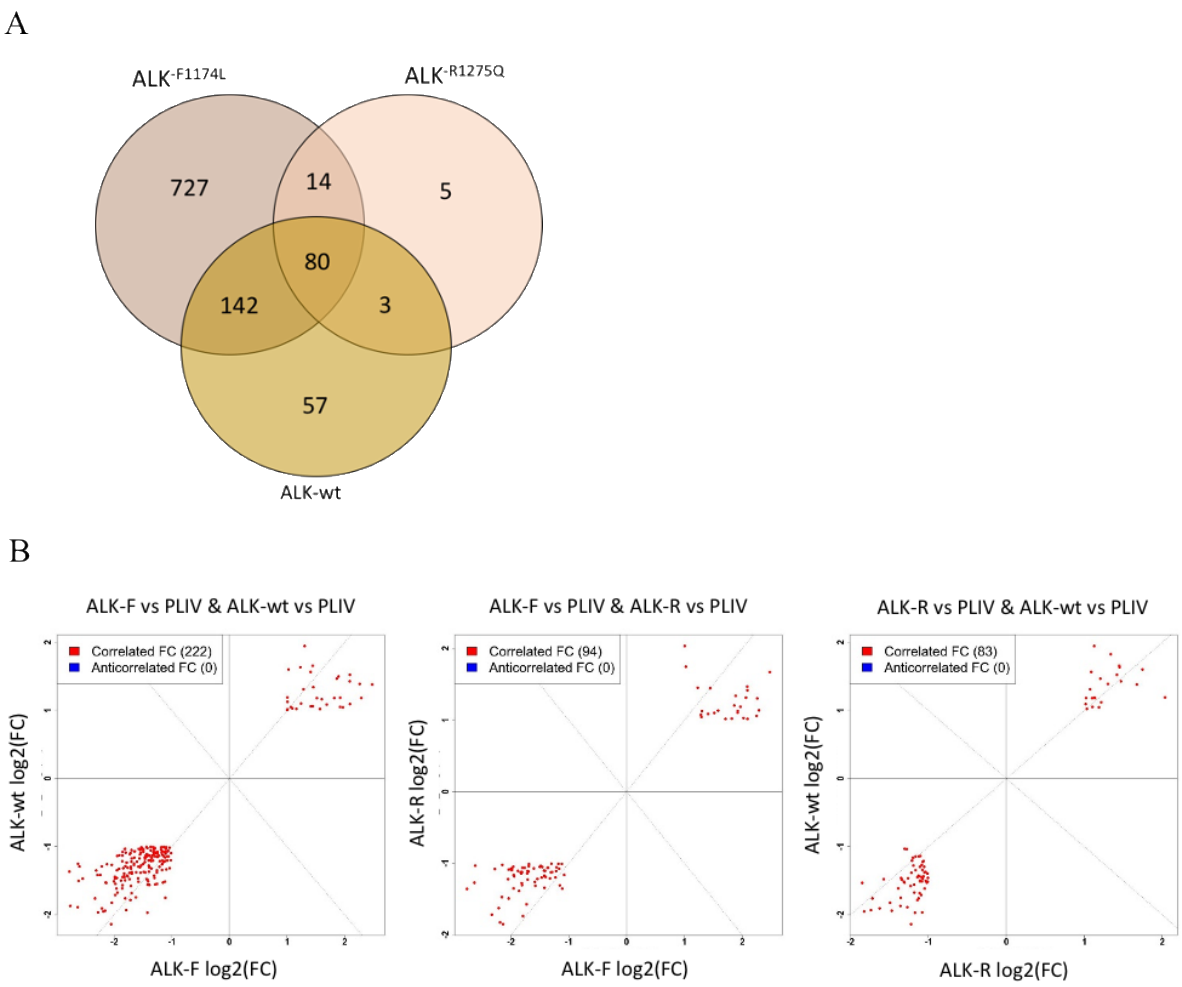

Figure 3. Number and correlation of the DE genes in ALK-expressing SK-N-Be2c tumors relative to control pLIV. (A) Venn diagram representing the common and specific DE genes in ALK-overexpressing tumors vs pLIV. **(B)** Graphs illustrating the DE genes found in common between the different tumor groups plotted according to the log2(FC) in ALK$^{-F1174L}$ and ALK-wt (left panel), ALK$^{-F1174L}$ and ALK$^{-R1275Q}$ (middle panel), and ALK$^{-R1275Q}$ and ALK-wt (right panel). Positively correlated genes are labelled in red, and anticorrelated (negatively correlated) genes in blue.

Overall, we observed the downregulation of several protocadherins (PCDH) in all ALK-overexpressing tumors, more specifically in the ALK$^{-F1174L}$ tumors (Figure 4). Protocadherins are a major subfamily of cadherins playing an important role in cellular interactions and cranial NCCs migration in embryonic development[195]. They are organized as non-clustered or clustered PCDH, the latter comprising the vast majority of the subfamily members[196]. We measured by RT Q-PCR the expression of each protocadherin cluster (Figure 5A), and the 8 protocadherins found deregulated in common in ALK-overexpressing tumors (Figure 5B). However, these analyses showed a relatively small difference in the level of gene expression, mainly due to the heterogenous expression level of the PCDH analyzed in the control tumors (Figure 5).

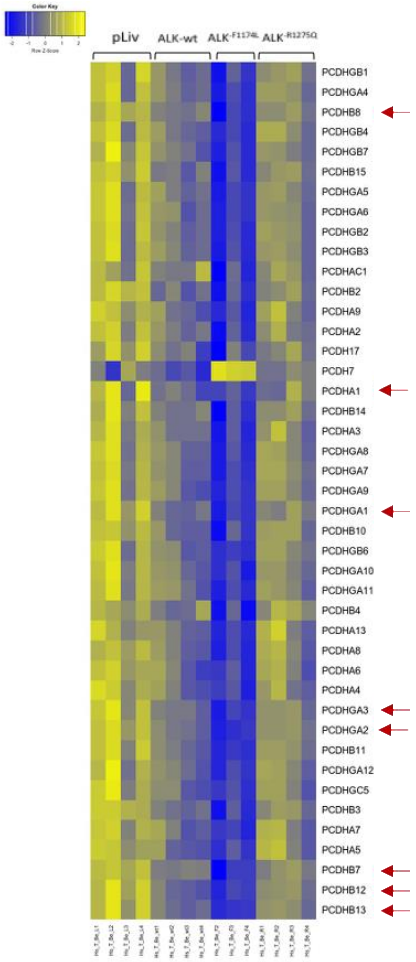

Figure 4. Expression of protocadherins in SK-K-N-Be2c-derived tumors. Heatmap illustrating the expression (z-score) of the protocadherins in control pLIV and ALK-expressing tumors. The protocadherins selected for validation are highlighted by red arrows.

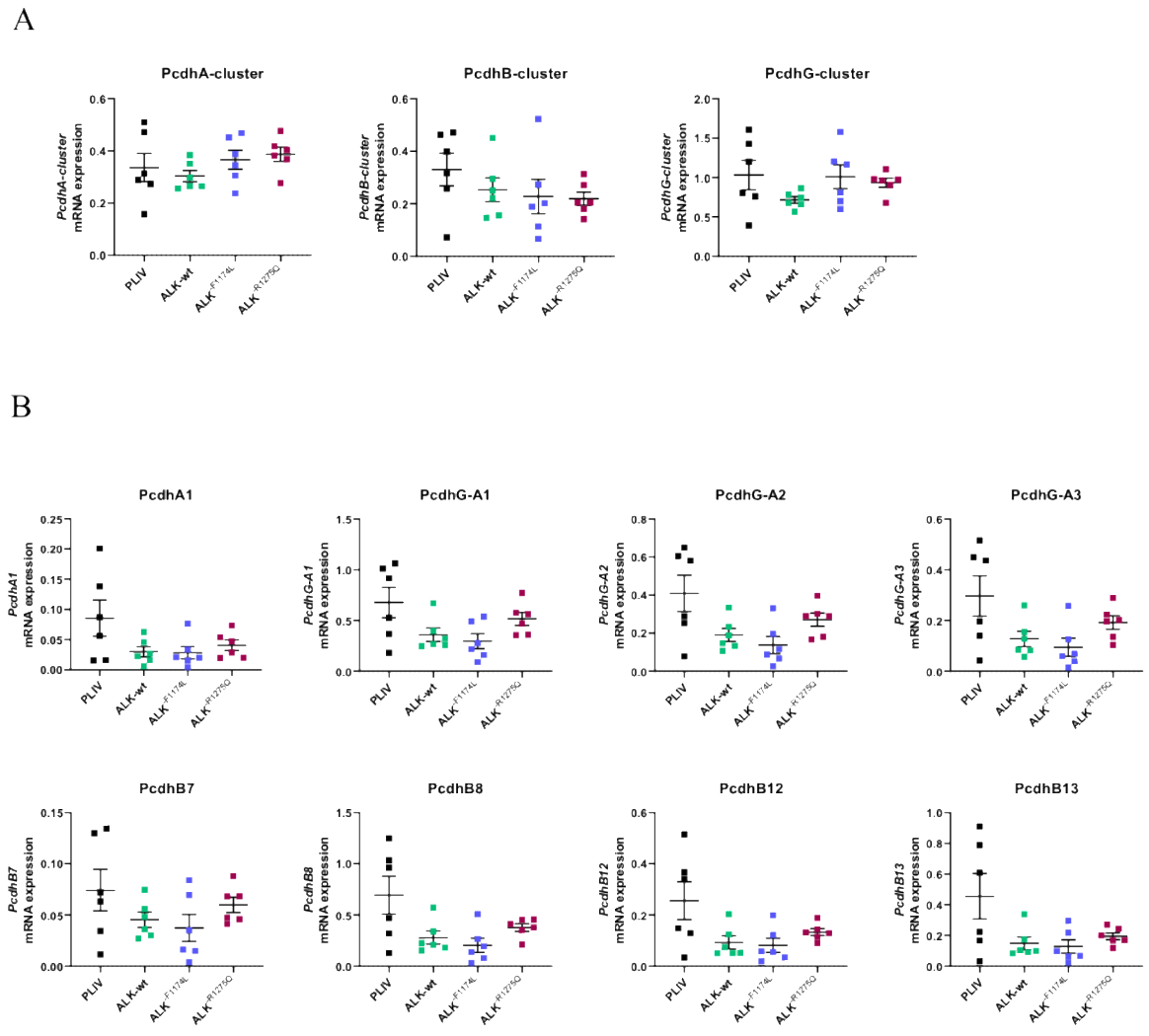

Figure 5. mRNA expression of protocadherins assessed by RT Q-PCR in SK-N-Be2c tumors. (A) mRNA expression ratio of the protocadherin α-cluster, β-cluster and γ-cluster. **(B)** mRNA expression ratio of the 8 protocadherins deregulated in common in ALK-overexpressing tumors vs pLIV. PCDH mRNA expression level relative to the *HPRT1* control gene are shown. One-way Anova multiples comparisons. pLIV n=6; ALK-wt n=6; ALK$^{-F1174L}$ n=6; ALK$^{-R1275Q}$ n=6.

The overexpression of ALK had a limited impact in this model, on the tumor growth, as well as well as on the results obtained by RNA sequencing and first validations. These results prompted us to conduct our further investigations in a weakly tumorigenic NB cell line.

ALK-overexpression increases the tumor growth capacity of the weakly tumorigenic SH-EP cell line

The ALK-wt, ALK$^{-F1174L}$ and ALK$^{-R1275Q}$ were stably expressed in the MYCN non-amplified and weakly tumorigenic SH-EP cell line. The transduced SH-EP cells were injected into NOD-SCID-γ mice subcutaneously to ensure tumor growth and avoid an invasive surgery. While no protein expression was detectable in SH-EP-pLIV cells, a strong expression of ALK was observed with the three ALK variants (Figure 6A). All mice implanted with SH-EP cells (6 mice/groups) developed tumors, and ALK$^{-F1174L}$ strongly enhanced their growth capacities, with mice developing tumors of 1000 mm^3 in 50 days as compared to 95 median days for the control group (Figure 6B). Although not statistically significant, tumor growth was also increased by ALK-wt overexpression, while the overexpression of ALK$^{-R1275Q}$ had no impact (Figure 6B).
The overexpression of ALK in ALK-wt, ALK$^{-F1174L}$ and ALK$^{-R1275Q}$ tumors relative to the control was confirmed by IHC staining (Figure 6C). The histologic analysis after H&E staining showed that ALK-overexpression altered the histology of SH-EP tumors. Indeed, tumor cells of the control group were characterized by the presence of mainly fusiform cells, with larger cytoplasm and were rich in collagenous stroma, reflecting a mesenchymal phenotype. ALK-wt and ALK$^{-R1275Q}$ tumors displayed heterogeneous profile, with either region with fusiform/spindle cells and stroma-rich regions, and areas composed of differentiated and/or differentiating neuroblasts (Figure 6D). Interestingly, ALK$^{-F1174L}$ tumors were mainly composed of undifferentiated/poorly differentiated neuroblasts, as reflected by the presence of small round blue cells (Figure 6D).

Altogether, these results show that ALK$^{-F1174L}$ increased the tumorigenic potential of the SH-EP cell line and may potentially favor a switch toward poorly differentiated neuroblasts.

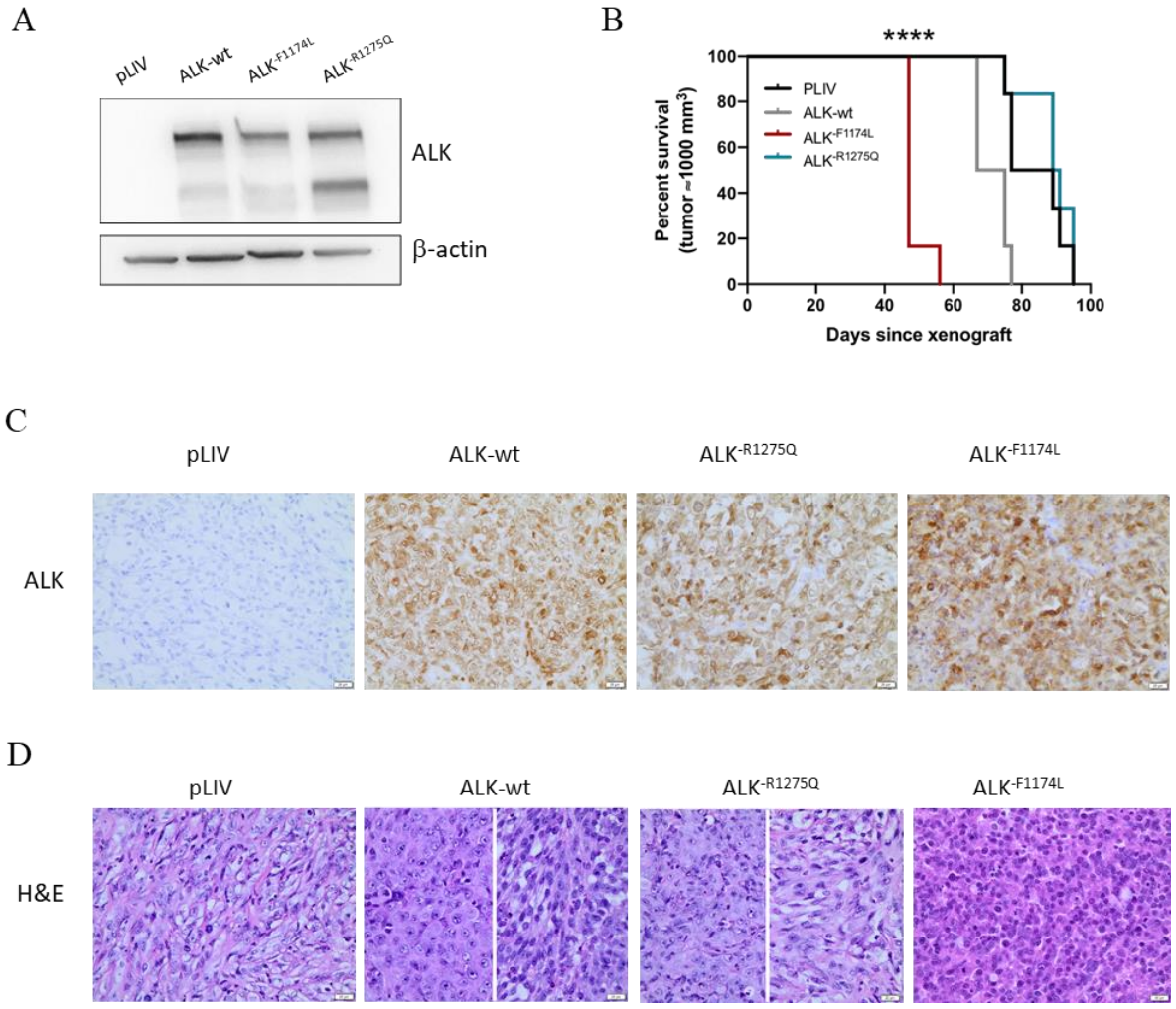

Figure 6. ALK overexpression increases the tumor growth properties of SH-EP cells. (A) Establishment of SH-EP-ALK-expressing cell lines. The expression of ALK was analyzed by western blot in SH-EP transduced cell lines. **(B)** Tumor growth of the SH-EP tumors. Survival curve comparison, Log-rank test, ****p<0.0001. Not significative results are not shown. N= 6 mice/group. **(C)** Representative images of ALK expression in SH-EP tumors (x40, scale bar = 20 μm). **(D)** Representative images of H&E staining of SH-EP tumors. For ALK-wt and ALK^{R1275Q} tumors, left images represent regions with differentiated and/or differentiating neuroblasts, and right images represent stroma-rich regions (x40, scale bar = 20 μm).

Impact of deregulated ALK activation on the transcriptome of SH-EP tumors

The transcriptional consequences of ALK overexpression were investigated by RNA sequencing of the SH-EP-derived tumors. Unsupervised hierarchical clustering showed that the tumors were clustered in distinct groups according to their ALK status, reflecting the expected heterogeneity among the different groups of tumors. However, one ALK$^{-R1275Q}$ tumor was clustered with the ALK$^{-F1174L}$ group (SH-EP_R6) and was thereby removed for the bioinformatic analysis (Supplementary Figure S2). Moreover, the hierarchical clustering and PCA analysis highlighted a proximity between ALK-wt and ALK$^{-F1174L}$ tumors (Supplementary Figure S2).

Genes with a log2(fold-change)≥ 1 or ≤ -1 and an adjusted *p* value ≤ 0.05 were considered as differentially expressed (DE). All ALK-overexpressing tumors displayed a high number of DE genes relative to control, as shown by the MVA plots for ALK-wt (1634 genes), ALK$^{-F1174L}$ (1369 genes) and ALK$^{-R1275Q}$ (1439 genes) (Figure 7A). Moreover, they all exhibited more upregulated than downregulated genes (Figure 7A). The Volcano plot of the DE genes of each group of ALK-expressing tumors first confirmed the overexpression of *ALK* in all groups (Figure 7B). Second, it revealed the strong downregulation of *VAV1* in ALK-wt and ALK$^{-F1174L}$ tumors and to a lesser extend in ALK$^{-R1275Q}$ tumors (Figure 7B). Of interest, low levels of *VAV1* expression are associated to a decrease in overall and event-free survival in a cohort of 498 NB patients[197] (Supplementary Figure S3). *VAV1* was thereby considered as an interesting target for further investigations.

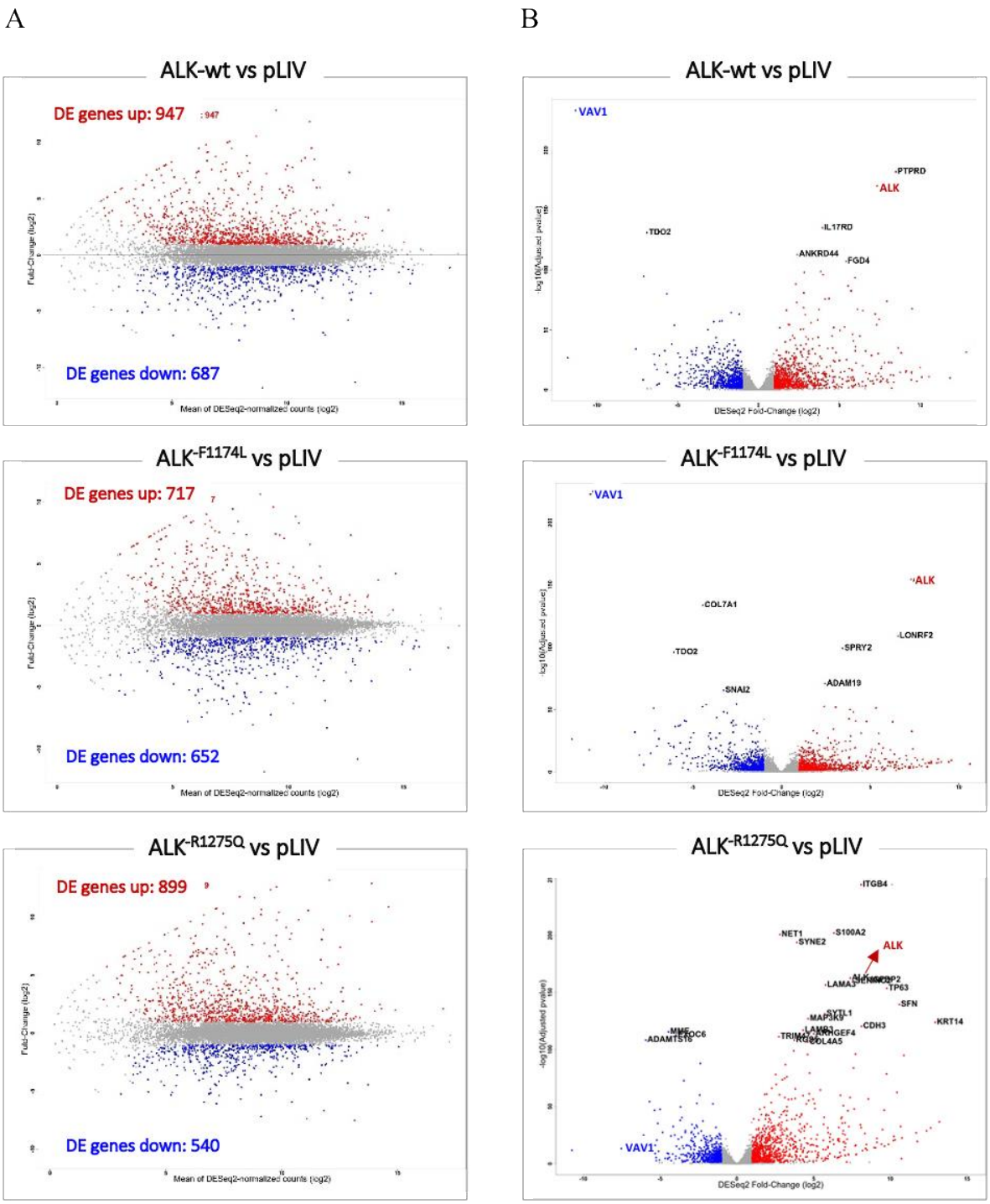

Figure 7. RNA sequencing analysis of SH-EP-ALK-overexpressing tumors relative to control pLIV tumors. (A) MVA plots representing the genes detected in ALK-expressing tumors relative to pLIV, plotted according to their log2(mean normalized counts) and log2(FC) with the DE genes upregulated (noted in red) and downregulated (noted in blue) genes. **(B)** Volcano plots representing the genes detected in ALK-expressing tumors relative to pLIV, plotted according to their log2(mean normalized counts) and log2(FC) with the DE genes upregulated (noted in red) and downregulated (noted in blue) genes. *VAV1* and *ALK* are highlighted in blue and red, respectively.

The three groups of ALK-expressing tumors shared 416 DE genes relative to the control tumors (Figure 8A). Interestingly, the ALK-wt and ALK$^{-F1174L}$ tumors shared the highest number of DE genes (915 genes), while 567 and 666 genes were found in common between ALK$^{-F1174L}$ and ALK$^{-R1275Q}$, and ALK$^{-R1275Q}$ and ALK-wt, respectively (Figure 8A). We investigated the correlation of the common DE genes between ALK-expressing tumors. For ALK$^{-F1174L}$ and ALK-wt tumors, almost all genes were positively correlated, with only 0.8% anti-correlated (8/915 genes) (Figure 8B, left panel). In contrast, the anti-correlated DE genes shared between ALK$^{-F1174L}$ and ALK$^{-R1275Q}$, or ALK$^{-R1275Q}$ and ALK-wt comprised respectively 18.3% (88/567 genes) and 17% (97/666 genes) (Figure 8B, middle and right panel).

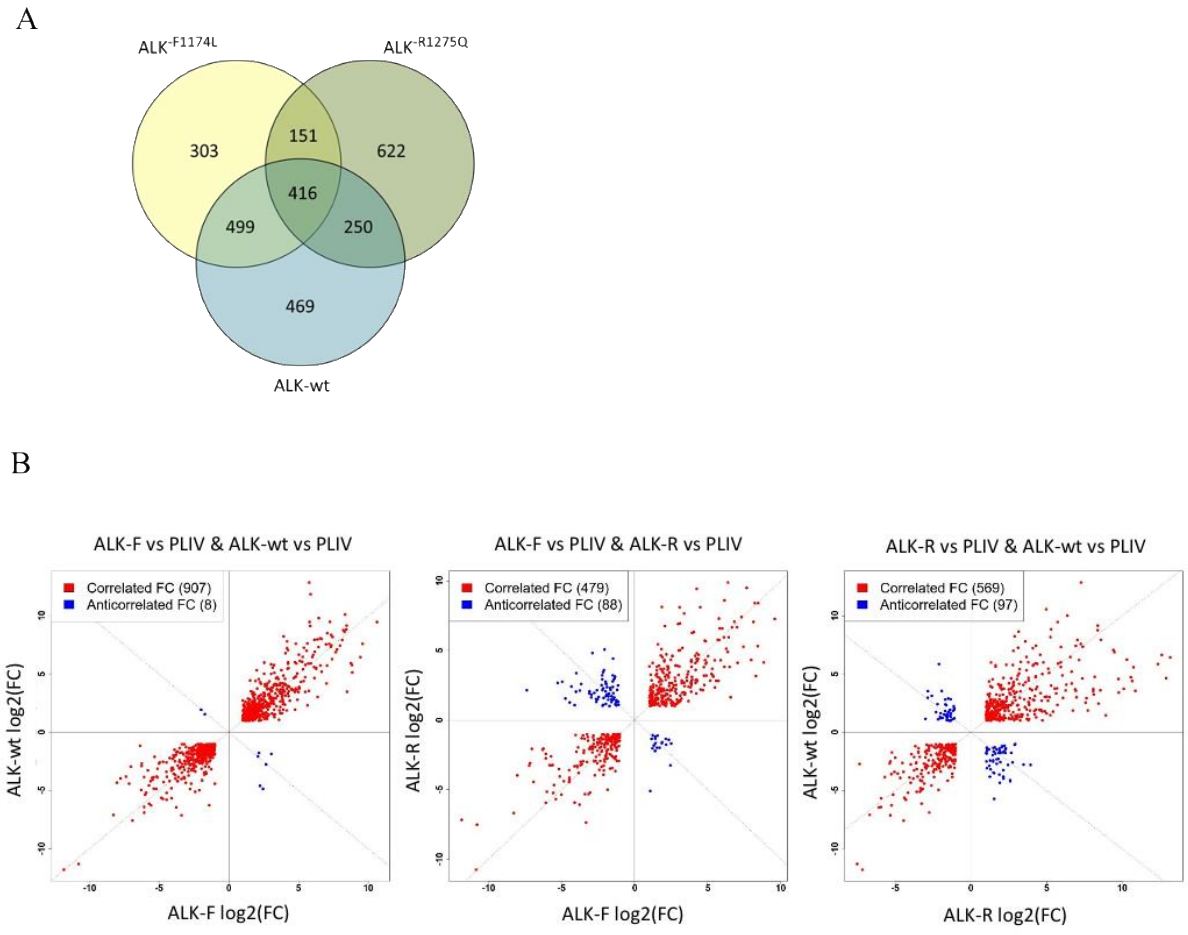

Figure 8. Number and correlation of the DE genes identified in SH-EP ALK-expressing tumors relative to control pLIV. (A) Venn diagram illustrating the common and specific DE genes in ALK-expressing tumors vs pLIV. **(B)** Graphs illustrating the DE genes found in common between the different tumor groups plotted according to the log2(FC) in ALK$^{-F1174L}$ and ALK-wt (left panel), ALK$^{-F1174L}$ and ALK$^{-R1275Q}$ (middle panel), and ALK$^{-R1275Q}$ and ALK-wt (right panel). Positively correlated genes are labelled in red, and anticorrelated (negatively correlated) genes in blue.

As we observed a phenotypic switch in SH-EP ALK-expressing tumors, Gene Set Enrichment Analysis (GSEA) were conducted for the ADRN and MES signature[46]. The results showed a significant enrichment of the ADRN signature in SH-EP ALK-wt and ALK$^{-F1174L}$ tumors (Figure 9A). In contrast, the ALK$^{-R1275Q}$ tumors were not significantly enriched neither for the MES and the ADRN signature relative to control tumor (data not shown). However, the MES signature was significantly enriched in the ALK$^{-R1275Q}$ tumors relative to ALK-wt and ALK$^{-F1174L}$ tumors (Figure 9B).

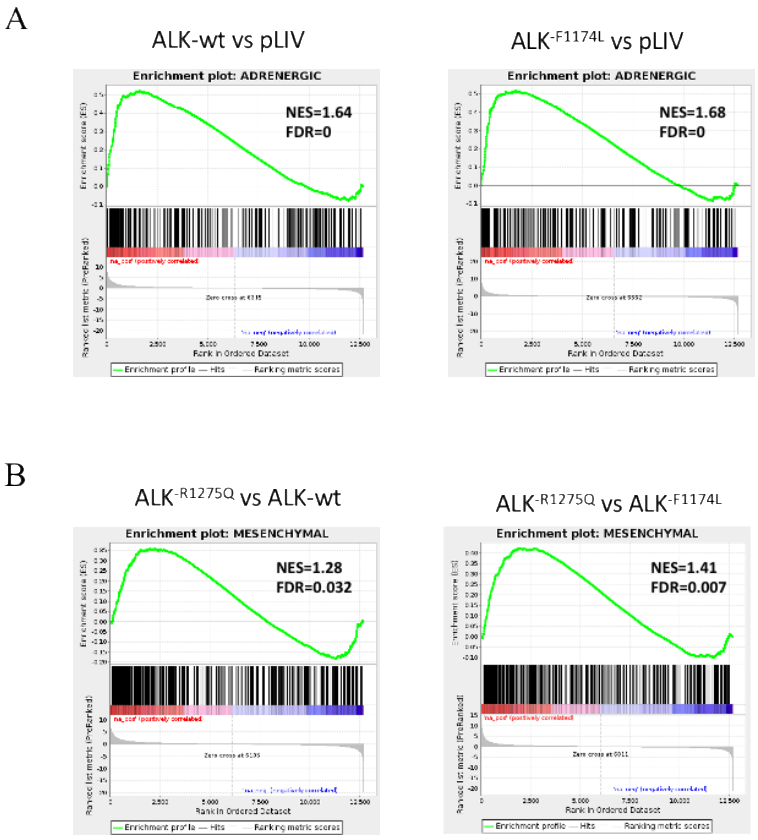

Figure 9. Enrichment of ADRN and MES signatures in SH-EP-derived tumors. (A) Enrichment plots of ADRN signature in ALK-wt vs pLIV and ALK$^{-F1174L}$ vs pLIV tumors. **(B)** GSEA analysis for enrichment in MES signature in ALK$^{-R1275Q}$ vs ALK-wt and ALK$^{-F1174L}$ tumors.

Taken together, the results show a higher correlation between ALK-wt and ALK$^{-F1174L}$ tumors. This was observed by the PCA and hierarchical clustering, as well as by the correlation of the DE expressed genes relative to control. Moreover, the ALK-wt and ALK$^{-F1174L}$ tumors displayed a similar enrichment for the ADRN signature, while ALK$^{-R1275Q}$ tumors displayed an enrichment for the MES signature relative to both ALK-wt and ALF$^{-F1174L}$ tumors.

The ALK-signature score is increased in SH-EP-ALK-expressing tumors

The 77-gene ALK signature has been established based on conserved transcriptional profile in NB cell lines harboring ALK hotspot mutations and further validated in NB primary tumors[186]. Among this signature, we identified 65 genes expressed in the SH-EP tumors, including for example *ETV5*, *DUSP5*, *DUSP6*. To validate the ALK-driven transcriptional consequences in our model, we calculated the enrichment of the ALK-signature in the control and ALK-expressing tumors as described[186]. The ALK-signature score was increased in the ALK-wt and ALK$^{-F1174L}$ relative to the control, as well as in the ALK$^{-R1275Q}$ tumors although we did not observe statistical differences for this latter group of tumors (Figure 10).To note, the ALK-signature was only increased in the SK-N-Be2c ALK$^{-F1174L}$ tumors relative to the control tumors reflecting the low transcriptomic difference of this signature in the ALK-wt and ALK$^{-R1275Q}$ groups (Supplementary Figure S4).

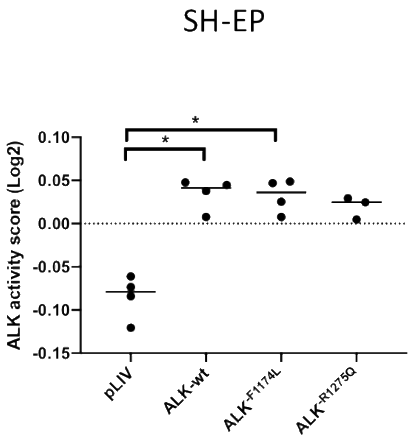

Figure 10. ALK-signature score in SH-EP-derived tumors. One-way Anova multiple comparisons. *p=0.0273 and p=0.0216. Not significant comparisons are not shown.

ALK overexpression deregulate genes involved in pathways related to axon guidance, extracellular matrix and cell-to-cell junction/communication

Gene Ontology (GO) analysis were performed on the DE genes in ALK-wt, ALK$^{-F1174L}$, or ALK$^{-R1275Q}$ vs controls to highlight the deregulated pathways. Figure 11 represents the most striking results (REACTOME). Overall, we observed an anticorrelation between ALK-wt/ALK$^{-F1174L}$ tumors and the ALK$^{-R1275Q}$ tumors, as the enriched pathways downregulated in ALK-wt/ALK$^{-F1174L}$ tumors (Figure 11A and B), were rather upregulated in the ALK$^{-R1275Q}$ tumors relative to the control (Figure 11C).

GO analysis revealed a deregulation of the Axon guidance gene set and pathways related to metastatic dissemination, including Extracellular matrix (ECM), Collagen formation, Hemostasis, Integrin Cell surface interaction, Cell junction organization, Cell communication in all ALK-expressing tumors (Figure 11). In addition, genes involved in the cell surface interactions at the vascular wall were downregulated in ALK$^{-F1174L}$ tumors. We sorted out genes deregulated in ALK-wt, ALK$^{-F1174L}$ and ALK$^{-R1275Q}$ tumors relative to the control tumors or between pairs of ALK-expressing tumors belonging to these pathways, and heatmaps were generated to illustrate their expression profiles in each group of tumors. Overall, the resulting heatmaps revealed similar expression patterns in ALK-wt and ALK$^{-F1174L}$ relative to control and ALK$^{-R1275Q}$ tumors, for either the axon guidance pathway (Figure 12) or pathways related to metastatic dissemination (Figure 13). Globally, the gene sets were downregulated in ALK-wt and ALK$^{-F1174L}$ tumors relative to the control and upregulated in the ALK$^{-R1275Q}$ tumors.

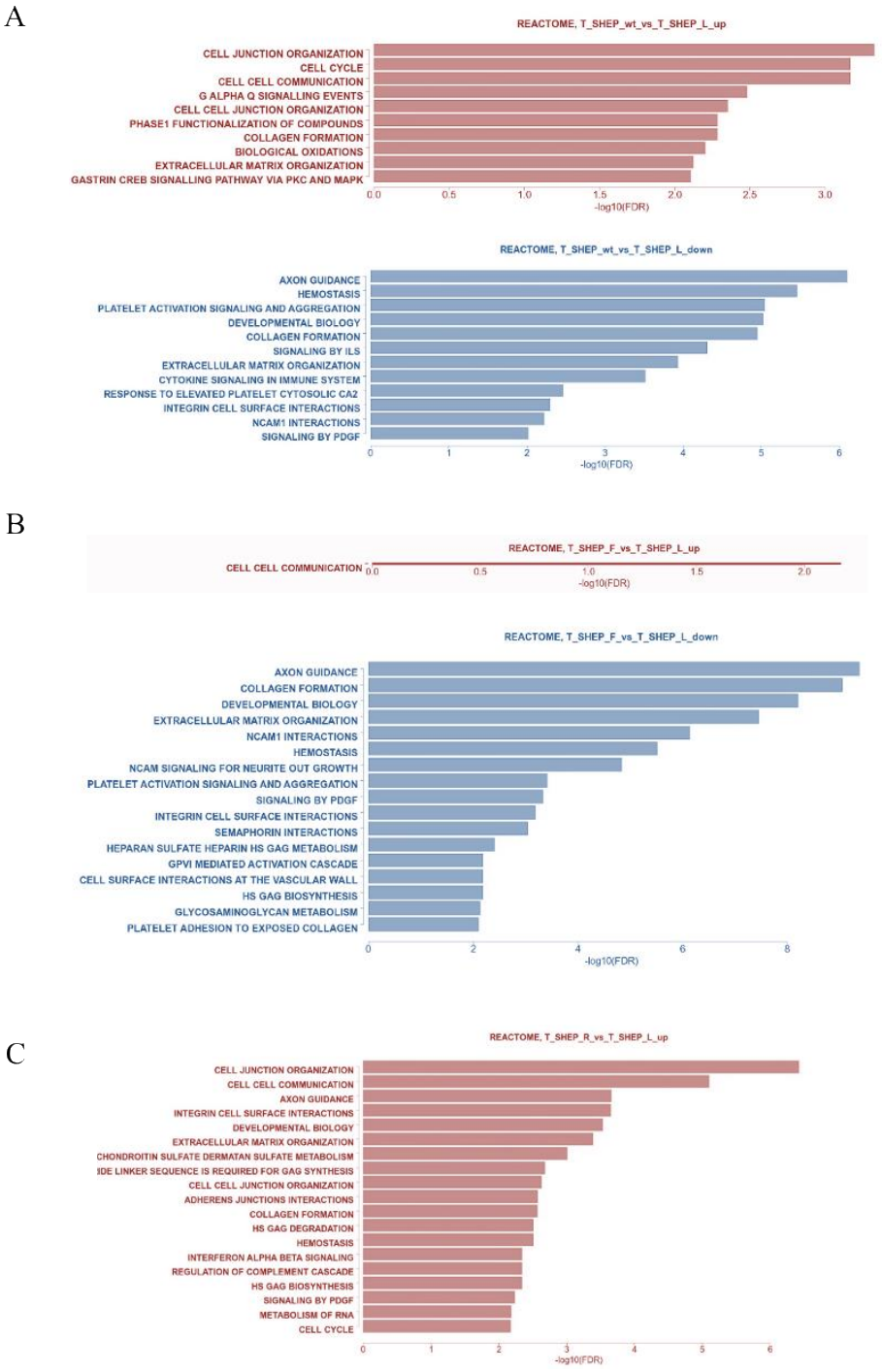

Figure 11. Expression of ALK-wt and ALK activating mutations deregulates pathways related to Axon guidance and ECM in SH-EP-derived tumors. GO analysis performed using either Up- or Down-regulated genes in ALK-expressing tumors vs pLIV. REACTOME_up and _down in **(A)** ALK-wt vs pLIV tumors, **(B)** ALK$^{-F1174L}$ vs pLIV tumors and **(C)** ALK$^{-R1275Q}$ vs pLIV tumors. Upregulated pathways are in red and downregulated pathways are in blue.

Of note, the Axon guidance gene set was the downregulated pathways with the smallest p-value in ALK-wt and ALK$^{-F1174L}$ tumors, and the third most upregulated pathway in ALK$^{-R1275Q}$ tumors (Figure 11). In this pathway, we identified genes belonging to the Slit/Robo family (*SRGAP3*, *SLIT2*), Rho-family (*RAC2*) and several semaphorins and their receptors were deregulated in ALK-overexpressing tumors (Figure 12). Moreover, we selected DE genes belonging both to the Axon guidance gene set and pathways related to EMT and Cell junction, Cell-cell communication. This included *RAC2*, a GTPase member of the Rho-family, *FYN*, a member of the protein-tyrosine kinase oncogene family, and *ITGAV*, an integrin involved in the interaction with the ECM component. In addition to the Axon guidance pathway (Figure 12), *RAC2*, *FYN* and *ITGAV* were found in the pathway Hemostasis, *FYN* and *ITGAV* were observed in Cell surface interaction at the vascular wall, *FYN* was in the pathway Cell-to-cell communication, and *ITGAV* in the Integrin cell surface interaction pathway (Figure 13). *VAV1*, which was the genes deregulated with the lowest FC and p-value in ALK-wt and ALK$^{-F1174L}$ tumors, was found in the pathway linked to homeostasis (Figure 13).

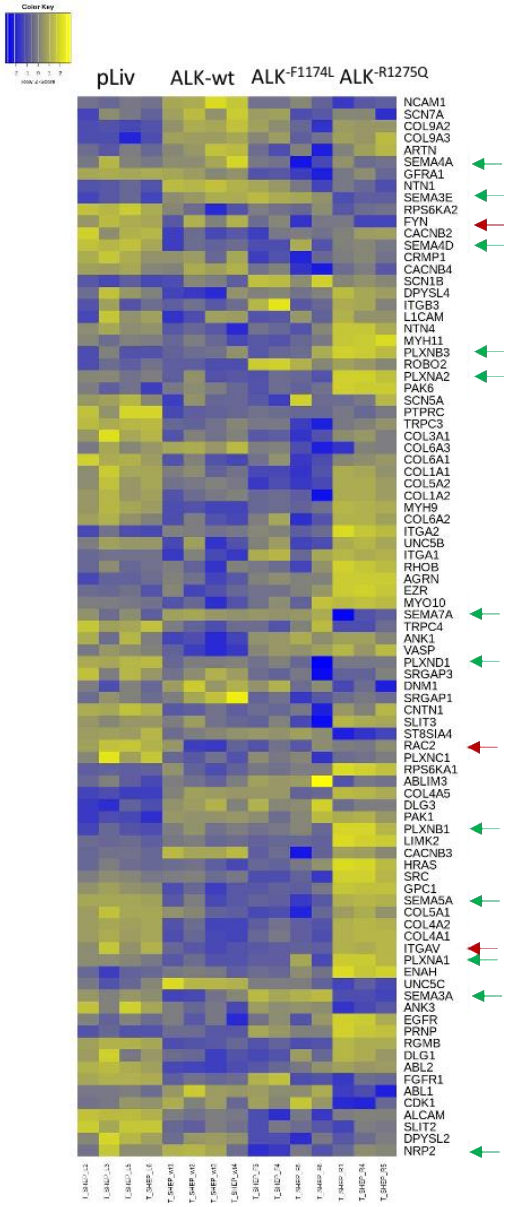

Figure 12. Expression of ALK-wt and ALK activating mutations deregulate pathways related to Axon guidance in SH-EP-derived tumors. Heatmap illustrating the expression (z-score) of the DE genes found in the REACTOME axon guidance pathway for all comparisons. Semaphorins and their receptors are highlighted by green arrows. *FYN*, *RAC2* and *ITGAV5* are highlighted in red arrows.

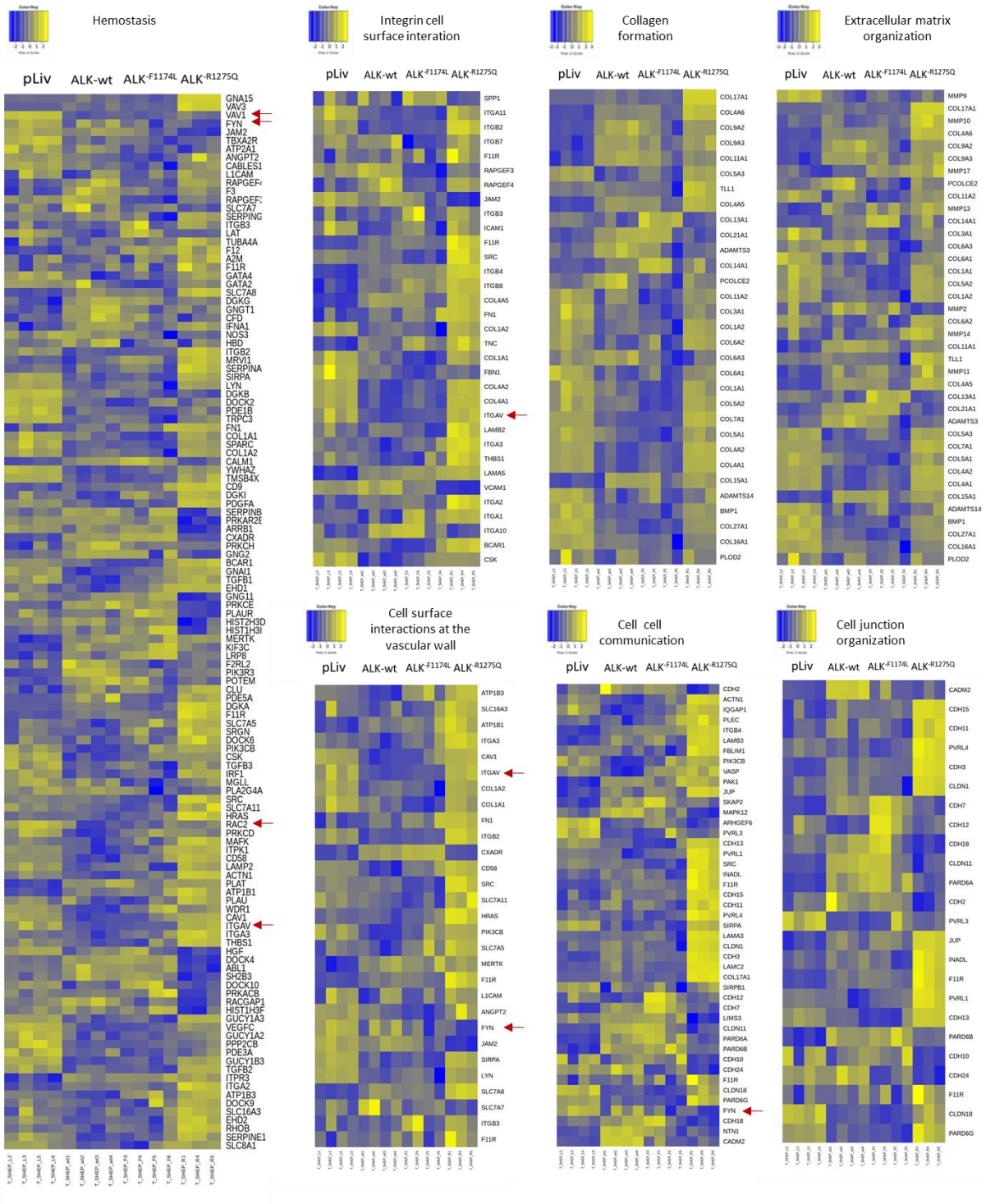

Figure 13. Expression of ALK-wt and ALK mutations deregulate pathways related to ECM and cell junction/communication in SH-EP-derived tumors. Heatmaps illustrating the expression (z-score) of the DE genes belonging to the REACTOME pathways Hemostasis, Integrin cell-surface interaction, Collagen formation, Extracellular-matrix organization, Cell surface interactions at the vascular wall, Cell-cell communication and Cell junction organization for all comparisons. *VAV1, FYN, ITGAV* and *RAC2* are highlighted by red arrows.

These genes were thus selected for further validations. According to the RNA sequencing, *VAV1* was downregulated in all ALK-expressing tumors relative to the control tumors (Figure 14A), *RAC2* in ALK-wt and ALK $^{-F1174L}$ tumors, *FYN* in ALK$^{-F1174L}$ and ALK$^{-R1275Q}$ tumors relative to the controls, *ITGAV* was downregulated in ALK-wt and ALK$^{-F1174L}$ tumors relative to controls (Figure 14A), but upregulated in ALK$^{-R1275Q}$ relative to ALK-wt and ALK$^{-F1174L}$ tumors (Figure 14B). To confirm the results observed by RNA sequencing, the mRNA expression levels of *FYN*, *RAC2*, *ITGAV* and *VAV1* were assessed by RT Q-PCR (Figure 14C). *FYN* expression was decreased in ALK$^{-F1174L}$ and ALK$^{-R1275Q}$ tumors relative to the control although without statistical significance. *RAC2* mRNA levels was decreased in ALK$^{-F1174L}$ and ALK$^{-R1275Q}$ tumors with no statistical difference. The expression of *ITGAV* was statistically increased in the ALK$^{-R1275Q}$ tumors relative to ALK-wt and ALK$^{-F1174L}$ tumors. In contrast, its expression was significantly decreased in ALK$^{-F1174L}$ tumors relative to control, and a trend was also observed in ALK-wt tumors. Finally, *VAV1* was completely abolished in all the ALK-expressing tumors (Figure 14C). We validated the results obtained by RNA sequencing regarding the downregulation of *VAV1* in all ALK-expressing tumors, and the upregulation of the integrin *ITGAV* in ALK$^{-R1275Q}$ tumors relative to ALK-wt and ALK$^{-F1174L}$, as well as in ALK$^{-F1174L}$ vs control tumors.

Globally, these observations suggest a role of activated ALK in deregulating genes involved in axon guidance and in EMT and cell junction/communication.

A

	ALK-wt vs pLiv	ALK$^{-F1174L}$ vs pLiv	ALK$^{-R1275Q}$ vs pLiv
FYN	ND	-2.07	-2.82
ITGAV	-1.61	-1.51	ND
VAV1	-11.30	-10.77	-7.51
RAC2	-1.10	-1.02	ND

B

	ALK$^{-R1275Q}$ vs ALK-wt	ALK$^{-R1275Q}$ vs ALK$^{-F1174L}$
ITGAV	1.79	1.69
VAV1	3.77	3.24
FYN	-2.26	ND

C

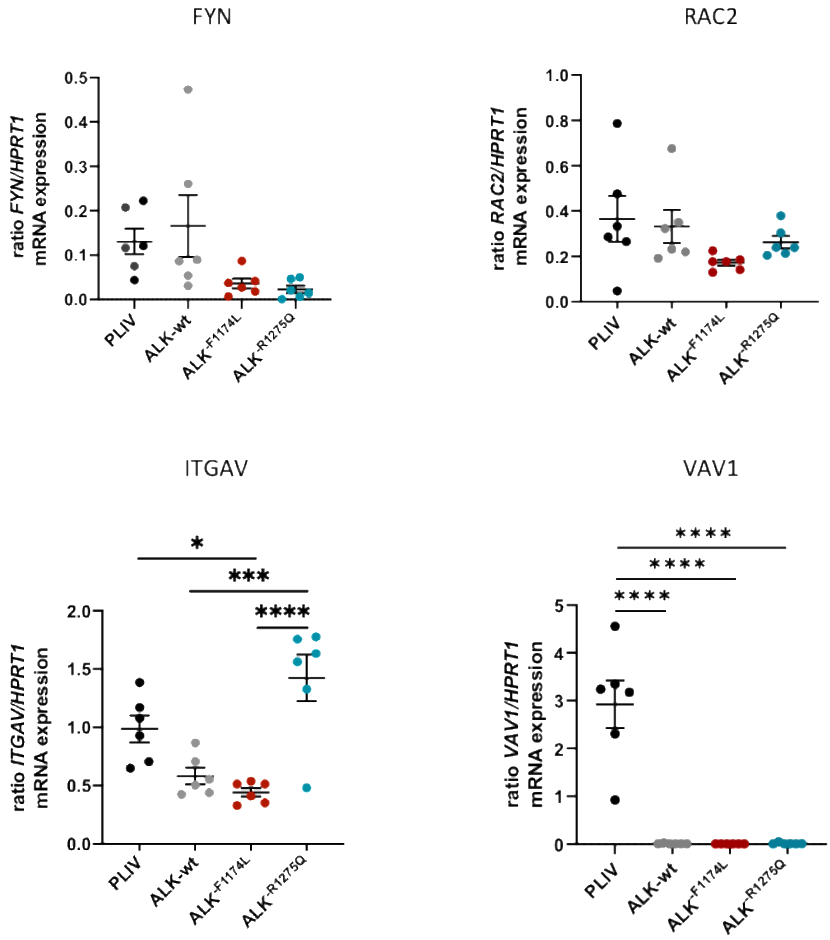

Figure 14. Expression levels of selected deregulated genes in SH-EP pLIV and ALK-expressing tumors. (A) Fold change in log2(FC) observed in RNA sequencing for *FYN*, *RAC2, ITGAV* and *VAV1* genes in ALK-wt, ALK$^{-F1174L}$ and ALK$^{-R1275Q}$ vs pLIV (ND means no difference). **(B)** Log2(FC) obtained by RNA sequencing for *ITGAV*, *VAV1* and *FYN* genes in ALK$^{-R1275Q}$ vs ALK-wt and ALK$^{-F1174L}$. **(C)** mRNA expression levels of *FYN, RAC2, ITGAV* and *VAV1* analyzed by RT Q-PCR. mRNA expression level relative to the *HPRT1* control gene are shown. One-way Anova multiple comparisons, not significant comparisons are not shown. *ITGAV* ****p<0.0001, ***p=0.0005, *p=0-0201; *VAV1* ****p<0.0001; pLIV n=6; ALK-wt n=6; ALK$^{-F1174L}$ n=6; ALK$^{-R1275Q}$ n=6.

Activated ALK increases the metastatic potential of the SH-EP derived tumors

The downregulation in ALK-wt and ALK$^{-F1174L}$, and the upregulation in ALK$^{-R1275Q}$ tumors of pathways related to ECM and cell-cell junction/communication in ALK-expressing tumors prompted us to investigate the occurrence of metastasis in the lung of mice engrafted with SH-EP cells. This was performed by ISH for the detection of human Alu sequences. Regarding the control group, we found only four isolated Alu-positive cells in the lungs of one mouse, while all lung sections analyzed from the remaining 5 mice of this group were negative (Figure 15). Remarkably, Alu staining revealed that all mice implanted subcutaneously with SH-EP-ALK-expressing cells displayed disseminated tumor cells in the lungs. Interestingly, the dissemination pattern exhibited heterogeneous characteristics across the ALK-expressing groups. In the ALK-wt group, the tumors cells invaded capillaries, as reflected by the presence of tumor cells in central and peripheral areas of the lung parenchyma. Small islets were observed in the lung tissue, and two mice exhibited larger metastases (500 µm) (Figure 15). Regarding the ALK$^{-F1174L}$ group, we detected only few isolated cells in the lungs. However, we observed an accumulation of tumor cells in the large vessels at the central area of the lung parenchyma (Figure 15) in 5 mice out of 6, one mouse displaying multiple small cell clusters (less than 5 cells). In contrast, in the ALK$^{-R1275Q}$ group, the lungs of all mice were invaded by numerous isolated cells, or small cell clusters present in capillaries and in pulmonary alveolus (Figure 15, represented by black arrows).

Taken together, these results show that activated ALK signaling increases the dissemination potential of the SH-EP tumor cells. In addition to the strong impact on the primary tumor growth, ALK$^{-F1174L}$ appears to favor the dissemination of tumor cells in cluster, as reflected by the accumulation of tumor cells in the large vessels of the lung. ALK-wt and ALK$^{-R1275Q}$ tumor cells appears to disseminate in single cells, as shown by the presence of tumor cells in the central and peripheral area of the lungs.

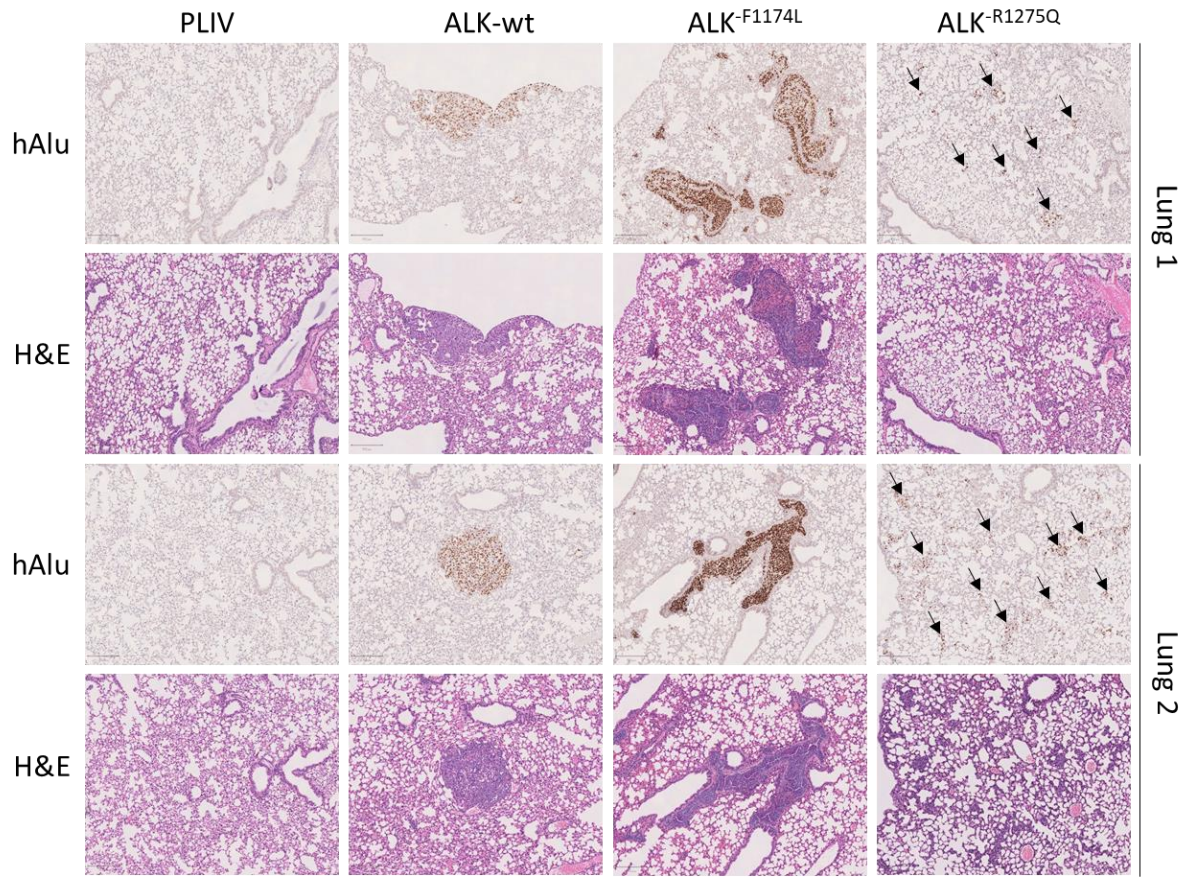

Figure 15. Activated ALK increases the dissemination potential of the SH-EP tumors. The lungs of mice were stained for H&E and hAlu-ISH for the detection of disseminated tumor cells (scale bar = 200 µm). Lungs of two representative mice (n=6 per group) implanted with SH-EP-pLIV, SH-EP-ALK-wt, SH-EP-ALK$^{-F1174L}$ and SH-EP-ALK$^{-R1275Q}$ cells.

Sensitivity of SH-EP tumor-derived cell lines to standard of care chemotherapy agents and the ALK inhibitor lorlatinib

Since we observed a potential cellular plasticity between MES/ADR phenotypes in the SH-EP tumors, we aimed to assess the sensitivity of the SH-EP-ALK-expressing tumor-derived cells to the standard of care chemotherapy agents doxorubicin and cisplatin. All tumor-derived cells were sensitive to doxorubicin, as reflected by a decrease of 50% of viability at 0.1 µM concentration (Figure 16A). In contrast, they were highly resistant to cisplatin, even at high drug concentrations (Figure 16B). ALK-overexpression had no impact on drug sensitivity, both for doxorubicin and cisplatin (Figure 16A and B).

Next, we assessed the effect of lorlatinib on control and ALK-expressing tumor-derived cells. All groups of ALK-expressing tumor-derived cells were sensitive to lorlatinib, as reflected by the significant decrease of viability observed relative to controls (Figure 16C). Interestingly, the ALK$^{-F1174L}$ tumor-derived cells were more sensitive to lorlatinib, relative to the ALK-wt and ALK$^{-R1275Q}$ tumor-derived cells as shown by the IC_{50} (Figure 16C). For example, at 2 µM concentrations of lorlatinib, the viability was significantly decreased in ALK-expressing tumor-derived cells relative to control. Moreover, the ALK$^{-F1174L}$ tumor-derived cells were significantly more sensitive relative to ALK-wt, and a trend was also observed relative to ALK$^{-R1275Q}$ tumor-derived cells (Figure 16C).
The *ETV5* mRNA expression has been reported to be rapidly decreased upon ALK inhibition with TAE-684[188,189]. To confirm a similar effect of lorlatinib, we evaluated the expression of *ETV5* by RT Q-PCR after treatment with 2 µM of lorlatinib for 8h in ALK-expressing tumor-derived cells. Although we did not obtain significant difference, we observed a marked trend for a strong decrease of *ETV5* mRNA expression in all ALK-overexpressing tumor-derived cells upon treatment with lorlatinib (Figure 16D).

These results were in line with previous observations regarding the sensitivity of the SH-EP cell line to doxorubicin and cisplatin. Moreover, we confirmed the sensitivity to lorlatinib of the ALK$^{-F1174L}$ and ALK$^{-R1275Q}$ tumor-derived cells. Interestingly, despite ALK$^{-F1174L}$ tumors displayed the most aggressive behavior, their derived-cells were also the most sensitive to lorlatinib when compared to the ALK-wt and ALK$^{-R1275Q}$ group.

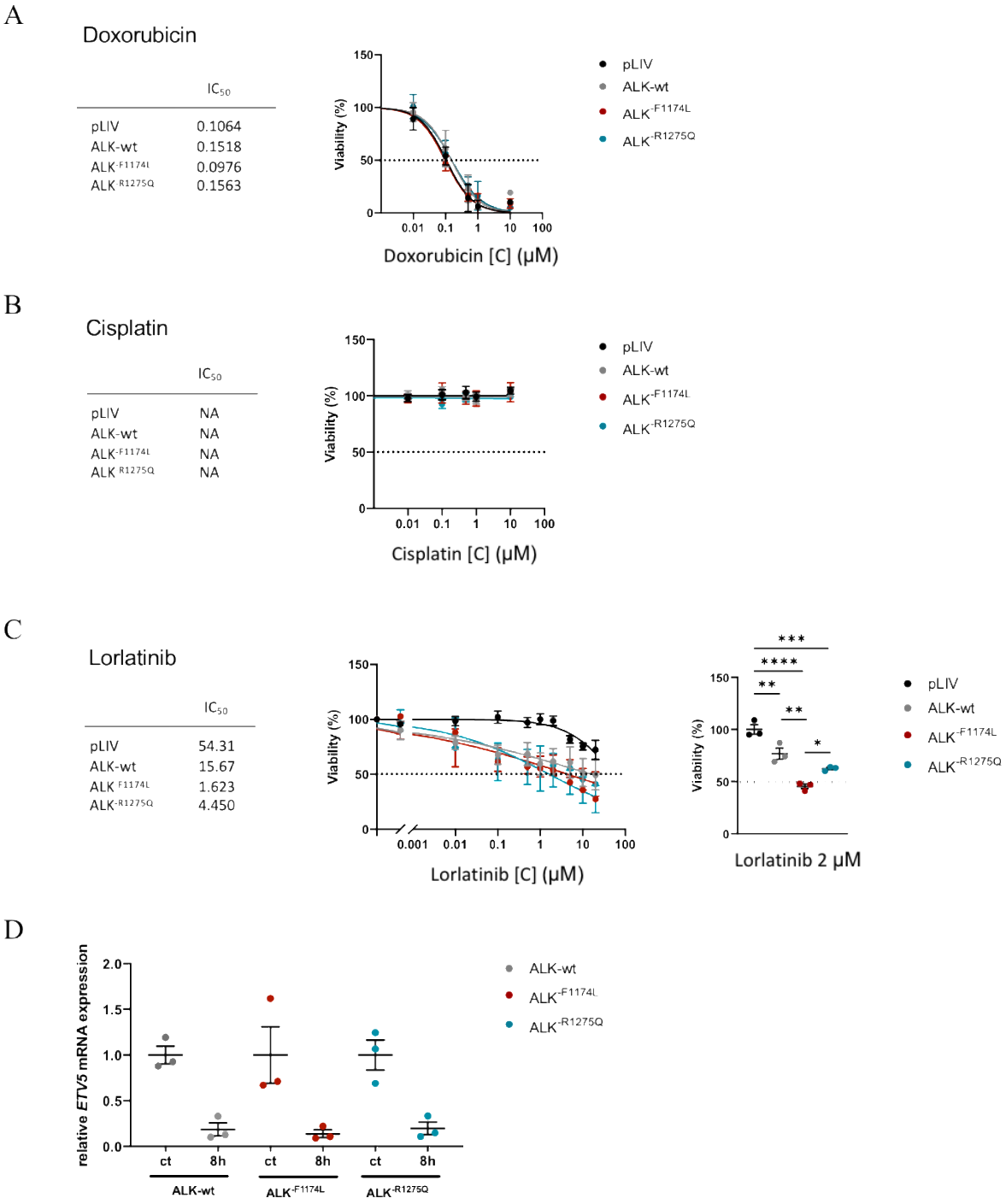

Figure 16. Assessment of the sensitivity of SH-EP tumor-derived cells to chemotherapy and lorlatinib. Cells were treated with **(A)** doxorubicin and **(B)** cisplatin at indicated concentration for 48h. IC_{50} values are represented in µM. n=3 tumor-derived cell lines. **(C)** Cells were treated with lorlatinib at indicated concentration for 48h. IC_{50} values are represented in µM. n=3 tumor-derived cell lines. The experiment was repeated three times. One-way Anova multiple comparisons, ****p<0.0001, ***p=0.0004, **p=0.0094 and p=0.0015, *p=0.480. **(D)** Relative mRNA expression of *ETV5* after treatment with 2 µM of lorlatinib for 8h. Results are shown as relative expression levels compared to the untreated cell lines. n=3 tumor-derived cell lines. Wilcoxon matched-pairs test.

DISCUSSION

In our experiments, the overexpression of ALK-wt, ALK$^{-R1275Q}$ and ALK$^{-F1174L}$ in the MYCN-amplified adrenergic SK-N-Be2c cells did not increase the tumor growth after orthotopic injection into the adrenal gland of athymic Swiss nude mice. Furthermore, they had weak transcriptional consequences in the generated tumors. Interestingly, SK-N-Be2c tumors were initially highly tumorigenic, expressed *MYCN* and low level of ALK-wt. From prior published evidence, the combination of the two oncogenes *ALK* and *MYCN* has been reported to drive highly aggressive tumors in patients, as well as in *in vivo* models[150,170]. We believe that, since the SK-N-Be2c tumors were already highly tumorigenic, the addition of ALK-wt or ALK mutations may not increase the aggressiveness of the tumor cells. Moreover, in this model, the ALK signature score was only increased in the ALK$^{-F1174L}$ tumors relative to the control. This is in accordance with the fact that ALK$^{-F1174L}$ tumors had the higher number of DE genes relative to control, while ALK-wt and ALK$^{-R1275Q}$ tumors had smaller number of DE genes. This leads us to speculate that the overexpression of the ALK variants had a low impact in this model because the level of endogenous ALK-wt receptor expressed in the control tumors is sufficient to activate its downstream signaling pathways.

In contrast, the overexpression of the ALK variants in the weakly tumorigenic and mesenchymal cell line SH-EP allowed us to investigate their roles during tumor progression. The strongest effect on tumor growth after subcutaneous injection in NOD-SCID-γ mice was observed with cells expressing ALK$^{-F1174L}$. These results are in line with previous observations, as ALK$^{-F1174L}$ has been reported to display a higher oncogenic potential relative to ALK$^{-R1275Q}$ or ALK-wt in several studies[148,164,170]. The overexpression of ALK$^{-R1275Q}$ had no impact on the primary tumor growth relative to the control group, which was relatively surprising since the oncogenic potential of ALK$^{-R1275Q}$ has been well reported in several studies[70,148,164]. Although ALK-wt was reported to be unable to transform Ba/3F and NIH/3T3 cells, prior data from our laboratory demonstrated that NCCs transduced with ALK-wt displayed the ability to generate tumors when subcutaneously and orthotopically injected into athymic Swiss nude mice, independently of *MYCN* expression[70,148,164]. In our model, the overexpression of the wild-type ALK receptor was able to increase the tumorigenic potential of the SH-EP cells. In SH-EP derived tumors we observed an increase of the ALK signature

score in ALK-wt, ALK$^{-F1174L}$ and ALK$^{-R1275Q}$ tumors relative to the control tumors. Our observations that ALK-wt tumors displayed an increased ALK signature score are contrasting with prior evidence. Indeed, the overexpression of ALK-wt, ALK$^{-R1275Q}$ and ALK$^{-F1174L}$ in the SK-N-AS cell line revealed an increased ALK signature in ALK$^{-R1275Q}$ and ALK$^{-F1174L}$ but not in ALK-wt cell lines, reflecting a similar activation of downstream ALK signaling between the two ALK mutants relative to the ALK-wt receptor *in vitro*[186]. In our model, results show that ALK-wt was also able to activate a downstream signaling as driven by ALK mutants. Also, the transcriptional profile of the ALK-wt tumors was found to be similar to the one in ALK$^{-F1174L}$ tumors, while the ALK$^{-R1275Q}$ tumors appear to display more specific transcriptional profile. In further and upcoming experiments, we will investigate the different and specific downstream effects of the ALK variants in our model.

In the SH-EP model, the histological analysis revealed a shift toward a neuroblastic phenotype in the ALK-expressing tumors. Indeed ALK-wt and ALK$^{-R1275Q}$ tumors displayed both mesenchymal and neuroblastic regions, and especially ALK$^{-F1174L}$ tumors were composed of undifferentiated/poorly differentiated neuroblasts, in contrast to control tumor that displayed a mesenchymal phenotype. GSEA analysis revealed an enrichment for an ADRN signature in ALK-wt and ALK$^{-F1174L}$ tumors relative to control, while the MES signature was enriched in ALK$^{-R1275Q}$ tumors relative to their ALK-wt and ALK$^{-F1174L}$ counterparts. Further validations will be needed to confirm this change in phenotype that potentially might be driven by ALK-wt or ALK mutations. First, it would be interesting to quantify the proportion of glial cells/stroma-rich and/or neuroblastic regions on H&E stained tumors. Second, investigations should be performed to better characterize the deregulation of MES and ADRN TFs that compose the CRC and define the cell lineage identity. For example, the MES TFs *PRRX1, NOTCH1, NOTCH3, MEOX2, SIX1, SIX4* and the ADRN TFs *DACH1, KLF7, HEY, HAND2* are expressed and modulated in the tumors. Of note, according to the RNA sequencing, *HAND2* is increased in ALK-wt and ALK$^{-F1174L}$ tumors relative to the control, and *NOTCH1* and *NOTCH3* are upregulated in ALK$^{-R1275Q}$ tumors. However, the SH-EP ALK-expressing tumors do not express *PHOX2B* and *GATA3*, as well as *TH* and *DBH*, suggesting that the transition toward the ADRN state is only partial. While the overexpression of the MES-TF PRRX1 or the activation of NOTCH pathway in ADRN NB cells induce a transition to a MES phenotype, the genes that control the

transition from MES to ADRN-like phenotype have not yet been reported[46,48]. Although our findings are preliminary and descriptive, they are interesting and novel considering that they may imply a role for ALK in the transition toward an ADRN-like phenotype in NB tumors.

In our experiments we identified a strong increase of the metastatic potential of SH-EP ALK-expressing tumors. Circulating tumor cells (CTCs) can disseminate as single cells or in clusters[198,199]. Once arriving at secondary sites, single cells invade capillaries, while CTCs clusters accumulate in large vessels[198]. However, CTCs clusters can also cross the capillary barrier by the formation of cell chains and transient deformation of individual tumors cells[200]. The histological analysis of the lung of mice suggested that ALK$^{-F1174L}$ may promote the dissemination of CTCs clusters, as reflected by the accumulation of tumor cells in the large vessels of the lungs. In contrast, ALK$^{-R1275Q}$ and ALK-wt may rather favor the dissemination of single CTCs, as cells could travel deeper in the lungs and were found in central and peripheral area of the parenchyma. CTC clusters are less prevalent than single CTCs but have been reported to be associated with poorer outcomes in patients[199]. Therefore, our observations suggest that ALK$^{-F1174L}$ might induce a more aggressive phenotype than ALK-wt and ALK$^{-R1275Q}$ by mediating the dissemination of CTC clusters.

Junctional plakoglobin (JUP), a desmosomal protein, has been reported to be associated to CTCs cluster in breast cancer and its expression is decreased in CTCs of other cancers[199,201]. Recently, the orthotopic implantation of NB LAN-1 cells into the adrenal gland was reported to form distant metastasis in various sites including ovary, lung, kidney, brain and liver[202]. The immunostaining for JUP revealed a strong expression in the primary tumors and large ovarian metastasis, but weak expression in the smaller liver and lung micro-metastases, suggesting a pro-metastatic role for *JUP* in NB tumors. It would be of interest to analyze JUP mRNA expression directly in the primary tumor, as well as in the lungs of our mice. Of note, *JUP* is more upregulated in ALK$^{-R1275Q}$ than in ALK-wt and ALK$^{-F1174L}$ tumors relative to controls in the RNA sequencing.

Interestingly, although ALK$^{-R1275Q}$ did not increase the growth of the primary tumors relative to the control, tumors cells were nevertheless able to disseminate. The ALK$^{-R1275Q}$ mutation has been previously reported to disturb the extracellular matrix (ECM) and to enhance cell invasion in a *KI* model[171]. Transcriptional analysis of sympathetic

neuronal cells revealed that ALK$^{-R1275Q}$ downregulates pathways related to EMT and focal adhesion[171]. Globally, major constituents of ECM including collagens, laminins and integrins were downregulated upon ALK$^{-R1275Q}$ expression[171]. These results are in contrast with our observations, which rather suggest an increased expression of components of the ECM and change in cell surface molecules in ALK$^{-R1275Q}$ tumors, such as integrins, cadherins or laminins. For example, we identified an increased expression of *ITGAV* in ALK$^{-R1275Q}$ tumors. ITGAV belongs to the family of integrin alpha chain family, that mediate adhesion to the ECM and cell-cell communication[203]. The overexpression of ITGAV has been reported in several cancer, where its overexpression favorize angiogenesis, migration, invasion, and spread of the tumor cells[204,205].

Moreover, the induction and reversion of EMT is a major mechanism during the metastatic process of solid tumors. Tumor cells down-regulate epithelial cell junction proteins during EMT at the primary tumor sites and re-express them at the metastatic site during the reversion of EMT, the mesenchymal-epithelial transition (MET), which occurs during metastatic outgrowth[206]. Our data suggests that ALK-wt might increase the ability of tumors cells to form established metastasis relative to the ALK$^{-R1275Q}$ mutation. Indeed, mice implanted with ALK$^{-R1275Q}$ expressing tumors displayed only isolated cells in the lungs, while two mice of the ALK-wt group presented established metastasis. Regarding the ALK$^{-F1174L}$ group, mice were sacrificed early due to the growth of the primary tumor, and the metastatic tumor cells were still blocked in capillaries at the time of sacrifice. The different metastatic profile observed in SH-EP ALK-expressing tumors suggest that the tumor cells might modulate the genes involved in cell junctions/communication and EMT-MET differently. Recent studies reported that the EMT of CTCs is a relevant process for invasion and metastasis in breast cancer, non-small cell lung cancer, prostate cancer, gastric cancer, colorectal cancer and hepatocellular carcinoma[207–211]. Therefore, we plan to identify and validate genes belonging to EMT-MET processes and cell junctions/communication that might be involved in the tumor cell dissemination.

In our experiments, RNA sequencing revealed the downregulation of genes involved in axon guidance in ALK-wt and ALK$^{-F1174L}$ expressing tumors, while these subsets of genes were upregulated in ALK$^{-R1275Q}$ tumors. We identified the deregulation of several semaphorins and their receptors in ALK-expressing tumors. For example,

SEMA3F and *SEMA5A* are downregulated in the ALK^{F1174L} tumors. Semaphorin proteins belong to axon guidance molecules that direct the neuronal network formation[212]. They mainly function via plexin receptors and are involved in a wide variety of processes during embryogenesis as well as in adult homeostasis[212]. For example, semaphorins are essential for the migration of cranial and trunk NCCs during embryonic development[213–215]. Besides their role in development, semaphorins can also promote tumor progression depending on their cellular context, while others function as *bona-fide* tumor suppressors inhibiting tumor development[216,217]. In an avian embryonic model driving NB tumorigenesis, the downregulation of Sema3C or its receptor PlexinA4 has been reported to induces NB dissemination[218]. The observations that the downregulation of Sema3C favors the dissemination of NB cells in embryonic development could suggest that semaphorins might be involved in the spread of the SH-EP-expressing tumor cells. Moreover, the link between activated ALK signaling and the deregulation of semaphorins has never been established, and it would be of interest to validate our observations by targeted experiments.

We also identified a downregulation of *VAV1* in all ALK-amplified tumors. VAV1 belongs to the VAV protein family, which are guanine nucleotide exchange factors (GEFs) for Rho family GTPases, such as Rac, leading to cell differentiation and/or proliferation in the hematopoietic system[219]. VAV1 has been reported as a proto-oncogene in pancreatic, lung and breast cancers, where its ectopic expression outside of the hematopoietic system leads to malignancy[220–223]. VAV1 has been described in human NB cell lines and tumors, under a wild type form, suggesting that VAV1 may play a role in the tumorigenic process of NB[224]. Moreover, alteration of several regulators of the Rac/Rho pathways, including structural variant in *VAV1*, have been described in NB and were associated to defects in neuritogenesis[64]. Our results are interesting considering that low levels of *VAV1* are associated to decrease in overall and event-free survival of NB patients. It would be of interest to further investigate if a putative correlation between the expression level of Vav1 and the ALK status of NB primary tumors exists, as it has yet not been reported. Finally, in breast cancer, the high expression of VAV1 was reported to decrease the invasive properties of breast-tumor derived cells *in vitro* and to reduce the ability of breast tumors to form metastasis *in vivo*[225]. Regarding the increased metastatic potential of SH-EP ALK-expressing

tumors, we could hypothesize that VAV1 might be involved in preventing the metastatic dissemination in NB as previously observed in breast cancer[225].

Finally, we confirmed the sensitivity of ALK-expressing cells to lorlatinib[180,181]. Indeed, the treatment with lorlatinib decreased the cell viability of ALK$^{-F1174L}$ and ALK$^{-R1275Q}$, and to a lesser extent ALK-wt SHEP-tumor derived cell lines. We also confirmed the decrease of *ETV5* mRNA expression after 8h of lorlatinib treatment, as previously described with the ALK inhibitor TAE-684[226]. Since the SH-EP tumors have the ability to disseminate *in vivo*, it would be of interest to evaluate the impact of lorlatinib not only on tumor growth, but also on metastatic dissemination, as well as on the cellular phenotype of the generated tumors.

The limitations of the experiments presented herein are mostly due to the fact the chosen experimental mouse models might not comprehensively reflect the NB tumors observed in humans. This is particularly true for SH-EP cells, which were injected subcutaneously. Orthotopic tumor models, as used for the SK-N-Be2c cells, are possibly more clinically relevant than those resulting from subcutaneous implantation because of the establishment of organ specific tumor microenvironment. In addition, we only studied the occurrence of metastasis in the lungs of our mice, which is rarely occurring in patients (3.6% of children with newly diagnosed NB)[227]. The most common sites of metastasis in NB include bone marrow, bone, lymph nodes, liver and intracranial and orbital sites[228]. It would be of interest to analyze the occurrence of metastasis in these secondary sites after orthotopic injection of the SH-EP cells in the adrenal gland. Moreover, xenografts models are *per se* limited as far as they allow the growth of clonally selected cells able to initiate cancer *in vivo*. Furthermore, we did not perform single colony selection after the lentiviral transduction of the NB cell lines, and we performed our experiments with a bulk of transduced cells. Therefore, we have to take into consideration the cellular heterogeneity of the resulting tumors. However, as lentiviral integration may produce off-target effects depending on its integration site, we limited these potential impacts by working with bulk cell populations. Finally, RNA sequencing analysis were performed on whole tumors, and not on single-cells, which would give a more precise characterization of the real tumor cell profile.

To conclude, although the results are preliminary and mainly descriptive, our first observations are encouraging for further investigations. We observed that activated ALK signaling might induce a transition toward an adrenergic phenotype in the generated tumors. To our knowledge, this is the first observation that ALK-wt overexpression and ALK$^{-F1174L}$ and ALK$^{-R1275Q}$ mutations could mediate specific process for metastatic dissemination. Further validations and experiments will be conducted to validate our observations and more precisely define the implication of the different ALK-amplification or mutation in NB tumorigenesis (Figure 17).

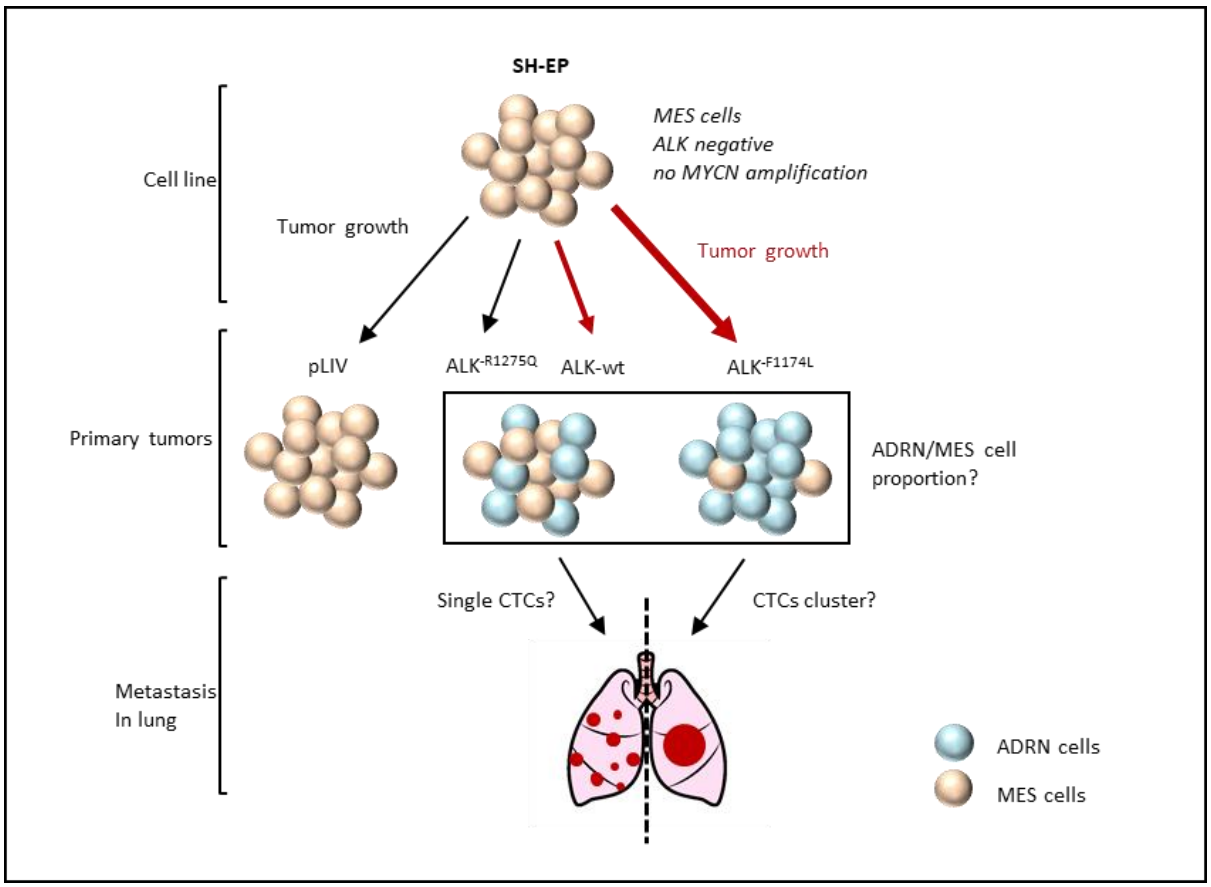

Figure 17. ALK$^{-F1174L}$ and to a lesser extent ALK-wt increase the tumor growth of the weakly tumorigenic SH-EP cells in a subcutaneous mice model. ALK activation appears to mediate a shift toward an adrenergic phenotype in the SH-EP tumors. Activated ALK signaling increases the metastatic potential of SH-EP tumors. ALK-wt and ALK$^{-R1275Q}$ would mediate a dissemination of single cells, while ALK$^{-F1174L}$ would rather promote the spread of CTC clusters. Further validations are needed to confirm our observations.

SUPPLEMENTARY FIGURES

A

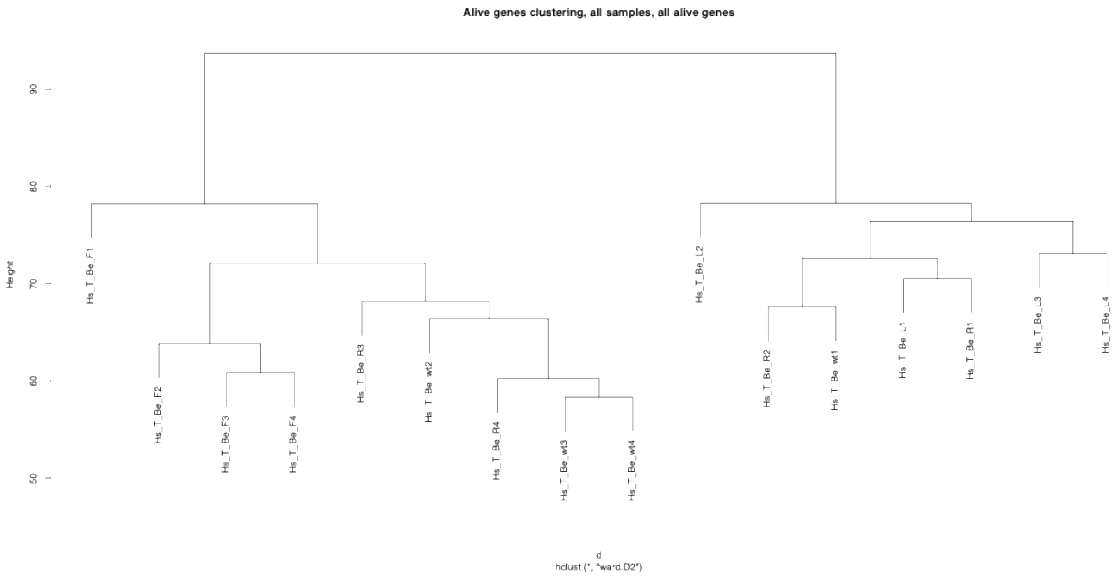

B

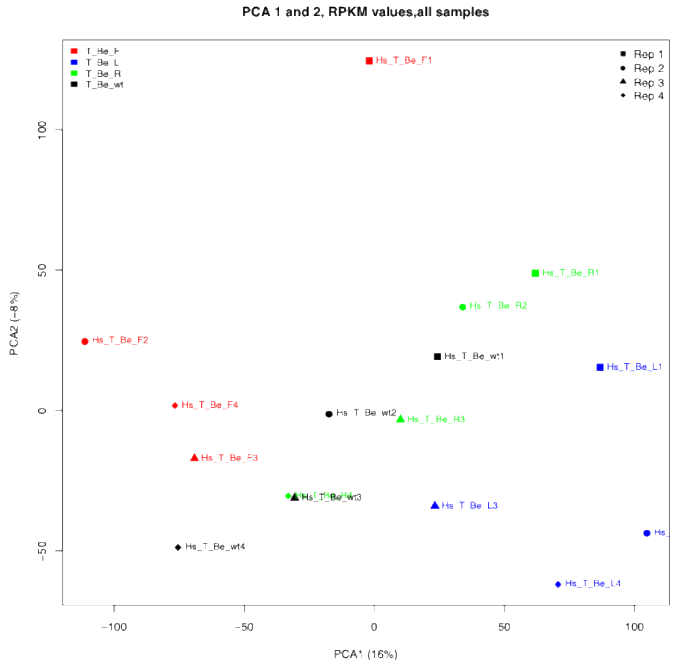

Supplementary Figure S1. (A) Unsupervised hierarchical clustering of SK-N-Be2c tumors (T_Be) performed using all detected genes. **(B)** PCA analysis showing the repartition of SK-N-Be2c tumors.

A

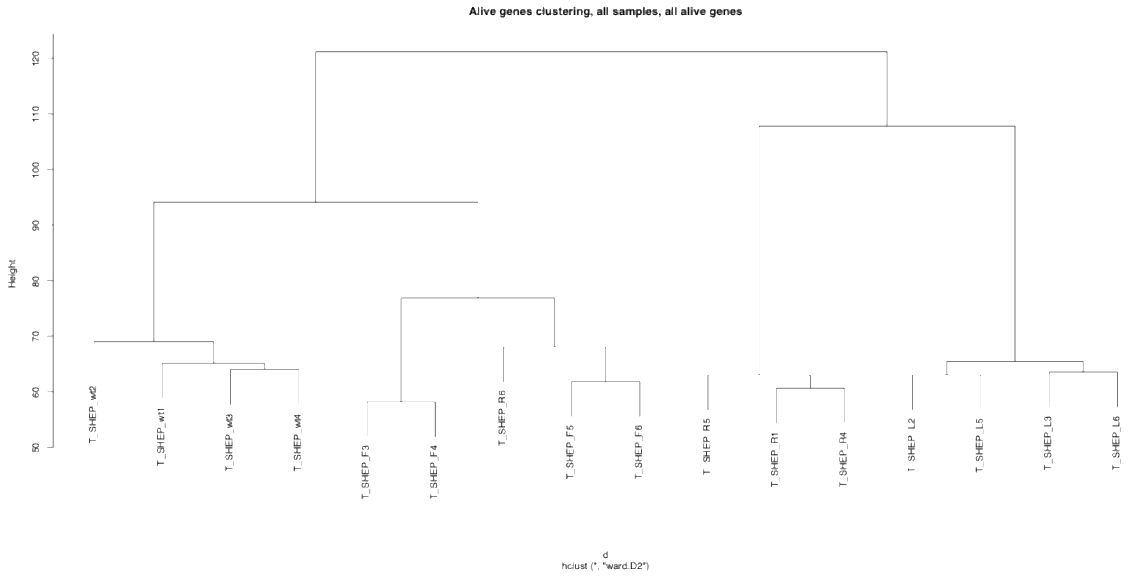

B

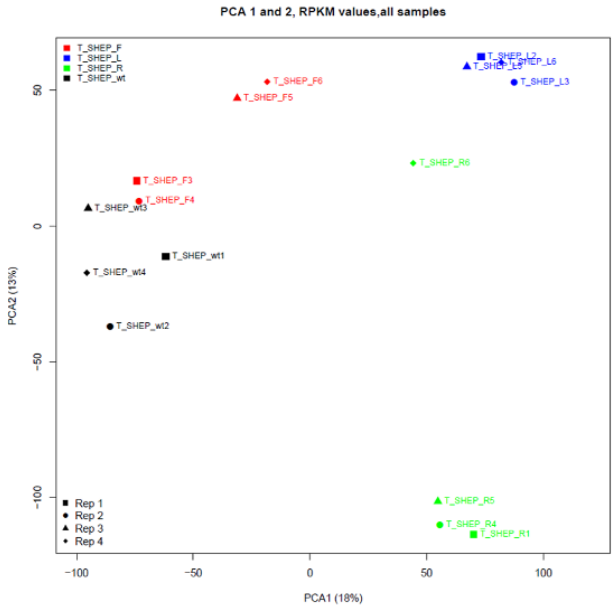

Supplementary Figure S2. (A) Unsupervised hierarchical clustering of SH-EP tumors (T_SHEP) performed using all detected genes. **(B)** PCA analysis showing the repartition of SH-EP tumors.

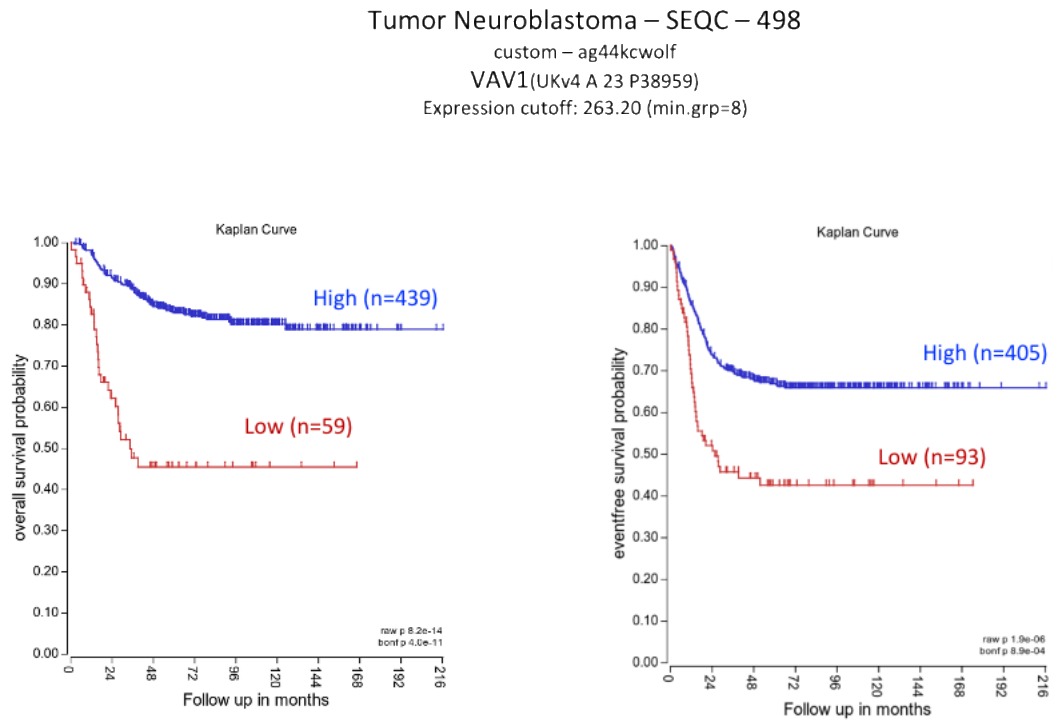

Supplementary Figure S3. Overall and event-free survival probability for patients according to VAV1 expression levels in 498 neuroblastoma tumors. *Zhang et al.,* Genome Biol., 2015, using the R2: Genomics Analysis and Visualization Platform (http://r2.amc.nl)

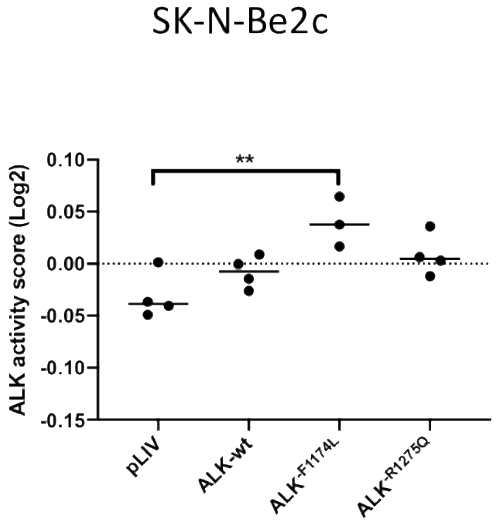

Supplementary Figure S4. ALK-signature score in SK-N-Be2c tumors. One-way Anova multiple comparisons. **p=0.0087. Not significant comparisons are not shown.

CONCLUSION AND PERSPECTIVES

This work aimed to increase the understanding of the impact of ALK deregulated signaling 1) on the formation of sympathetic ganglia at early stages of embryonic development to characterize its involvement as a first hit in NB tumor initiation, 2) by investigating the implication of the ALK$^{-F1174L}$ and ALK$^{-R1275Q}$ activating mutations relative to the wild-type isoform *in vivo* in NB pathogenesis.

Using a *Sox10-Cre;LSL-ALK-F1174L* mouse model, we report for the first time a role for the ALK-F1174L mutation in disturbing the balance between proliferation and differentiation in the sympathetic lineage *in vivo* at early embryonic stages between E9.5 and E11.5. In our model, one of the limitation was that the expression of the ALK-F1174L mutation was anterior by nearly 1.5 days than the endogenous gene. In addition, the early expression of ALK-F1174L led to an embryonic lethality from E12.5 and had more striking impacts relative to the observations made in the ALK$^{-F1178L}$ KI model. Indeed, in the KI model, the offspring display lethality between 24h and 48h after birth in homozygous mice[123]. Furthermore, the time-frame for the analysis of SG differentiation was limited by the embryonic lethality and we cannot exclude that the SA differentiation was delayed as observed in murine Ascl1 and Insm1 know-out models[27,28]. Moreover, one question that remains unanswered is by which specific mechanisms ALK-F1174L impairs the SA differentiation. One of our hypotheses was that ALK-F1174L may mediate a dysregulation of the TF network involved in noradrenergic specification. However, our data showed that Ascl1 and Insm1 may not be involved, suggesting that other TFs might drive the block in noradrenergic differentiation. One approach would be to investigate the impact of the ALK mutations in murine NCCs *in vitro*. NCCs cells are pluripotent cells that can be differentiated into particular cells lineage[229]. We could analyze the modulation of TFs after the differentiation of NCCs expressing the ALK mutations into the sympathetic lineage upon differentiating agents, such as BMP4 and retinoid acid as previously described[230].

One other approach would be to analyze the impact of deregulated ALK on the formation of the SNS in the ALK$^{-F1174L}$ or ALK$^{-R1275Q}$ *KI* model where the mutations are expressed under the control of the endogenous promoter[170]. Since the offspring of this model are viable, it would allow us to study the impact of the ALK mutations on the

sympathetic differentiation at later embryonic stages and on the differentiation of adrenal chromaffin cells, which acquire adrenergic and chromaffin markers between E14.5 and E16.5. Moreover, Schwann cell precursors have recently been reported to generate chromaffin cells of the adrenal gland, highlighting an additional cellular origin for adrenal NB[35]. It would thus be of interest to study the impact of the ALK mutations on the differentiation of this particular cell lineage.

In the *KI* model the mutations are expressed around E10.5 in Phox2b+ precursors in SG that already have started to acquire noradrenergic features. Such models could help to clarify the timeframe during which ALK deregulated signaling affects the development and differentiation of the SNS. Other alternatives would be to cross the *LSL-ALK-F1174L* mice with Phox2b-Cre mice to express the mutation in Phox2b+ sympathetic progenitors, or the use of ligand-dependent Cre recombinases system (i.e Sox10-CreER^{T2}) that can be activated by administration of tamoxifen to the mice to control the timing and the tissues in which the ALK mutations would be expressed. Using these mice models, the ALK$^{-F1174L}$ mutation could be expressed at a higher expression level than in the *KI* model and might potentially be sufficient to drive NB. Indeed, the expression of the ALK$^{-F1174L}$ mutation in sympathetic precursors (TH+, DBH+) under the control of the β-actin promoter has been reported to generate NB but with incomplete penetrance and long latency[168].

Over the last years, the comprehension of the ALK downstream signaling has been largely improved by proteomic and transcriptomic profiling of NB cells and/or tumors[145,146,186]. However, the mechanisms by which ALK promotes aggressive NB remain largely to be discovered. In the second part of this work, we identified potential new processes by which ALK deregulated signaling may promote NB pathogenesis. We first observed that ALK might favor a switch between mesenchymal and adrenergic phenotype into the tumors. As the link between activated ALK signaling and cellular plasticity has not been reported, it could be an important aspect to further investigate. One interesting approach would be to perform microdissection of mesenchymal and adrenergic areas in SH-EP tumor sections, and conduct RNA sequencing analysis to get further insight into the cellular properties of these distinct tumor regions. Another alternative would be to perform single-cell RNA sequencing analyses of newly generated tumors, which may provide a better characterization of

the cell lineage and of the intratumoral heterogeneity. Finally, the overexpression of ALK-wt, ALK$^{-R1275Q}$ and ALK$^{-F1174L}$ in other NB mesenchymal cell lines, such as CA2E or GIMEN cells, could be of interest to confirm our results.

Second, one very interesting aspect was that the expression of ALK-wt, ALK$^{-R1275Q}$ and ALK$^{-F1174L}$ increased the dissemination potential of the SH-EP tumors. Our preliminary observations suggested that ALK-wt and ALK$^{-R1275Q}$ could allow the dissemination of single CTCs, while ALK$^{-F1174L}$ appeared to mediate the spread of CTCs in clusters, which was associated to poor prognosis. To further investigate this aspect and to understand the specific process by which ALK-wt, ALK$^{-R1275Q}$ and ALK$^{-F1174L}$ mediate tumor cell dissemination, an interesting approach would isolate single CTCs and clusters in circulation by flow-cytometry followed by their molecular characterization[231].

To conclude, this work contributed to increase the understanding of ALK mutation as a path to initiate NB-genesis during embryonic development by promoting a precancerous state. Moreover, we reported potential new mechanisms of ALK deregulated signaling in promoting the aggressive phenotype of NB tumors. The transcriptional profiling of SH-EP tumors will help to provide information regarding the deregulation of genes that might be crucial for the transition toward an adrenergic phenotype and/or metastatic dissemination of ALK-wt, ALK$^{-F1174L}$ and ALK$^{-R1275Q}$-expressing tumors cells, as well as to discover new potential ALK signaling targets, such as semaphorins or Rho GTPase signaling.

REMERCIEMENTS

Je souhaite tout d'abord remercier le Dr. Raffaele Renella pour m'avoir donné l'opportunité de travailler au sein de son laboratoire. Je le remercie pour sa confiance, son soutient, et son précieux encadrement. Je remercie également le Dr. Annick Mühlethaler pour sa supervision et ses conseils. Je les remercie tous les deux pour leur aide indispensable à la réalisation de ce travail.

Je remercie mes collègues avec qui j'ai passé de merveilleuses années. Je souhaite exprimer mon immense gratitude à Katia Balmas Bourloud pour sa gentillesse, son écoute et sa bonne humeur durant ces quatre années. Je la remercie pour tout ce qu'elle m'a appris. Je remercie également les Dr. Julien Delobel et Dr. Maria-Vittoria Sepporta pour leur encouragements continus, tous ces bons moments partagés au travail ainsi qu'à l'extérieur, nos pauses thés et petit-déjeuner du mercredi.

Je remercie Véronique Noguet et Elena Lemel pour leur bonne humeur tous les midis. Je remercie également le Dr. Nadja Chevalier pour toutes nos petites sorties et discussions interminables. Merci au Dr. Marjorie Flahaut pour nos journée Zoé4Life, merci au Dr. Emma Garcia et à Katia Nardou pour leur gentillesse.

Je remercie les Prof. Nicolo Riggi, Dr. Viviane Praz, Dr. Olga Shakhova, Dr. Marco Gualandi, Dr. Jean-Marc Joseph, Dr. Nicolas Jauquier, dont les collaborations ont permis l'accomplissement de ce travail. Je remercie également tous les membres de mon jury pour leurs conseils.

Je remercie de tout mon cœur ma famille, notamment mes parents, ma petite sœur et mes grands-parents, qui m'ont toujours beaucoup soutenu tout au long de ces études. Je tiens également à remercier tous mes amis.

Enfin, ma plus grande gratitude va à mon mari Jimmy, pour ses encouragements et tout ce qu'il fait au quotidien pour me soutenir.

REFERENCES

1. Bray, F. *et al.* Global cancer statistics 2018: GLOBOCAN estimates of incidence and mortality worldwide for 36 cancers in 185 countries. *CA Cancer J Clin* **68**, 394–424 (2018).
2. Stratton, M. R., Campbell, P. J. & Futreal, P. A. The cancer genome. *Nature* **458**, 719–724 (2009).
3. Poon, S. L., McPherson, J. R., Tan, P., Teh, B. T. & Rozen, S. G. Mutation signatures of carcinogen exposure: genome-wide detection and new opportunities for cancer prevention. *Genome Med* **6**, 24 (2014).
4. Feinberg, A. P., Koldobskiy, M. A. & Göndör, A. Epigenetic modulators, modifiers and mediators in cancer aetiology and progression. *Nat. Rev. Genet.* **17**, 284–299 (2016).
5. Hanahan, D. & Weinberg, R. A. Hallmarks of cancer: the next generation. *Cell* **144**, 646–674 (2011).
6. Downing, J. R. *et al.* The Pediatric Cancer Genome Project. *Nat. Genet.* **44**, 619–622 (2012).
7. Siegel, R. L., Miller, K. D. & Jemal, A. Cancer statistics, 2019. *CA Cancer J Clin* **69**, 7–34 (2019).
8. Gröbner, S. N. *et al.* The landscape of genomic alterations across childhood cancers. *Nature* **555**, 321–327 (2018).
9. Ma, X. *et al.* Pan-cancer genome and transcriptome analyses of 1,699 paediatric leukaemias and solid tumours. *Nature* **555**, 371–376 (2018).
10. Wu, G. *et al.* The genomic landscape of diffuse intrinsic pontine glioma and pediatric non-brainstem high-grade glioma. *Nat. Genet.* **46**, 444–450 (2014).
11. Lannon, C. L. & Sorensen, P. H. B. ETV6-NTRK3: a chimeric protein tyrosine kinase with transformation activity in multiple cell lineages. *Semin. Cancer Biol.* **15**, 215–223 (2005).
12. Filbin, M. & Monje, M. Developmental origins and emerging therapeutic opportunities for childhood cancer. *Nat. Med.* **25**, 367–376 (2019).
13. Brodeur, G. M., Nichols, K. E., Plon, S. E., Schiffman, J. D. & Malkin, D. Pediatric Cancer Predisposition and Surveillance: An Overview, and a Tribute to Alfred G. Knudson Jr. *Clin. Cancer Res.* **23**, e1–e5 (2017).
14. Zhang, J. *et al.* Germline Mutations in Predisposition Genes in Pediatric Cancer. *N Engl J Med* **373**, 2336–2346 (2015).
15. Han, Z.-Y. *et al.* The occurrence of intracranial rhabdoid tumours in mice depends on temporal control of Smarcb1 inactivation. *Nat Commun* **7**, 10421 (2016).
16. Jones, D. T. W. *et al.* Molecular characteristics and therapeutic vulnerabilities across paediatric solid tumours. *Nat. Rev. Cancer* **19**, 420–438 (2019).
17. Maris, J. M. Recent advances in neuroblastoma. *N. Engl. J. Med.* **362**, 2202–2211 (2010).
18. McCorry, L. K. Physiology of the autonomic nervous system. *Am J Pharm Educ* **71**, 78 (2007).
19. Sommer. Neural crest-derived stem cells. *StemBook* (2010) doi:10.3824/stembook.1.51.1.
20. Rohrer, H. Transcriptional control of differentiation and neurogenesis in autonomic ganglia. *Eur. J. Neurosci.* **34**, 1563–1573 (2011).
21. Morikawa, Y. *et al.* BMP signaling regulates sympathetic nervous system development through Smad4-dependent and -independent pathways. *Development* **136**, 3575–3584 (2009).
22. Schneider, C., Wicht, H., Enderich, J., Wegner, M. & Rohrer, H. Bone morphogenetic

proteins are required in vivo for the generation of sympathetic neurons. *Neuron* **24**, 861–870 (1999).
23. Kelsh, R. N. Sorting out Sox10 functions in neural crest development. *Bioessays* **28**, 788–798 (2006).
24. Tsarovina, K., Schellenberger, J., Schneider, C. & Rohrer, H. Progenitor cell maintenance and neurogenesis in sympathetic ganglia involves Notch signaling. *Mol. Cell. Neurosci.* **37**, 20–31 (2008).
25. Callahan, T., Young, H. M., Anderson, R. B., Enomoto, H. & Anderson, C. R. Development of satellite glia in mouse sympathetic ganglia: GDNF and GFR alpha 1 are not essential. *Glia* **56**, 1428–1437 (2008).
26. Pattyn, A., Morin, X., Cremer, H., Goridis, C. & Brunet, J. F. The homeobox gene Phox2b is essential for the development of autonomic neural crest derivatives. *Nature* **399**, 366–370 (1999).
27. Wildner, H., Gierl, M. S., Strehle, M., Pla, P. & Birchmeier, C. Insm1 (IA-1) is a crucial component of the transcriptional network that controls differentiation of the sympatho-adrenal lineage. *Development* **135**, 473–481 (2008).
28. Pattyn, A., Guillemot, F. & Brunet, J.-F. Delays in neuronal differentiation in Mash1/Ascl1 mutants. *Developmental Biology* **295**, 67–75 (2006).
29. Hendershot, T. J. *et al.* Conditional deletion of Hand2 reveals critical functions in neurogenesis and cell type-specific gene expression for development of neural crest-derived noradrenergic sympathetic ganglion neurons. *Dev. Biol.* **319**, 179–191 (2008).
30. Tsarovina, K. *et al.* The Gata3 transcription factor is required for the survival of embryonic and adult sympathetic neurons. *J. Neurosci.* **30**, 10833–10843 (2010).
31. Coppola, E., d'Autreaux, F., Rijli, F. M. & Brunet, J.-F. Ongoing roles of Phox2 homeodomain transcription factors during neuronal differentiation. *Development* **137**, 4211–4220 (2010).
32. Reiff, T. *et al.* Neuroblastoma phox2b variants stimulate proliferation and dedifferentiation of immature sympathetic neurons. *J. Neurosci.* **30**, 905–915 (2010).
33. Lucas, M. E., Müller, F., Rüdiger, R., Henion, P. D. & Rohrer, H. The bHLH transcription factor hand2 is essential for noradrenergic differentiation of sympathetic neurons. *Development* **133**, 4015–4024 (2006).
34. Ernsberger, U. & Rohrer, H. The development of the noradrenergic transmitter phenotype in postganglionic sympathetic neurons. *Neurochem. Res.* **21**, 823–829 (1996).
35. Furlan, A. *et al.* Multipotent peripheral glial cells generate neuroendocrine cells of the adrenal medulla. *Science* **357**, eaal3753 (2017).
36. Maris, J. M., Hogarty, M. D., Bagatell, R. & Cohn, S. L. Neuroblastoma. *Lancet* **369**, 2106–2120 (2007).
37. Yanagisawa, M., Yoshimura, S. & Yu, R. K. Expression of GD2 and GD3 gangliosides in human embryonic neural stem cells. *ASN Neuro* **3**, (2011).
38. Schulz, G. *et al.* Detection of ganglioside GD2 in tumor tissues and sera of neuroblastoma patients. *Cancer Res.* **44**, 5914–5920 (1984).
39. Smith, S. J., Diehl, N. N., Smith, B. D. & Mohney, B. G. Urine catecholamine levels as diagnostic markers for neuroblastoma in a defined population: implications for ophthalmic practice. *Eye (Lond)* **24**, 1792–1796 (2010).
40. Eisenhofer, G., Kopin, I. J. & Goldstein, D. S. Catecholamine metabolism: a contemporary view with implications for physiology and medicine. *Pharmacol. Rev.* **56**, 331–349 (2004).
41. Ciccarone, V., Spengler, B. A., Meyers, M. B., Biedler, J. L. & Ross, R. A. Phenotypic diversification in human neuroblastoma cells: expression of distinct neural crest lineages. *Cancer Res.* **49**, 219–225 (1989).

42. Ross, R. A., Biedler, J. L. & Spengler, B. A. A role for distinct cell types in determining malignancy in human neuroblastoma cell lines and tumors. *Cancer Lett.* **197**, 35–39 (2003).
43. Ross, R. A. *et al.* Human neuroblastoma I-type cells are malignant neural crest stem cells. *Cell Growth Differ.* **6**, 449–456 (1995).
44. Walton, J. D. *et al.* Characteristics of stem cells from human neuroblastoma cell lines and in tumors. *Neoplasia* **6**, 838–845 (2004).
45. Veschi, V., Verona, F. & Thiele, C. J. Cancer Stem Cells and Neuroblastoma: Characteristics and Therapeutic Targeting Options. *Front Endocrinol (Lausanne)* **10**, 782 (2019).
46. van Groningen, T. *et al.* Neuroblastoma is composed of two super-enhancer-associated differentiation states. *Nature Genetics* **49**, 1261–1266 (2017).
47. Boeva, V. *et al.* Heterogeneity of neuroblastoma cell identity defined by transcriptional circuitries. *Nat. Genet.* **49**, 1408–1413 (2017).
48. van Groningen, T. *et al.* A NOTCH feed-forward loop drives reprogramming from adrenergic to mesenchymal state in neuroblastoma. *Nat Commun* **10**, 1530 (2019).
49. Jiang, M., Stanke, J. & Lahti, J. M. The connections between neural crest development and neuroblastoma. *Curr. Top. Dev. Biol.* **94**, 77–127 (2011).
50. Marshall, G. M. *et al.* The prenatal origins of cancer. *Nat Rev Cancer* **14**, 277–289 (2014).
51. Wakamatsu, Y., Watanabe, Y., Nakamura, H. & Kondoh, H. Regulation of the neural crest cell fate by N-myc: promotion of ventral migration and neuronal differentiation. *Development* **124**, 1953–1962 (1997).
52. Seeger, R. C. *et al.* Association of Multiple Copies of the N-myc Oncogene with Rapid Progression of Neuroblastomas. *New England Journal of Medicine* **313**, 1111–1116 (1985).
53. Schwab, M. *et al.* Amplified DNA with limited homology to myc cellular oncogene is shared by human neuroblastoma cell lines and a neuroblastoma tumour. *Nature* **305**, 245–248 (1983).
54. Cohn, S. L. *et al.* The International Neuroblastoma Risk Group (INRG) classification system: an INRG Task Force report. *J. Clin. Oncol.* **27**, 289–297 (2009).
55. Janoueix-Lerosey, I. *et al.* Overall Genomic Pattern Is a Predictor of Outcome in Neuroblastoma. *JCO* **27**, 1026–1033 (2009).
56. Schleiermacher, G. *et al.* Accumulation of segmental alterations determines progression in neuroblastoma. *J. Clin. Oncol.* **28**, 3122–3130 (2010).
57. Attiyeh, E. F. *et al.* Chromosome 1p and 11q deletions and outcome in neuroblastoma. *N. Engl. J. Med.* **353**, 2243–2253 (2005).
58. Bown, N. *et al.* Gain of chromosome arm 17q and adverse outcome in patients with neuroblastoma. *N. Engl. J. Med.* **340**, 1954–1961 (1999).
59. Caron, H. *et al.* Allelic Loss of Chromosome 1p as a Predictor of Unfavorable Outcome in Patients with Neuroblastoma. *N Engl J Med* **334**, 225–230 (1996).
60. Plantaz, D. *et al.* Comparative genomic hybridization (CGH) analysis of stage 4 neuroblastoma reveals high frequency of 11q deletion in tumors lacking MYCN amplification. *Int. J. Cancer* **91**, 680–686 (2001).
61. Rubie, H. *et al.* Loss of chromosome 1p may have a prognostic value in localised neuroblastoma: results of the French NBL 90 Study. Neuroblastoma Study Group of the Société Française d'Oncologie Pédiatrique (SFOP). *Eur. J. Cancer* **33**, 1917–1922 (1997).
62. Schleiermacher, G. *et al.* Clinical relevance of loss heterozygosity of the short arm of chromosome 1 in neuroblastoma: a single-institution study. *Int. J. Cancer* **69**, 73–78 (1996).
63. Lastowska, M. *et al.* Comprehensive genetic and histopathologic study reveals three

types of neuroblastoma tumors. *J. Clin. Oncol.* **19**, 3080–3090 (2001).
64. Molenaar, J. J. *et al.* Sequencing of neuroblastoma identifies chromothripsis and defects in neuritogenesis genes. *Nature* **483**, 589–593 (2012).
65. Boeva, V. *et al.* Breakpoint features of genomic rearrangements in neuroblastoma with unbalanced translocations and chromothripsis. *PLoS ONE* **8**, e72182 (2013).
66. Pugh, T. J. *et al.* The genetic landscape of high-risk neuroblastoma. *Nat Genet* **45**, 279–284 (2013).
67. Sausen, M. *et al.* Integrated genomic analyses identify ARID1A and ARID1B alterations in the childhood cancer neuroblastoma. *Nat. Genet.* **45**, 12–17 (2013).
68. Chen, Y. *et al.* Oncogenic mutations of ALK kinase in neuroblastoma. *Nature* **455**, 971–974 (2008).
69. Janoueix-Lerosey, I. *et al.* Somatic and germline activating mutations of the ALK kinase receptor in neuroblastoma. *Nature* **455**, 967–970 (2008).
70. George, R. E. *et al.* Activating mutations in ALK provide a therapeutic target in neuroblastoma. *Nature* **455**, nature07397 (2008).
71. Mossé, Y. P. *et al.* Identification of *ALK* as a major familial neuroblastoma predisposition gene. *Nature* **455**, nature07261 (2008).
72. Cheung, N.-K. V. *et al.* Association of age at diagnosis and genetic mutations in patients with neuroblastoma. *JAMA* **307**, 1062–1071 (2012).
73. Zeineldin, M. *et al.* MYCN amplification and ATRX mutations are incompatible in neuroblastoma. *Nat Commun* **11**, 913 (2020).
74. Peifer, M. *et al.* Telomerase activation by genomic rearrangements in high-risk neuroblastoma. *Nature* **526**, 700–704 (2015).
75. Ackermann, S. *et al.* A mechanistic classification of clinical phenotypes in neuroblastoma. *Science* **362**, 1165–1170 (2018).
76. Keshelava, N. *et al.* Loss of p53 function confers high-level multidrug resistance in neuroblastoma cell lines. *Cancer Res.* **61**, 6185–6193 (2001).
77. Tweddle, D. A., Malcolm, A. J., Bown, N., Pearson, A. D. & Lunec, J. Evidence for the development of p53 mutations after cytotoxic therapy in a neuroblastoma cell line. *Cancer Res.* **61**, 8–13 (2001).
78. Carr, J. *et al.* Increased frequency of aberrations in the p53/MDM2/p14(ARF) pathway in neuroblastoma cell lines established at relapse. *Cancer Res.* **66**, 2138–2145 (2006).
79. Eleveld, T. F. *et al.* Relapsed neuroblastomas show frequent RAS-MAPK pathway mutations. *Nature Genetics* **47**, 864–871 (2015).
80. Schramm, A. *et al.* Mutational dynamics between primary and relapse neuroblastomas. *Nat. Genet.* **47**, 872–877 (2015).
81. Schleiermacher, G. *et al.* Emergence of New ALK Mutations at Relapse of Neuroblastoma. *JCO* **32**, 2727–2734 (2014).
82. Duan, C. *et al.* Whole exome sequencing reveals novel somatic alterations in neuroblastoma patients with chemotherapy. *Cancer Cell Int.* **18**, 21 (2018).
83. Maris, J. M. *et al.* Molecular genetic analysis of familial neuroblastoma. *Eur. J. Cancer* **33**, 1923–1928 (1997).
84. Roshkow, J. E., Haller, J. O., Berdon, W. E. & Sane, S. M. Hirschsprung's disease, Ondine's curse, and neuroblastoma--manifestations of neurocristopathy. *Pediatr Radiol* **19**, 45–49 (1988).
85. Weese-Mayer, D. E. *et al.* Idiopathic congenital central hypoventilation syndrome: analysis of genes pertinent to early autonomic nervous system embryologic development and identification of mutations in PHOX2b. *Am. J. Med. Genet. A* **123A**, 267–278 (2003).
86. Bourdeaut, F. *et al.* Germline mutations of the paired-like homeobox 2B (PHOX2B)

gene in neuroblastoma. *Cancer Lett.* **228**, 51–58 (2005).
87. Mosse, Y. P. *et al.* Germline PHOX2B Mutation in Hereditary Neuroblastoma. *Am J Hum Genet* **75**, 727–730 (2004).
88. Tolbert, V. P., Coggins, G. E. & Maris, J. M. Genetic susceptibility to neuroblastoma. *Current Opinion in Genetics & Development* **42**, 81–90 (2017).
89. Devoto, M. *et al.* Genome-wide linkage analysis to identify genetic modifiers of ALK mutation penetrance in familial neuroblastoma. *Hum. Hered.* **71**, 135–139 (2011).
90. Birch, J. M. *et al.* Relative frequency and morphology of cancers in carriers of germline TP53 mutations. *Oncogene* **20**, 4621–4628 (2001).
91. Vandepoele, K. *et al.* A constitutional translocation t(1;17)(p36.2;q11.2) in a neuroblastoma patient disrupts the human NBPF1 and ACCN1 genes. *PLoS ONE* **3**, e2207 (2008).
92. Schleiermacher, G., Janoueix-Lerosey, I. & Delattre, O. Recent insights into the biology of neuroblastoma. *Int. J. Cancer* **135**, 2249–2261 (2014).
93. Capasso, M. *et al.* Common variations in BARD1 influence susceptibility to high-risk neuroblastoma. *Nat. Genet.* **41**, 718–723 (2009).
94. Maris, J. M. *et al.* Chromosome 6p22 locus associated with clinically aggressive neuroblastoma. *N. Engl. J. Med.* **358**, 2585–2593 (2008).
95. Russell, M. R. *et al.* CASC15-S Is a Tumor Suppressor lncRNA at the 6p22 Neuroblastoma Susceptibility Locus. *Cancer Res.* **75**, 3155–3166 (2015).
96. Wang, K. *et al.* Integrative genomics identifies LMO1 as a neuroblastoma oncogene. *Nature* **469**, 216–220 (2011).
97. Diskin, S. J. *et al.* Common variation at 6q16 within HACE1 and LIN28B influences susceptibility to neuroblastoma. *Nat. Genet.* **44**, 1126–1130 (2012).
98. Zhang, L. *et al.* The E3 ligase HACE1 is a critical chromosome 6q21 tumor suppressor involved in multiple cancers. *Nat. Med.* **13**, 1060–1069 (2007).
99. Viswanathan, S. R. *et al.* Lin28 promotes transformation and is associated with advanced human malignancies. *Nat. Genet.* **41**, 843–848 (2009).
100. Nguyen, L. B. *et al.* Phenotype restricted genome-wide association study using a gene-centric approach identifies three low-risk neuroblastoma susceptibility Loci. *PLoS Genet.* **7**, e1002026 (2011).
101. Peuchmaur, M. *et al.* Revision of the International Neuroblastoma Pathology Classification: confirmation of favorable and unfavorable prognostic subsets in ganglioneuroblastoma, nodular. *Cancer* **98**, 2274–2281 (2003).
102. Shimada, H. *et al.* The International Neuroblastoma Pathology Classification (the Shimada system). *Cancer* **86**, 364–372 (1999).
103. Brodeur, G. M. *et al.* International criteria for diagnosis, staging, and response to treatment in patients with neuroblastoma. *J. Clin. Oncol.* **6**, 1874–1881 (1988).
104. Brodeur, G. M. *et al.* Revisions of the international criteria for neuroblastoma diagnosis, staging, and response to treatment. *J. Clin. Oncol.* **11**, 1466–1477 (1993).
105. Monclair, T. *et al.* The International Neuroblastoma Risk Group (INRG) staging system: an INRG Task Force report. *J. Clin. Oncol.* **27**, 298–303 (2009).
106. Meany, H. J. Non-High-Risk Neuroblastoma: Classification and Achievements in Therapy. *Children (Basel)* **6**, (2019).
107. Smith, V. & Foster, J. High-Risk Neuroblastoma Treatment Review. *Children (Basel)* **5**, (2018).
108. Cole, K. A. & Maris, J. M. New strategies in refractory and recurrent neuroblastoma: translational opportunities to impact patient outcome. *Clin. Cancer Res.* **18**, 2423–2428 (2012).
109. Zage, P. E. Novel Therapies for Relapsed and Refractory Neuroblastoma. *Children*

(Basel) **5**, (2018).
110. Minturn, J. E. *et al.* Phase I trial of lestaurtinib for children with refractory neuroblastoma: a new approaches to neuroblastoma therapy consortium study. *Cancer Chemother. Pharmacol.* **68**, 1057–1065 (2011).
111. Umapathy, G., Mendoza-Garcia, P., Hallberg, B. & Palmer, R. H. Targeting anaplastic lymphoma kinase in neuroblastoma. *Apmis* **127**, 288 (2019).
112. Weiss, W. A., Aldape, K., Mohapatra, G., Feuerstein, B. G. & Bishop, J. M. Targeted expression of MYCN causes neuroblastoma in transgenic mice. *EMBO J.* **16**, 2985–2995 (1997).
113. Teitz, T. *et al.* Th-MYCN mice with caspase-8 deficiency develop advanced neuroblastoma with bone marrow metastasis. *Cancer Res.* **73**, 4086–4097 (2013).
114. Althoff, K. *et al.* A Cre-conditional *MYCN*-driven neuroblastoma mouse model as an improved tool for preclinical studies. *Oncogene* **34**, 3357 (2015).
115. Molenaar, J. J. *et al.* LIN28B induces neuroblastoma and enhances MYCN levels via let-7 suppression. *Nat. Genet.* **44**, 1199–1206 (2012).
116. De Wilde, B. *et al.* The mutational landscape of MYCN, Lin28b and ALK F1174L driven murine neuroblastoma mimics human disease. *Oncotarget* **9**, 8334–8349 (2018).
117. Janoueix-Lerosey, I., Lopez-Delisle, L., Delattre, O. & Rohrer, H. The ALK receptor in sympathetic neuron development and neuroblastoma. *Cell Tissue Res.* **372**, 325–337 (2018).
118. Hallberg, B. & Palmer, R. H. The role of the ALK receptor in cancer biology. *Ann. Oncol.* **27 Suppl 3**, iii4–iii15 (2016).
119. Morris, S. W. *et al.* ALK, the chromosome 2 gene locus altered by the t(2;5) in non-Hodgkin's lymphoma, encodes a novel neural receptor tyrosine kinase that is highly related to leukocyte tyrosine kinase (LTK). *Oncogene* **14**, 2175–2188 (1997).
120. Hurley, S. P., Clary, D. O., Copié, V. & Lefcort, F. Anaplastic Lymphoma Kinase is Dynamically Expressed on Subsets of Motor Neurons and in the Peripheral Nervous System. *J Comp Neurol* **495**, 202–212 (2006).
121. Vernersson, E. *et al.* Characterization of the expression of the ALK receptor tyrosine kinase in mice. *Gene Expr. Patterns* **6**, 448–461 (2006).
122. Degoutin, J., Brunet-de Carvalho, N., Cifuentes-Diaz, C. & Vigny, M. ALK (Anaplastic Lymphoma Kinase) expression in DRG neurons and its involvement in neuron–Schwann cells interaction. *European Journal of Neuroscience* **29**, 275–286 (2009).
123. Lopez-Delisle, L. *et al.* Hyperactivation of Alk induces neonatal lethality in knock-in AlkF1178L mice. *Oncotarget* **5**, 2703–2713 (2014).
124. Weiss, J. B. *et al.* Anaplastic lymphoma kinase and leukocyte tyrosine kinase: functions and genetic interactions in learning, memory and adult neurogenesis. *Pharmacol. Biochem. Behav.* **100**, 566–574 (2012).
125. Yao, S. *et al.* Anaplastic Lymphoma Kinase Is Required for Neurogenesis in the Developing Central Nervous System of Zebrafish. *PLOS ONE* **8**, e63757 (2013).
126. Stoica, G. E. *et al.* Identification of Anaplastic Lymphoma Kinase as a Receptor for the Growth Factor Pleiotrophin. *J. Biol. Chem.* **276**, 16772–16779 (2001).
127. Stoica, G. E. *et al.* Midkine Binds to Anaplastic Lymphoma Kinase (ALK) and Acts as a Growth Factor for Different Cell Types. *J. Biol. Chem.* **277**, 35990–35998 (2002).
128. Lorente, M. *et al.* Stimulation of the midkine/ALK axis renders glioma cells resistant to cannabinoid antitumoral action. *Cell Death Differ.* **18**, 959–973 (2011).
129. Reiff, T. *et al.* Midkine and Alk signaling in sympathetic neuron proliferation and neuroblastoma predisposition. *Development* **138**, 4699–4708 (2011).
130. Mathivet, T., Mazot, P. & Vigny, M. In contrast to agonist monoclonal antibodies,

both C-terminal truncated form and full length form of Pleiotrophin failed to activate vertebrate ALK (anaplastic lymphoma kinase)? *Cell. Signal.* **19**, 2434–2443 (2007).
131. Miyake, I. *et al.* Activation of anaplastic lymphoma kinase is responsible for hyperphosphorylation of ShcC in neuroblastoma cell lines. *Oncogene* **21**, 5823–5834 (2002).
132. Moog-Lutz, C. *et al.* Activation and inhibition of anaplastic lymphoma kinase receptor tyrosine kinase by monoclonal antibodies and absence of agonist activity of pleiotrophin. *J. Biol. Chem.* **280**, 26039–26048 (2005).
133. Murray, P. B. *et al.* Heparin is an activating ligand of the orphan receptor tyrosine kinase ALK. *Sci Signal* **8**, ra6 (2015).
134. Guan, J. *et al.* FAM150A and FAM150B are activating ligands for anaplastic lymphoma kinase. *eLife Sciences* **4**, e09811 (2015).
135. Reshetnyak, A. V. *et al.* Augmentor α and β (FAM150) are ligands of the receptor tyrosine kinases ALK and LTK: Hierarchy and specificity of ligand-receptor interactions. *Proc. Natl. Acad. Sci. U.S.A.* **112**, 15862–15867 (2015).
136. Fadeev, A. *et al.* ALKALs are in vivo ligands for ALK family receptor tyrosine kinases in the neural crest and derived cells. *Proc. Natl. Acad. Sci. U.S.A.* **115**, E630–E638 (2018).
137. Mo, E. S., Cheng, Q., Reshetnyak, A. V., Schlessinger, J. & Nicoli, S. Alk and Ltk ligands are essential for iridophore development in zebrafish mediated by the receptor tyrosine kinase Ltk. *Proc. Natl. Acad. Sci. U.S.A.* **114**, 12027–12032 (2017).
138. Reshetnyak, A. V. *et al.* Identification of a biologically active fragment of ALK and LTK-Ligand 2 (augmentor-α). *Proc. Natl. Acad. Sci. U.S.A.* **115**, 8340–8345 (2018).
139. Zhang, H. *et al.* Deorphanization of the human leukocyte tyrosine kinase (LTK) receptor by a signaling screen of the extracellular proteome. *Proc. Natl. Acad. Sci. U.S.A.* **111**, 15741–15745 (2014).
140. Bilsland, J. G. *et al.* Behavioral and neurochemical alterations in mice deficient in anaplastic lymphoma kinase suggest therapeutic potential for psychiatric indications. *Neuropsychopharmacology* **33**, 685–700 (2008).
141. Lasek, A. W. *et al.* An evolutionary conserved role for anaplastic lymphoma kinase in behavioral responses to ethanol. *PLoS ONE* **6**, e22636 (2011).
142. Witek, B. *et al.* Targeted Disruption of ALK Reveals a Potential Role in Hypogonadotropic Hypogonadism. *PLoS ONE* **10**, e0123542 (2015).
143. Morris, S. W. *et al.* Fusion of a kinase gene, ALK, to a nucleolar protein gene, NPM, in non-Hodgkin's lymphoma. *Science* **263**, 1281–1284 (1994).
144. Hallberg, B. & Palmer, R. H. Mechanistic insight into ALK receptor tyrosine kinase in human cancer biology. *Nature Reviews Cancer* **13**, nrc3580 (2013).
145. Van den Eynden, J. *et al.* Phosphoproteome and gene expression profiling of ALK inhibition in neuroblastoma cell lines reveals conserved oncogenic pathways. *Sci. Signal.* **11**, eaar5680 (2018).
146. Chen, K. *et al.* Phosphoproteomics reveals ALK promote cell progress via RAS/ JNK pathway in neuroblastoma. *Oncotarget* **7**, 75968–75980 (2016).
147. Umapathy, G. *et al.* The kinase ALK stimulates the kinase ERK5 to promote the expression of the oncogene MYCN in neuroblastoma. *Sci Signal* **7**, ra102 (2014).
148. Schönherr, C. *et al.* Anaplastic Lymphoma Kinase (ALK) regulates initiation of transcription of MYCN in neuroblastoma cells. *Oncogene* **31**, 5193–5200 (2012).
149. Sattu, K. *et al.* Phosphoproteomic analysis of anaplastic lymphoma kinase (ALK) downstream signaling pathways identifies signal transducer and activator of transcription 3 as a functional target of activated ALK in neuroblastoma cells. *FEBS J.* **280**, 5269–5282 (2013).
150. Brouwer, S. D. *et al.* Meta-analysis of Neuroblastomas Reveals a Skewed ALK Mutation Spectrum in Tumors with MYCN Amplification. *Clin Cancer Res* **16**, 4353–4362

(2010).
151. Ogawa, S., Takita, J., Sanada, M. & Hayashi, Y. Oncogenic mutations of ALK in neuroblastoma. *Cancer Science* **102**, 302–308 (2011).
152. Lamant, L. *et al.* Expression of the ALK Tyrosine Kinase Gene in Neuroblastoma. *Am J Pathol* **156**, 1711–1721 (2000).
153. Carén, H., Abel, F., Kogner, P. & Martinsson, T. High incidence of DNA mutations and gene amplifications of the ALK gene in advanced sporadic neuroblastoma tumours. *Biochemical Journal* **416**, 153–159 (2008).
154. Bresler, S. C. *et al.* Differential Inhibitor Sensitivity of Anaplastic Lymphoma Kinase Variants Found in Neuroblastoma. *Science Translational Medicine* **3**, 108ra114-108ra114 (2011).
155. de Pontual, L. *et al.* Germline gain-of-function mutations of ALK disrupt central nervous system development. *Hum. Mutat.* **32**, 272–276 (2011).
156. Chand, D. *et al.* Cell culture and Drosophila model systems define three classes of anaplastic lymphoma kinase mutations in neuroblastoma. *Dis Model Mech* **6**, 373–382 (2013).
157. Schönherr, C. *et al.* The neuroblastoma ALK(I1250T) mutation is a kinase-dead RTK in vitro and in vivo. *Transl Oncol* **4**, 258–265 (2011).
158. Bresler, S. C. *et al.* ALK mutations confer differential oncogenic activation and sensitivity to ALK inhibition therapy in neuroblastoma. *Cancer Cell* **26**, 682–694 (2014).
159. Bellini, A. *et al.* Deep Sequencing Reveals Occurrence of Subclonal ALK Mutations in Neuroblastoma at Diagnosis. *Clin Cancer Res* **21**, 4913–4921 (2015).
160. Okubo, J. *et al.* Aberrant activation of ALK kinase by a novel truncated form ALK protein in neuroblastoma. *Oncogene* **31**, 4667–4676 (2012).
161. Cazes, A. *et al.* Characterization of rearrangements involving the ALK gene reveals a novel truncated form associated with tumor aggressiveness in neuroblastoma. *Cancer Res.* **73**, 195–204 (2013).
162. Olsen, R. R. *et al.* MYCN induces neuroblastoma in primary neural crest cells. *Oncogene* **36**, 5075–5082 (2017).
163. Schulte, J. H. *et al.* MYCN and ALKF1174L are sufficient to drive neuroblastoma development from neural crest progenitor cells. *Oncogene* **32**, 1059 (2013).
164. Montavon, G. *et al.* Wild-type ALK and activating ALK-R1275Q and ALK-F1174L mutations upregulate Myc and initiate tumor formation in murine neural crest progenitor cells. *Oncotarget* **5**, 4452–4466 (2014).
165. Kramer, M., Ribeiro, D., Arsenian-Henriksson, M., Deller, T. & Rohrer, H. Proliferation and Survival of Embryonic Sympathetic Neuroblasts by MYCN and Activated ALK Signaling. *J. Neurosci.* **36**, 10425–10439 (2016).
166. Gouzi, J. Y., Moog-Lutz, C., Vigny, M. & Carvalho, N. B. Role of the subcellular localization of ALK tyrosine kinase domain in neuronal differentiation of PC12 cells. *Journal of Cell Science* **118**, 5811–5823 (2005).
167. Motegi, A., Fujimoto, J., Kotani, M., Sakuraba, H. & Yamamoto, T. ALK receptor tyrosine kinase promotes cell growth and neurite outgrowth. *Journal of Cell Science* **117**, 3319–3329 (2004).
168. Heukamp, L. C. *et al.* Targeted Expression of Mutated ALK Induces Neuroblastoma in Transgenic Mice. *Science Translational Medicine* **4**, 141ra91-141ra91 (2012).
169. Berry, T. *et al.* The ALK(F1174L) mutation potentiates the oncogenic activity of MYCN in neuroblastoma. *Cancer Cell* **22**, 117–130 (2012).
170. Cazes, A. *et al.* Activated Alk triggers prolonged neurogenesis and Ret upregulation providing a therapeutic target in ALK-mutated neuroblastoma. *Oncotarget* **5**, 2688–2702 (2014).

171. Ueda, T. *et al.* ALK(R1275Q) perturbs extracellular matrix, enhances cell invasion and leads to the development of neuroblastoma in cooperation with MYCN. *Oncogene* **35**, 4447–4458 (2016).
172. Zhu, S. *et al.* Activated ALK Collaborates with MYCN in Neuroblastoma Pathogenesis. *Cancer Cell* **21**, 362–373 (2012).
173. Mossé, Y. P. *et al.* Safety and activity of crizotinib for paediatric patients with refractory solid tumours or anaplastic large-cell lymphoma: a Children's Oncology Group phase 1 consortium study. *The Lancet Oncology* **14**, 472–480 (2013).
174. Debruyne, D. N. *et al.* ALK inhibitor resistance in ALK(F1174L)-driven neuroblastoma is associated with AXL activation and induction of EMT. *Oncogene* **35**, 3681–3691 (2016).
175. Sakamoto, H. *et al.* CH5424802, a selective ALK inhibitor capable of blocking the resistant gatekeeper mutant. *Cancer Cell* **19**, 679–690 (2011).
176. Krytska, K. *et al.* Crizotinib Synergizes with Chemotherapy in Preclinical Models of Neuroblastoma. *Clin. Cancer Res.* **22**, 948–960 (2016).
177. Moore, N. F. *et al.* Molecular rationale for the use of PI3K/AKT/mTOR pathway inhibitors in combination with crizotinib in ALK-mutated neuroblastoma. *Oncotarget* **5**, 8737–8749 (2014).
178. Wood, A. C. *et al.* Dual ALK and CDK4/6 Inhibition Demonstrates Synergy against Neuroblastoma. *Clin. Cancer Res.* **23**, 2856–2868 (2017).
179. Wang, H. Q. *et al.* Combined ALK and MDM2 inhibition increases antitumor activity and overcomes resistance in human ALK mutant neuroblastoma cell lines and xenograft models. *Elife* **6**, (2017).
180. Guan, J. *et al.* The ALK inhibitor PF-06463922 is effective as a single agent in neuroblastoma driven by expression of ALK and MYCN. *Dis Model Mech* **9**, 941–952 (2016).
181. Infarinato, N. R. *et al.* The ALK/ROS1 Inhibitor PF-06463922 Overcomes Primary Resistance to Crizotinib in ALK-Driven Neuroblastoma. *Cancer Discov* **6**, 96–107 (2016).
182. Martinsson, T. *et al.* Appearance of the Novel Activating F1174S ALK Mutation in Neuroblastoma Correlates with Aggressive Tumor Progression and Unresponsiveness to Therapy. *Cancer Res* **71**, 98–105 (2011).
183. Schulte, J. H. *et al.* High ALK Receptor Tyrosine Kinase Expression Supersedes ALK Mutation as a Determining Factor of an Unfavorable Phenotype in Primary Neuroblastoma. *Clin Cancer Res* **17**, 5082–5092 (2011).
184. Carpenter, E. L. & Mossé, Y. P. Targeting ALK in neuroblastoma—preclinical and clinical advancements. *Nature Reviews Clinical Oncology* **9**, 391 (2012).
185. Lovly, C. M. & Shaw, A. T. Molecular pathways: resistance to kinase inhibitors and implications for therapeutic strategies. *Clin. Cancer Res.* **20**, 2249–2256 (2014).
186. Lambertz, I. *et al.* Upregulation of MAPK Negative Feedback Regulators and RET in Mutant ALK Neuroblastoma: Implications for Targeted Treatment. *Clin. Cancer Res.* **21**, 3327–3339 (2015).
187. Claeys, S. *et al.* Early and late effects of pharmacological ALK inhibition on the neuroblastoma transcriptome. *Oncotarget* **8**, 106820–106832 (2017).
188. Lopez-Delisle, L. *et al.* Activated ALK signals through the ERK-ETV5-RET pathway to drive neuroblastoma oncogenesis. *Oncogene* **37**, 1417–1429 (2018).
189. Mus, L. M. *et al.* The ETS transcription factor ETV5 is a target of activated ALK in neuroblastoma contributing to increased tumour aggressiveness. *Sci Rep* **10**, 218 (2020).
190. Corey, J. M. *et al.* Patterning N-type and S-type neuroblastoma cells with Pluronic F108 and ECM proteins. *J Biomed Mater Res A* **93**, 673–686 (2010).
191. Mazot, P. *et al.* The constitutive activity of the ALK mutated at positions F1174 or

R1275 impairs receptor trafficking. *Oncogene* **30**, 2017–2025 (2011).
192. Suvà, M. L. *et al.* Reconstructing and reprogramming the tumor-propagating potential of glioblastoma stem-like cells. *Cell* **157**, 580–594 (2014).
193. Joseph, J.-M. *et al.* In vivo echographic evidence of tumoral vascularization and microenvironment interactions in metastatic orthotopic human neuroblastoma xenografts. *Int. J. Cancer* **113**, 881–890 (2005).
194. Meier, R. *et al.* The chemokine receptor CXCR4 strongly promotes neuroblastoma primary tumour and metastatic growth, but not invasion. *PLoS ONE* **2**, e1016 (2007).
195. Bradley, R. S. Neural crest development in Xenopus requires Protocadherin 7 at the lateral neural crest border. *Mechanisms of Development* **149**, 41–52 (2018).
196. Hayashi, S. & Takeichi, M. Emerging roles of protocadherins: from self-avoidance to enhancement of motility. *Journal of Cell Science* **128**, 1455–1464 (2015).
197. Zhang, W. *et al.* Comparison of RNA-seq and microarray-based models for clinical endpoint prediction. *Genome Biol.* **16**, 133 (2015).
198. Fares, J., Fares, M. Y., Khachfe, H. H., Salhab, H. A. & Fares, Y. Molecular principles of metastasis: a hallmark of cancer revisited. *Signal Transduct Target Ther* **5**, 28 (2020).
199. Aceto, N. *et al.* Circulating tumor cell clusters are oligoclonal precursors of breast cancer metastasis. *Cell* **158**, 1110–1122 (2014).
200. Au, S. H. *et al.* Clusters of circulating tumor cells traverse capillary-sized vessels. *Proc. Natl. Acad. Sci. U.S.A.* **113**, 4947–4952 (2016).
201. Aktary, Z., Alaee, M. & Pasdar, M. Beyond cell-cell adhesion: Plakoglobin and the regulation of tumorigenesis and metastasis. *Oncotarget* **8**, 32270–32291 (2017).
202. Hänel, L. *et al.* Differential Proteome Analysis of Human Neuroblastoma Xenograft Primary Tumors and Matched Spontaneous Distant Metastases. *Sci Rep* **8**, 13986 (2018).
203. Desgrosellier, J. S. & Cheresh, D. A. Integrins in cancer: biological implications and therapeutic opportunities. *Nat. Rev. Cancer* **10**, 9–22 (2010).
204. Waisberg, J. *et al.* Overexpression of the ITGAV gene is associated with progression and spread of colorectal cancer. *Anticancer Res.* **34**, 5599–5607 (2014).
205. van der Horst, G. *et al.* Targeting of alpha-v integrins reduces malignancy of bladder carcinoma. *PLoS ONE* **9**, e108464 (2014).
206. Lambert, A. W., Pattabiraman, D. R. & Weinberg, R. A. Emerging Biological Principles of Metastasis. *Cell* **168**, 670–691 (2017).
207. Yu, M. *et al.* Circulating breast tumor cells exhibit dynamic changes in epithelial and mesenchymal composition. *Science* **339**, 580–584 (2013).
208. Lecharpentier, A. *et al.* Detection of circulating tumour cells with a hybrid (epithelial/mesenchymal) phenotype in patients with metastatic non-small cell lung cancer. *Br. J. Cancer* **105**, 1338–1341 (2011).
209. Armstrong, A. J. *et al.* Circulating tumor cells from patients with advanced prostate and breast cancer display both epithelial and mesenchymal markers. *Mol. Cancer Res.* **9**, 997–1007 (2011).
210. Zhao, R. *et al.* Expression and clinical relevance of epithelial and mesenchymal markers in circulating tumor cells from colorectal cancer. *Oncotarget* **8**, 9293–9302 (2017).
211. Li, T.-T. *et al.* Evaluation of epithelial-mesenchymal transitioned circulating tumor cells in patients with resectable gastric cancer: Relevance to therapy response. *World J. Gastroenterol.* **21**, 13259–13267 (2015).
212. Alto, L. T. & Terman, J. R. Semaphorins and their Signaling Mechanisms. *Methods Mol. Biol.* **1493**, 1–25 (2017).
213. Gammill, L. S., Gonzalez, C., Gu, C. & Bronner-Fraser, M. Guidance of trunk neural crest migration requires neuropilin 2/semaphorin 3F signaling. *Development* **133**, 99–106

(2006).
214. Yu, H.-H. & Moens, C. B. Semaphorin signaling guides cranial neural crest cell migration in zebrafish. *Dev. Biol.* **280**, 373–385 (2005).
215. Osborne, N. J., Begbie, J., Chilton, J. K., Schmidt, H. & Eickholt, B. J. Semaphorin/neuropilin signaling influences the positioning of migratory neural crest cells within the hindbrain region of the chick. *Dev. Dyn.* **232**, 939–949 (2005).
216. Chédotal, A., Kerjan, G. & Moreau-Fauvarque, C. The brain within the tumor: new roles for axon guidance molecules in cancers. *Cell Death Differ.* **12**, 1044–1056 (2005).
217. Neufeld, G. *et al.* The role of the semaphorins in cancer. *Cell Adh Migr* **10**, 652–674 (2016).
218. Delloye-Bourgeois, C. *et al.* Microenvironment-Driven Shift of Cohesion/Detachment Balance within Tumors Induces a Switch toward Metastasis in Neuroblastoma. *Cancer Cell* **32**, 427-443.e8 (2017).
219. Guo, F. & Zheng, Y. Vav1: Friend and Foe of Cancer. *Trends in Cell Biology* **27**, 879–880 (2017).
220. Fernandez-Zapico, M. E. *et al.* Ectopic expression of VAV1 reveals an unexpected role in pancreatic cancer tumorigenesis. *Cancer Cell* **7**, 39–49 (2005).
221. Lazer, G., Idelchuk, Y., Schapira, V., Pikarsky, E. & Katzav, S. The haematopoietic specific signal transducer Vav1 is aberrantly expressed in lung cancer and plays a role in tumourigenesis. *J. Pathol.* **219**, 25–34 (2009).
222. Sebban, S. *et al.* Vav1 promotes lung cancer growth by instigating tumor-microenvironment cross-talk via growth factor secretion. *Oncotarget* **5**, 9214–9226 (2014).
223. Sebban, S. *et al.* Vav1 fine tunes p53 control of apoptosis versus proliferation in breast cancer. *PLoS ONE* **8**, e54321 (2013).
224. Hornstein, I. *et al.* The haematopoietic specific signal transducer Vav1 is expressed in a subset of human neuroblastomas. *J. Pathol.* **199**, 526–533 (2003).
225. Grassilli, S. *et al.* High nuclear level of Vav1 is a positive prognostic factor in early invasive breast tumors: a role in modulating genes related to the efficiency of metastatic process. *Oncotarget* **5**, 4320–4336 (2014).
226. Zhang, Z. *et al.* Transcription factor Etv5 is essential for the maintenance of alveolar type II cells. *Proc. Natl. Acad. Sci. U.S.A.* **114**, 3903–3908 (2017).
227. Dubois, S. G. *et al.* Lung metastases in neuroblastoma at initial diagnosis: A report from the International Neuroblastoma Risk Group (INRG) project. *Pediatr Blood Cancer* **51**, 589–592 (2008).
228. DuBois, S. G. *et al.* Metastatic sites in stage IV and IVS neuroblastoma correlate with age, tumor biology, and survival. *J. Pediatr. Hematol. Oncol.* **21**, 181–189 (1999).
229. Lee, G. *et al.* Isolation and directed differentiation of neural crest stem cells derived from human embryonic stem cells. *Nat. Biotechnol.* **25**, 1468–1475 (2007).
230. Kirino, K., Nakahata, T., Taguchi, T. & Saito, M. K. Efficient derivation of sympathetic neurons from human pluripotent stem cells with a defined condition. *Sci Rep* **8**, 12865 (2018).
231. Bhagwat, N. *et al.* An integrated flow cytometry-based platform for isolation and molecular characterization of circulating tumor single cells and clusters. *Sci Rep* **8**, 5035 (2018).